2

F W Kallmeyer, 832

X

ANALYSIS OF ANGULAR ALIGNMENT PROCEDURES FOR UNIFIED S-BAND 30-FOOT ANTENNA SYSTEM

MARCH 1970

CONTRACT NO NAS 5-10854

PREPARED BY

COMPUTER SCIENCES CORPORATION
GEONAUTICS OPERATION
803 WEST BROAD STREET
FALLS CHURCH, VIRGINIA 22046

DATA EVALUATION BRANCH
MANNED FLIGHT PLANNING AND ANALYSIS DIVISION
GODDARD SPACE FLIGHT CENTER
GREENBELT, MARYLAND

ANALYSIS OF ANGULAR ALIGNMENT PROCEDURES FOR UNIFIED S-BAND 30-FOOT ANTENNA SYSTEM

H MacDonald Harper

Computer Sciences Corporation
Falls Church, Virginia

March 1970

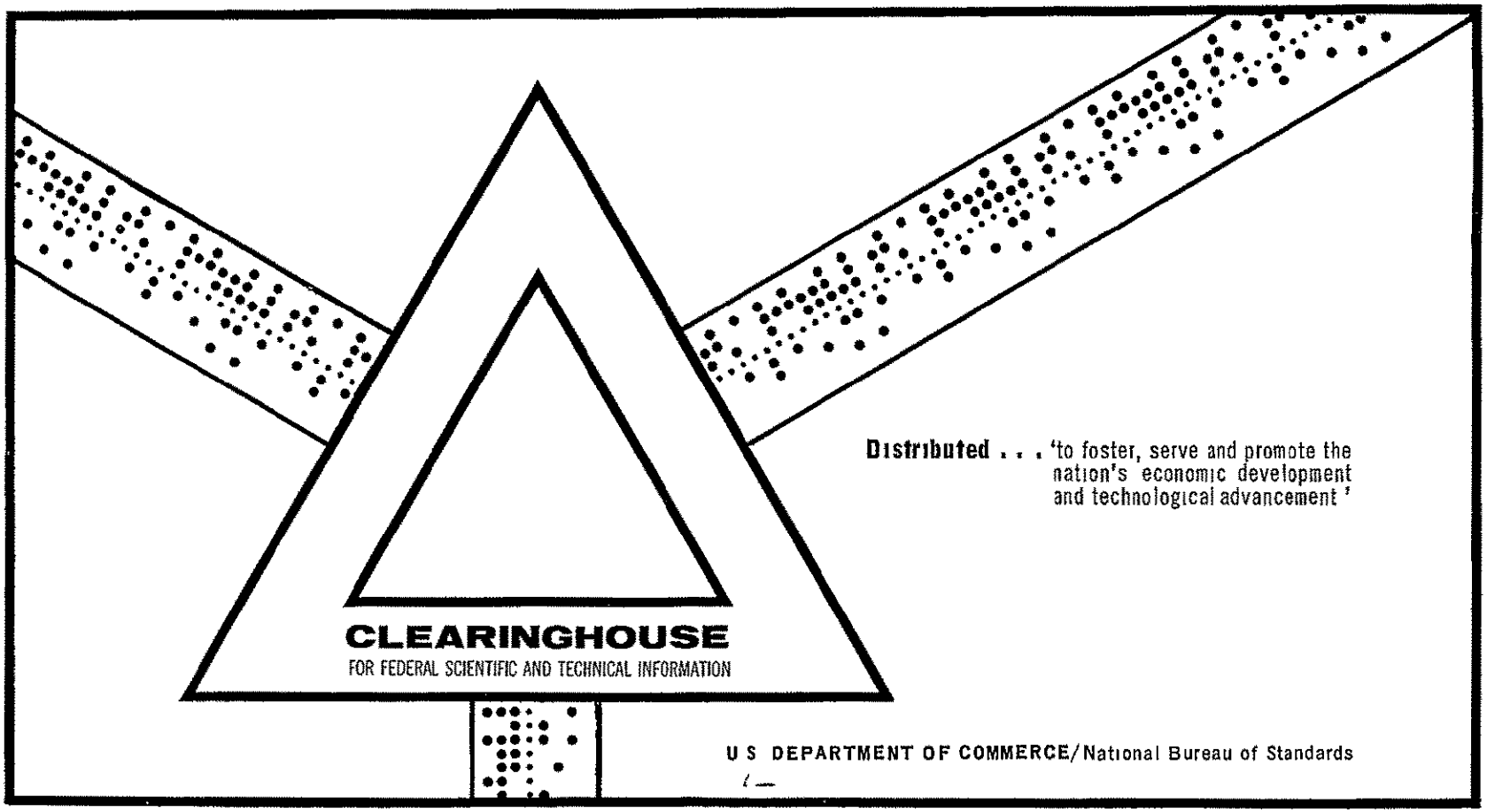

ANALYSIS OF ANGULAR ALIGNMENT PROCEDURES FOR UNIFIED S-BAND 30-FOOT ANTENNA SYSTEM

March 1970

Contract No. NAS 5-10854

Goddard Space Flight Center
Contract Officer Miss J C Arena
Technical Officer Mr F W Kallmeyer 832

Prepared by

Computer Sciences Corporation
803 West Broad Street
Falls Church, Virginia 22046

Project Manager H MacDonald Harper

For
Data Evaluation Branch
Manned Flight Planning and Analysis Division
Goddard Space Flight Center
Greenbelt, Maryland

SUMMARY

Investigations performed under this contract represent the second part of a two-phase study program to establish field procedures for angular alignment and orientation of the unified S-band 30-foot antennas

The ultimate purpose of this study was to analyze various techniques and procedures which may be applicable for angular calibration of the unified S-band antennas, and to devise optimum methods which will be suitable for monitoring antenna orientation on a near real-time basis

This report describes field investigations and tests that were made with the 30-foot unified S-band antenna at the Network Training and Test Facility (NTTF), Goddard Space Flight Center Investigations involved various efforts including final field testing of procedures for using level readings and star observations for calibrating the mechanical axis of the antenna, assessment of existing optical-electronic boresighting procedures, and a preliminary evaluation of methods for using celestial radio sources for rf axis alignment

Analytical studies were made in conjunction with these field experiments to define an appropriate error model for using star observations to calibrate the mechanical axis of the antenna Based on an analysis of eight sets of star observations, a star calibration model was developed This included nine error terms for defining antenna misalignment due to angle encoder bias, azimuth misalignment, tilt with respect to the local gravity vector, and nonorthogonalities of the X axis to Y axis and optical axis to Y axis, and X and Y structural deflections Results of solutions indicated that the nine error coefficients could be determined within a standard deviation not exceeding $\pm 0^{\circ}004$ and a standard deviation of a single observation, σ_o, of $\pm 0.^{\circ}003$

During the star observations and periodically between sets of star observations optical targets and Y-wheelhouse spirit levels were monitored It was found that the levels provide a reliable means of monitoring antenna

change between sets of star observations, and that optical targets are useful in supporting evidence of change Use of the two systems indicated that the X encoder drifted more than $0.^{\circ}125$ in 5 months

Tests conducted on the standard boresighting technique indicated that, despite multipath, optical-rf alignment can be determined by this technique to within a standard error of about $0^{\circ}02$

Preliminary testing and analysis was made to determine the feasibility of using celestial radio sources and the ALSEP transponder for rf axis alignment Five radio stars were detected with the available equipment set-up, but the low signal to noise ratio limited useful observations to two stars, Cassiopeia A and Cygnus A Three methods for observing the radio sources were tested but because of the limited observations each method could not be thoroughly assessed Despite the limited data, the technique of single axis scanning gave encouraging results, comparing favorably with ALSEP (both autotrack and photos) and rf-optical boresighting The standard error of the single axis scan method was about $0^{\circ}03$

The use of the field instruction manual, "Operation Manual for Angular Alignment and Static Calibration of Unified S-Band 30-foot Antenna," written as part of this contract is recommended to maintain and monitor antenna angular calibration. The procedures outlined in this manual would be enhanced by the addition of extra sets of Y-wheelhouse spirit levels

The radio star and ALSEP experiments for rf axis alignment are encouraging and it is strongly recommended that these methods of calibration be refined

TABLE OF CONTENTS

TABLE OF CONTENTS - (Continued)

TABLE OF CONTENTS - (Continued)

LIST OF FIGURES

LIST OF FIGURES - (Continued)

LIST OF TABLES

SECTION 1
INTRODUCTION

1.1 PURPOSE AND SCOPE

The investigations performed under this contract were concerned with the development of field procedures for the geodetic alignment and orientation of the unified S-band 30-foot antenna system

The objective of the studies was to establish alignment procedures to improve the reliability of angular tracking data from the unified S-band antennas and to provide a means for accurately relating these data to the adopted geodetic reference system. To be of maximum benefit for tracking operations, these procedures should be capable of readily furnishing the geodetic orientation of the antenna prior to, and possibly during, tracking missions

To determine the geodetic orientation of a tracking antenna such as the unified S-band antenna system, it is necessary to know the relationship of its mechanical and electronic axes, the orientation of its mechanical axes to the local gravity vector, the relationship of its azimuth plane to geodetic north, and the deflection of the vertical at the site All of these factors must be known to an accuracy commensurate with the angular measurement capability of the antenna Since the antenna structure is affected to some extent by atmospheric changes (diurnal solar heating, wind load, etc.) and settlement of its foundation, antenna orientation varies with time and the initial geodetic orientation is of little value unless some means can be devised to monitor the relative change in orientation Such means may be either internal to the antenna structure, such as permanently installed spirit levels, or external, such as star calibration techniques and optical targets

The ultimate purpose of this study, therefore, was to analyze various techniques and procedures which may be applicable for angular alignment and calibration of the unified S-band antennas, and to devise efficient methods

which will be suitable for monitoring antenna orientation on a near real-time basis

1.2 STUDY PLAN AND SCHEDULE

The work performed under this contract represents the second part of a two-phase study program approved by technical representatives of the Data Evaluation Branch, Manned Flight Planning and Analysis Division In accordance with this study program, geodetic alignment procedures were to be developed by undertaking the following investigations 1) an assessment of existing field methods used for the initial alignment of the antenna structure, 2) an analysis of terrestrial targets and star observation procedures for providing orientation and alignment data, 3) operational tests and analyses of selected alignment procedures to determine their capabilities and compatibility with existing site calibration procedures, and 4) the preparation of an instruction manual detailing specifications and procedures for geodetic alignment of the antennas These investigations were to be performed with the unified S-band 30-foot antenna at the Network Training and Test Facility (NTTF), Goddard Space Flight Center

For contractual purposes the investigations were programmed in two phases, each of six month duration The first phase involved a preliminary analysis of items 1) and 2) above and was accomplished under contract NAS 5-10638 during the period 16 April through 15 October 1968 The results of this phase of the work were presented in Geonautics' report, "Geodetic Alignment Procedures for Unified S-band Antenna System (Preliminary Analysis)", dated November 1968.

The second phase of the study program was undertaken under the present contract beginning on 26 February 1969. Work was scheduled for a six-month period and was divided into three major tasks 1) completion of field evaluation of procedures tested during the first phase of the study, 2) investigation of existing electronic boresighting techniques, and 3) preparation of the instruction manual for site personnel (Note: The instruction manual is separate from this report)

During the second month of the contract, project personnel were requested to consider the possibility of using celestial radio sources for aligning the electronic axis of the antenna This led to a redirection of the work for task 2) above to include a preliminary analysis of the feasibility of celestial radio sources and lunar beacons, such as ALSEP, for calibration of the electronic axis of the 30-foot antenna system.

Field experiments and operational tests at the NTTF site were originally scheduled over a three-month period beginning the first month of the contract However, because of training classes, maintenance, and test programs already scheduled at NTTF, field work did not begin until the week of April 27th, two months after the contract starting date In addition to this delay, extensive maintenance was required on the antenna after the Apollo 10 mission, this prevented any field work during the period 26 May through 23 June. Because of these delays, the contract period of performance was extended by GSFC for four months This made it possible to continue the field work intermittently as often as NTTF schedules would permit through the last week in September. At this time, the antenna underwent a five week maintenance overhaul which precluded any further field testing under this contract

1.3 REPORT ORGANIZATION

Section 2 of this report describes the field investigations and observational data obtained at the NTTF unified S-band 30-foot antenna site Investigations involved various efforts including the installation and survey of new optical targets around the antenna, final field testing of procedures for using level readings and star observations for calibrating the mechanical axis of the antenna, assessment of existing electronic boresighting procedures, and preliminary evaluation of methods for observing celestial radio sources.

Section 3 discusses the results of the field experiments and observational data. This section describes the data reduction methods for performing star calibrations and using level readings for monitoring the

orientation of the antenna, and the methods used in reducing observations of celestial radio sources.

Section 4 presents conclusions and recommendations derived from the study.

SECTION 2
INVESTIGATIONS AND FIELD EXPERIMENTS

2.1 GENERAL CONSIDERATIONS

The rationale for the experiments and procedures developed under this study is provided in the following discussion which summarizes the operational requirements, constraints, and possible approaches for angular alignment of the USB (unified S-band) 30-foot antenna system

2.1.1 Angular Alignment Requirements

Angular tolerances were not specified at the start of this study since the problems involved in aligning and calibrating the antenna axes were not known at the time. A review of the system performance specifications [1] indicated that the pointing accuracy of the antenna should be ±0.6 minutes of arc ($^{\circ}_{.}010$) and the tracking accuracy should be within 1.5 minutes of arc ($^{\circ}_{.}025$). Pointing accuracy is defined as the closeness to which the antenna can be directed (programmed) to a given coordinate position It may also be considered a measure of the accuracy to which the mechanical axis of the antenna can be aligned to the geodetic reference system Tracking accuracy indicates the overall angular error of the antenna system during autotrack and is a measure in part of how accurately the mechanical and electronic axes can be aligned.

Initial alignment of the 30-foot antennas was performed by the Collins Radio Company when the antennas were erected The procedures used to align the optical, mechanical, and electronic axes are outlined in references [2] and [3] A review of these methods was made at the beginning of this study and they were found to be adequate for their intended purpose After the antenna is erected and fully equipped it is impracticable to perform some of these basic procedures, particularly alignment of the mechanical axes. The tasks that were required to accomplish this initial alignment are summarized as follows·

a) Alignment of mechanical axes This involved the alignment of the X-Y axes and the reflector. Pre-construction survey monuments were utilized to orient the X and Y axes into the meridian and prime-vertical planes within a tolerance of ± 5 seconds of arc This was accomplished by optical sighting on the survey monuments from each end of the axes shafts During this operation spirit levels representing the X and Y axes were oriented norma to the local gravity vector and the X and Y angle encoders were indexed The reflector surface was aligned after X and Y axes alignment by optical sighting on targets from the center of the Y axis

b) Alignment of optical and mechanical axes The optical axis of the boresight telescope was placed parallel to the local gravity vector while the antenna was aligned to the zenith Adjustments were the made to the telescope reticle to make it coincident to the optical path

c) Alignment of optical and electronic axes This was accomplished in the usual manner by optical sighting on the boresight tower whil rf signals were transmitted from either the boresight transmitter or the test transponder

It was not possible to perform a field evaluation of all these methods, however, tests were made of the collimating device used to adjust the optica axes and of the electronic boresighting procedures since these methods are periodically used to re-align the antenna axes For practical reasons it is necessary to accept the initial alignment of the mechanical axes and to devis appropriate methods for measuring any misalignment errors that may exist

For the investigations under this contract (and the previous contract, NAS-5-10638) it has been convenient to consider the field alignment problem as involving four principal operations 1) alignment of the optical and mechan cal axes, 2) calibration of the optical-mechanical axes, 3) monitoring the ori tation of the mechanical axes to the local gravity vector, and 4) alignment of

the electronic axis Operations 1), 2), and 3) establish the static pointing accuracy of the antenna while all four operations determine the total angular tracking capability Accepting the performance specifications quoted earlier as guidelines for this study, it follows that it is desirable to develop methods wherein the errors of each of the first three operations do not exceed $\pm^{o}010$ and wherein the total error contribution of all four operations is held within a maximum tolerance of $^{o}025$

2 1 2 Operational Requirements

The objective of this study was to develop operation procedures which would provide field personnel with a complete on-site capability for aligning and calibrating the antenna system These procedures were to be capable of establishing the geodetic alignment and orientation of the antenna prior to a tracking mission, and periodically during a mission, if necessary They were to be compatible with the existing pre-mission calibration techniques and were not to require any significant hardware changes or use of additional equipment The on-site Univac 1218 computer was to be used for the data processing and any computational analysis that may be required

Operational requirements and field routines for calibrating the antenna were to be described in an instruction manual It was intended that this manual would completely define the observation and data reduction procedures so that site personnel could accomplish the angular calibration directly in the field

2 1 3 Review of Applicable Calibration Techniques

At the beginning of this study there were two techniques which appeared most applicable for angular calibration external optical targets for monitoring the antenna orientation with respect to the gravity vector, and star observations for calibrating the mechanical axes

Optical targets seemed promising since they had been used successfully in the past for measuring the tilt plane of precision az-el antennas [4] It was realized that there would be some limitations in their use with the unified

S-band X-Y mount because of the 20° keyhole cones in the north and south directions, and the need to have the targets high enough above ground so the could be observed from the boresight telescope For the planned field experiments, optical targets would be particularly valuable for assessing the stability of the antenna structure and the static pointing capability of the system Another advantage in having optical targets was that they could provide an independent check on the suitability of the Y-wheelhouse level vials for referencing the antenna axes to the local gravity vector

Star observations offer a practical method for determining misalignment errors that may be present in the mechanical axis They also provide a means for relating the mechanical axis to the optical axis Errors due to azimuth referencing, lack of orthogonality of the X-Y axes, angle encoder biases, antenna tilt, and other factors can be determined from analysis of star observations if the antenna system is capable of making precise angular measurements The main prerequisite in using star observations, apart from the need to have good visibility, is that the optical system must be capable of detecting stars dimmer than second magnitude so that a sufficient number and distribution of star observations can be obtained

Alignment of the optical axis to rf axis is normally done by boresighting on a nearby collimation tower Sightings are made on the boresight optical target while signals are received from the boresight transmitter or transponder The coordinates of the optical target are well determined by geodetic surveys and checked by the antenna itself By repeated pointings and autotracking on the boresight tower, the angular relation between the optical and rf axis is obtained in terms of the angle encoder differences The principal limitation of this method is that multipath effects often introduce large errors, particularly in the elevation plane of the antenna beam

The optical and rf axes can also be collimated by tracking an aircraft equipped with an optical target and transponder, but this is expensive and inconvenient The use of a calibration type satellite, such as the GEOS satellites, would be desirable except there are none available with an S-band transponder which could be used for this purpose

Because of the disadvantages in using the boresight tower for rf axis alignment, GSFC engineers suggested the possibility of using celestial radio sources. Two radio sources had been detected with the Bermuda 30-foot S-band antenna If these sources can be accurately observed they should be superior to any other method of rf axis collimation Thus, one of the main efforts under this contract was to determine the feasibility of using radio stars for aligning the electronic axis of the antenna

Another method for rf axis alignment is the use of the Apollo ALSEP transponders which are being left on the moon Since they can be autotracked by the 30-foot antennas, they should provide an excellent means for rf alignment There are certain disadvantages with their use because of the restricted path of the moon and because ALSEP does not continuously transmit signals and must be interrogated from a master station Even with these limitations, they should be useful as an independent check on other alignment techniques Since the Apollo 11 mission was to take place during this contract period, it was decided that an attempt should be made to investigate this method

The various tests and experimental data obtained to evaluate the capabilities of these different methods are discussed in the following sections

2 2 OPTICAL TARGET EXPERIMENTS

2 2 1 Installation of Targets

Five optical ground targets were installed around the S-band antenna in June 1968 under the previous contract These were used during the first phase of the study to evaluate the repeatability (precision) in pointing the antenna and to monitor the tilt of the antenna with respect to the local gravity vector

At the beginning of this contract period it was found that several targets had been removed and others were badly weathered and needed replacing Therefore, new target boards were made and emplaced A

geodetic survey was then made to position the targets and to obtain their angular coordinates with respect to the mechanical axis of the antenna Six targets were located around the antenna as shown in figure 1 As before, targets could not be spaced evenly because of the topography and dense tree coverage The layout of the targets was very similar to the previous arrangement, except for the target on the Operations Building

Several tests were made prior to installing the targets to select a target pattern which would be best for viewing through the TV monitor located at the antenna console The previous target boards used a standard K & E survey target (red-and-white checkerboard pattern) but these were difficult to see when they were not in direct sunlight A black and white "bull's eye" pattern was selected for the new targets The circle of the pattern was white and its size was varied for each target board so it would fit within the innermost fiducial marks of the reticle when viewed through the TV A small electric lamp of about 0 5 inch diameter was set in the center of the circle so that the targets could be used at night

2 2 2 Observing Procedures

Tests conducted during the previous contract indicated that the standard deviation (σ_s) of a single pointing of the S-band antenna was $0^{\circ}0045$ for the X angle and $0^{\circ}0024$ for the Y angle These pointing tests were made on the optical targets and thus the X angle was near 90° and the Y axis was nearly vertical It is felt that the large σ_s for X may be caused by the weight of the entire superstructure of the antenna straining against the X axis gears when $X = 90^{\circ}$ If this is so, then the better measure of pointing error is the σ_s for Y To be on the conservative side, $\sigma_s = 0^{\circ}0035$ is considered as representative for all angles of X and Y

In obtaining angular observations to the optical targets, 5 pointings to each target were previously recommended Experience has shown that 3 pointings are sufficient for any type of calibration tests This should provide an average standard deviation of approximately $0^{\circ}002$ for each set of observations It also reduces the time to make a round of observations on all targets by about 10 minutes

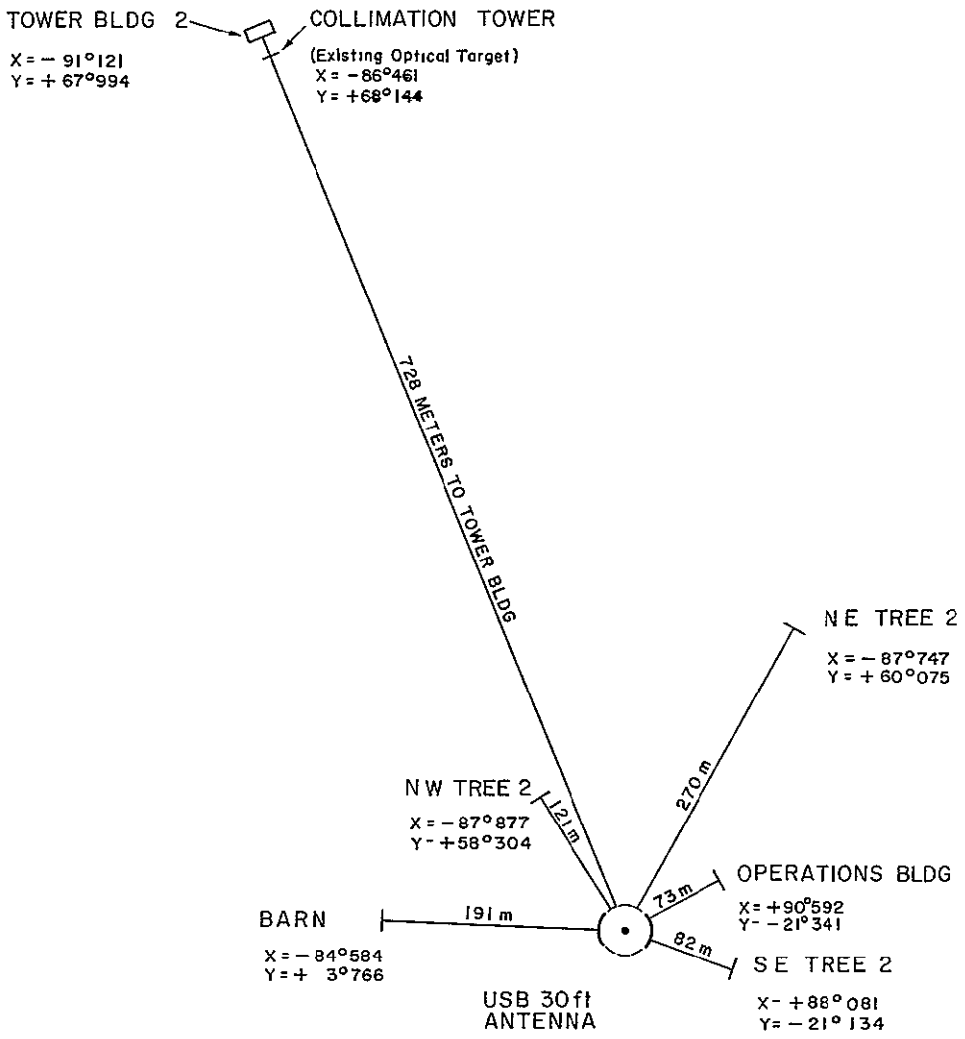

Figure 1

LOCATION OF OPTICAL TARGETS AT
NTTF USB - 30 FT ANTENNA

It took about 5 minutes on the average to obtain 3 pointings on each target This included the time to slew the antenna from one target to the next Care had to be taken in moving the antenna since all target directions were either close to, or within, the pre-limits of the X axis Three of the targets were in the pre-limit range where it is tedious for the antenna operator to precisely control the movement of the antenna Observations on these targets often took twice as long to obtain as those on the other targets

2 2 3 Target Observations

Table 1 of appendix I provides a summary of all the field test data obtained under this contract As indicated, optical target observations were obtained over the period 30 April through 23 July 1969 It was intended that the targets would be observed when star observations were made and over a period of several days to monitor any changes in the orientation of the antenn with respect to the gravity vector. This was followed until the end of July when the dead-limits of the X axis were changed from 89° back to about 87°. This placed three of the targets past the dead-limit, and as a result no further observations were made on the optical targets Approximately 40 sets of observations were made prior to the change in the dead-limit settings As discussed later in section 3 2, these observations were useful in evaluating the drift in the X angle encoder

2 3 STAR OBSERVATIONS

2 3 1 Development of Observing Technique

During this contract period, the method for obtaining star observations was improved and fully tested The improvement was based on finding a convenient procedure for timing the star observations For this purpose, site personnel at NTTF were able to develop a computer program which would print the X and Y angle encoder readings together with the time of the star observation to the nearest 0 1 second

The observing procedure was selected during the previous study effort and is based on marking the time when a star "drifts" through the center of

the reticle of the optical system In practice the console operator locates the star at the pre-selected position and observes the direction of the "drift" of the star until he is satisfied that he can position the antenna ahead of the star so that the star will pass through the center of the reticle The time of the event is marked by the operator pushing the "good/bad" switch The X and Y angles and time of the event are then printed on a teletype at the antenna console This procedure is repeated for four or five pointings on the same star

The event marker program greatly improves the reliability and efficiency of the observing technique by eliminating the need to manually record the observational data Usually a set of pointings can be obtained in less than 2 minutes Field tests have shown that when the visibility is good it is possible to obtain 20-30 observations per hour with an experienced console operator While the operator is observing a set of pointings, an assistant sets the X and Y angles of the next star into the Antenna Position Programmer When the operator is ready to move to the next star, he pushes the program mode button and the antenna immediately slews to the new star position If pre-arrangements have been made to select the stars to be observed, the whole operation proceeds very efficiently

The only drawback to this operation is the video system Tests have repeatedly shown that only stars of about 2 5 magnitude or brighter will be visible through the video system This imposes severe limitations as it restricts the distribution and number of stars that can be observed at any given time With a star magnitude of 2 5 as the lower limit of visibility, there will be only 20-30 different stars that can be observed from any given site throughout the year During the field tests it was found that second magnitude stars were seldom visible through the system below 30° from the zenith even when visibility was good This further limits the number of stars that can be observed

2 3 2 Observations Obtained

Stars were observed periodically throughout the field tests to calibrate the mechanical axis Observations were obtained more often than originally

planned because the X angle encoder was constantly drifting Since this affected the calibration results and would have an effect on other field experiments, it was necessary to have updated observational data to accurately determine the X angle bias

Table 2 of appendix I summarizes the useful star observations that were obtained on 8 nights The table lists the different stars observed and the number of sets of observations made on each night As indicated, only stars of 2 4 magnitude or brighter were observed All observations of the 2 3 and 2 4 magnitude stars (Alphecca and Eltanin) were made within 25° of the zenith The fact that stars of greater magnitude were seen on one night and not another is believed to be attributable to the video camera and the adjustment of the TV monitor Site personnel had difficulty in keeping the TV in adjustment and they were required to refocus the picture tube periodically when star observations were being obtained Atmospheric seeing conditions were not considered a limiting factor since on several nights visibility in the area was unrestricted

2 4 LEVEL VIAL OBSERVATIONS

Tests were conducted during the previous study effort to determine the stability and precision of the level vials (spirit bubbles) in the Y-wheelhouse These vials are oriented so that one is parallel to the Y axis and the other is parallel to the X axis During the initial alignment procedures, after the antenna has been oriented to the zenith, the bubbles in these vials are centered by rotating the capstan screws in the vial mounts, the bubbles then theoretically provide a permanent reference for orienting the antenna to the astronomic zenith

The early tests demonstrated that the bubbles enable positioning the antenna in the zenith to a repeatability of $\pm 0^{\circ}001$ If it is assumed that the bubbles were aligned during the initial alignment procedure and that there has been no movement of the capstan screws or the mounting plate, the antenna can be positioned to zenith to within $\pm 0^{\circ}001$ using the level vials

Periodic "levelings" were conducted during the star and target observations as indicated in table 1 of appendix I For these "levelings," the antenna was positioned so that both level bubbles were centered and the angle encoder readings were recorded The ambient temperature and pressure were recorded at this time Table 3 of appendix I lists the level data obtained during this contract Analysis and interpretation of these data are presented in Section 3 2

2 5 BORESIGHTING

Tests were made to determine the repeatability of aligning the optical - rf axes by boresighting on the collimation tower The boresight procedures outlined by Collins Radio Company were used initially for this purpose These procedures were found to be satisfactory but they are somewhat cumbersome and redundant for normal field operations It was found that they could be improved with slight modifications and without any degradation in the end result

Boresight errors can be relatively large when using the collimation tower because of multipath effects These are dependent on the height and location of the tower, terrain conditions along the transmission path, and the environment conditions Reflectivity characteristics of the ground are affected significantly by environmental conditions and this causes the apparent rf alignment to vary accordingly Since boresight errors are normally larger in the elevation plane than the azimuth plane, the alignment errors in the X axis would be expected to be larger than in the Y axis Analysis of the multipath effects for the NTTF site indicates that under worse conditions the X angle error may vary as much as $\pm 0^{o}025$

Boresight observations were obtained periodically between 29 April and 25 May as shown in table I of appendix I Results and comparison of the optical and electronic boresight data are presented in section 3 4

2 6 OBSERVATIONS OF CELESTIAL RADIO SOURCES

Field experiments were undertaken in the third month of this contract to investigate the feasibility of using celestial radio sources for aligning the electronic axis of the antenna If these sources could be observed accurately enough they would provide an ideal method for rf alignment and would eliminate the multipath problems that exist when the collimation tower is used

At the start of these tests the capabilities of the receiver system were unknown, however, possibilities for detecting celestial sources were promising as GSFC engineers had previously observed two radio stars at Bermuda

It must be stated at the outset that the investigation and experiments performed under this contract provide only a preliminary assessment of the capabilities of radio star calibration techniques As will be noted in the discussion which follows, further experimentation and analysis will be required to evaluate the full potential of these sources for the 30-foot antenna system

2 6 1 System Configuration

Initial experiments were concerned with determining an appropriate system configuration for detecting and recording radio star signals Several equipment set-ups and tests were made before it was found that signals could be detected by tapping the receiver at the 50mHz IF junction between the S-band mixer and the switched attenuator (See figure 2) Initially, the rf input signals were recorded on a Beckman Dynograph with the serial time code added Difficulty was experienced in obtaining sufficient sensitivity from the analog recorder without driving the recording pen completely off scale Consequently, a bucking voltage circuit was added to cancel noise bias in the system thus allowing maximum sensitivity to be derived from the analog recorder After several trials at reducing data, it was determined that the Beckman recorder could not be accurately correlated with X and Y angle recordings Therefore, it was supplemented by a digital voltmeter which was sampled every 0 1 second by the Univac 1218 The TDP was recorded simultaneously to obtain X and Y angle readings A computer program was prepared by site personnel to provide a printout of digital voltages

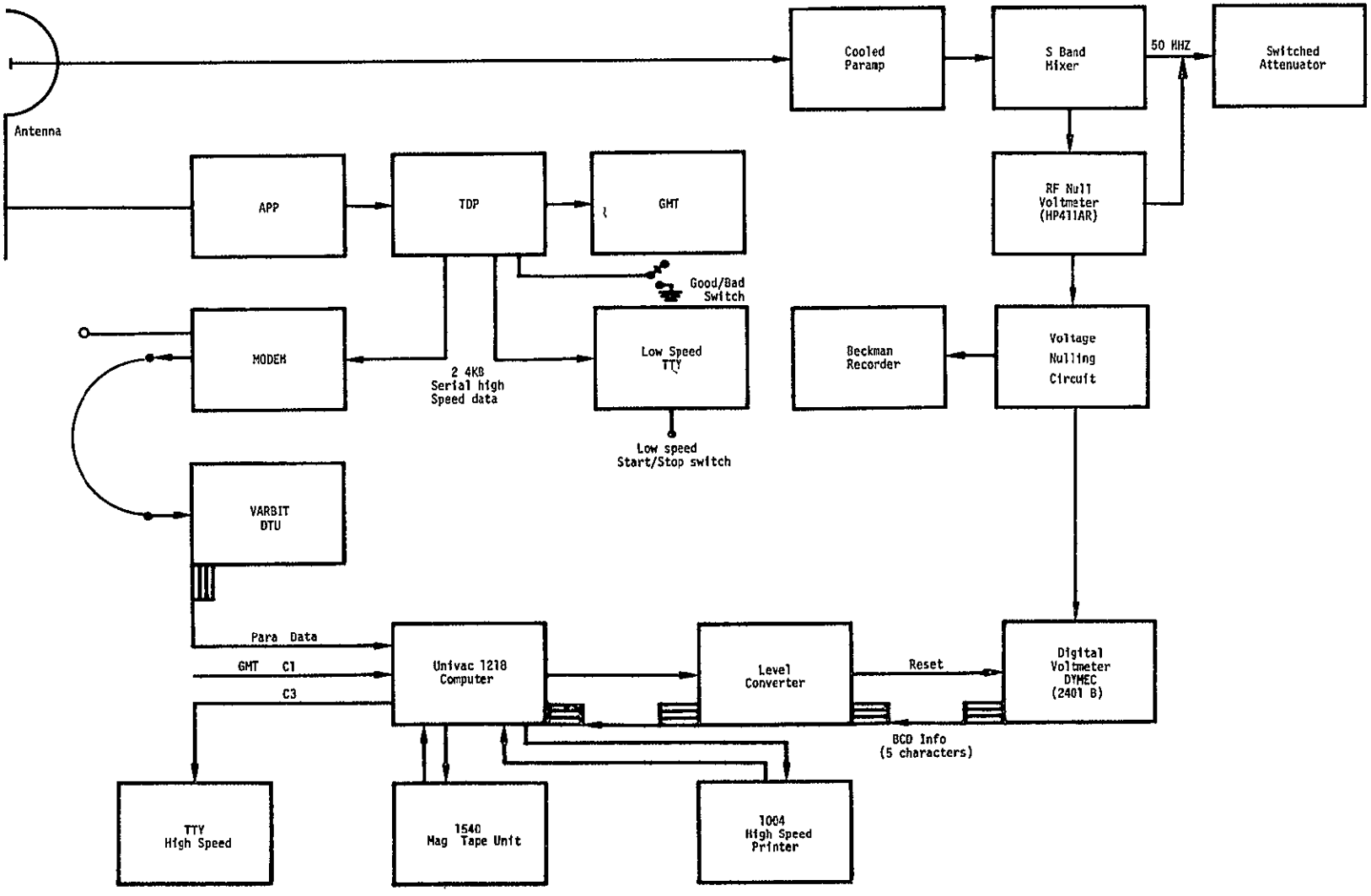

FIGURE 2

SYSTEM CONFIGURATION FOR OBSERVING CELESTIAL RADIO SOURCES

and X and Y angles for every 0 1 second of time A program was also prepared to average the voltages over a 1 second period and to print the mean voltage for every second of time, with the corresponding X and Y angles

It must be emphasized that the equipment configuration shown in figure 2 was a preliminary test set-up and represented only those arrangements which could be provided by site personnel at the time Further investigation of the system configuration is needed to design circuitry to reduce noise in the system and if possible to amplify the received signals Also, further experimentation is needed to determine the optimum point in the receiver system for detecting the radio star signals As will be seen, the digital recording system was not fully tested although it appeared quite promising during the few experiments performed

2 6 2 Selection of Radio Sources

A brief analysis was made at the beginning of this effort to estimate the amount of power flux that would have to be available from a radio source for detection with the 30-foot antenna system As indicated in appendix III, any radio source having a flux density greater than about 2×10^{-26} watts m^{-2} Hz^{-1} at S-band frequencies could theoretically be detected with the system For antennas equipped with the cryogenic preamplifier, as is the case at NTTF, the minimum flux density in theory is approximately 1×10^{-26} watts m^{-2} Hz^{-1} Atmospheric attentuation and system noise levels will undoubtedly require that the energy be somewhat greater than these values

Based on these considerations, a review was made of available literature and catalogs to determine which radio sources could be considered Since Cassiopeia A and Cygnus A had been detected at the Bermuda site, it was decided that these sources should be considered first After reviewing several catalogs it was evident that there are not many sources with the required power flux Also, the positional coordinates of most sources are questionable as there are many values, all obtained by different equipment at different frequencies A few sources with a wide range of flux densities

were selected for the initial experiments as shown in table 1 Accurate right ascensions and declinations were not available for all the sources, but they were adequate for the preliminary tests which were concerned with detection and recording of the radio signals The positional accuracy of source 3C400 was particularly low but it was included in the tests because it would be available for observation during the same time period as Cassiopeia A and Cygnus A

Because of the limited availability of the antenna, it was necessary to restrict the field experiments to the strongest sources and those which could be observed over a period of 3 - 4 hours Consequently, the only sources that were consistently detected were Cassiopeia A, Cygnus A and 3C400 Taurus A and Virgo A were not detected until late in the test program and were not used for evaluation of the various observing methods discussed below

Centaurus A was too close to the horizon to be observed No attempt was made to observe source 3C157 as it was always below or too close to the horizon when tests were being conducted

All recorded radio signals contained an appreciable amount of noise which made it difficult to assess the potential capabilities of the observing schemes Inspection of the graphical records indicated that the largest portion of the noise wave form consisted of a 10 Hz sine wave modulated by a 60 Hz signal This noise problem could not be investigated as the antenna schedules at NTTF did not permit time to experiment with the system configuration

Input signals from Cassiopeia A and Cygnus A were found to be reasonably strong with signal to noise ratios of about 7 db and 3 db, with their maximum voltages ranging from about 140 - 160 mv and 80 - 120 mv , respectively Signals from source 3C400 were very weak but always detectable The maximum signal voltages for 3C400 varied from about 50 - 70 mv Since system noise level ranged between 20 - 30 mv during the test period, it is doubtful that any radio source weaker than 3C400 could have been useful in these experiments with the existing system configuration Virgo A, with

TABLE 1

RADIO SOURCES SELECTED FOR FIELD TESTS

Source	Right Ascension	Std Error	(1) Ref	Declination	Std Error	Ref	Flux (2) Density
3 C 144, Taurus A	$5^h\ 31^m\ 30^s5$	$\pm 0^s3$	c	+21° 59' 02"	± 5"	a,b	830
3 C 157	6 14 08	±6	b	+22 43 37	±15	a,b	70
3CC 274, Virgo A	12 28 18 4	±0 5	c	+12 39 57	± 4	a,b	120
Centaurus A	13 22 34 8	±0 6	c	-42 48 24	±80	b	190
3 C 400	19 21 30	±24	b	+14 24	±2700	b	200
3 C 405, Cygnus A	19 57 44 5	±0 4	c	+40 37 26	±30	b	870
3 C 461, Cassiopeia A	23 21 06 8	±0 8	c	+58 32 48	± 3	b	1700

NOTES

(1) References

a "Accurate Measurement of Declinations of Radio Sources," R B Read, Astrophysical Journal, 1963

b "General Catalogue of Discrete Radio Sources," Howard & Maran, Astronomical Journal, 1964

c "Accurate Right Ascensions for 226 Radio Sources," Formalont et al, Astronomical Journal, 1964

(2) Unit of 10^{-26} watts m^{-2} Hz^{-1}, estimated for S-band frequency

an estimated 120 flux units, was barely detected and would not have been a usable source for the observing schemes described below

2 6 3 Possible Observing Techniques

After succeeding in receiving radio signals from several sources and developing some facility and technique for recording them, the problem of developing observational techniques that would allow calibration of the antenna electrical axis was considered

The adoption of an ephemeris for the observable radio stars is necessary for all observational schemes Computations based on the ephemeris are used to point the antenna in the direction to acquire the star at a given time, and then to compute the exact location of the source (in X and Y) for the instant of observation

Definitions and assumptions under which observations are taken are

1) The electrical axis of the antenna is the direction or position where the received signal strength of a radio source is maximum Therefore, ideally a maximum signal occurs when pointing the electrical axis at the radio source, practically, however, the maximum for an observation will occur at the point of closest approach to this ideal pointing

2) The celestial radio sources are considered to be point sources A point source is here defined as one whose angular dimensions are much smaller than that of the antenna's beamwidth ($0^{o}85$)

3) The received signal does not contain any significant time bias or distortion, i e , there is no time constant to consider in using the graphical or digital printouts

4) The angular coordinates of the antenna's electrical axis are stable, and will remain so under normal operating conditions (The circumstances under which these coordinates might change have not been assessed)

5) The spectra of the signal being measured and the receiver noise are considered to be uniform with a Gaussian distribution, and the output will have statistical oscillations about its true mean

Various methods for taking radio star observations were investigated The three methods described below were judged most promising and were the techniques that were experimentally tested during this study

2.6 3 1 Fixed Position Method

In this method of observing, the antenna is set and locked at a preselected direction (X and Y angles) obtained from an approximate star ephemeris This direction is so chosen that at a short time later, due to the Earth's rotation, the star drifts through the antenna's field of view During the star's passage, the received signal voltages are recorded with the corresponding time of the received signal The time at which the peak voltage occurred is taken as the instant at which the star most closely approached the electrical axis The observing procedure should be repeated three or four times over a short time period (15 - 20 minutes) During each star passage (after the initial pass) the direction of the antenna is offset normal to the star path by a few hundreds of a degree so the star will drift through the antenna's field of view along different tracks as shown in figure 3

The calibration of the electrical axis is determined in the following manner Using the time of occurrence of the maximum voltage, the direction in which the mechanical axis of the antenna should have been pointing is computed in terms of the X and Y angles A comparison of this computed value with the observed direction when the maximum voltage occurred determines the "mispointing" to the radio source in both the X and Y axes The mispointing is referred to as the O minus C value (O-C) in X and Y This O-C value is computed for each passage of the star and reduced for the mechanical to optical relationship so as to refer these values to the optical reticle Any single set of O-C values is taken as a point on a line passing through the electrical axis A line fitted to the series of O-C points is considered to pass through the electrical axis as shown in figure 3 The whole

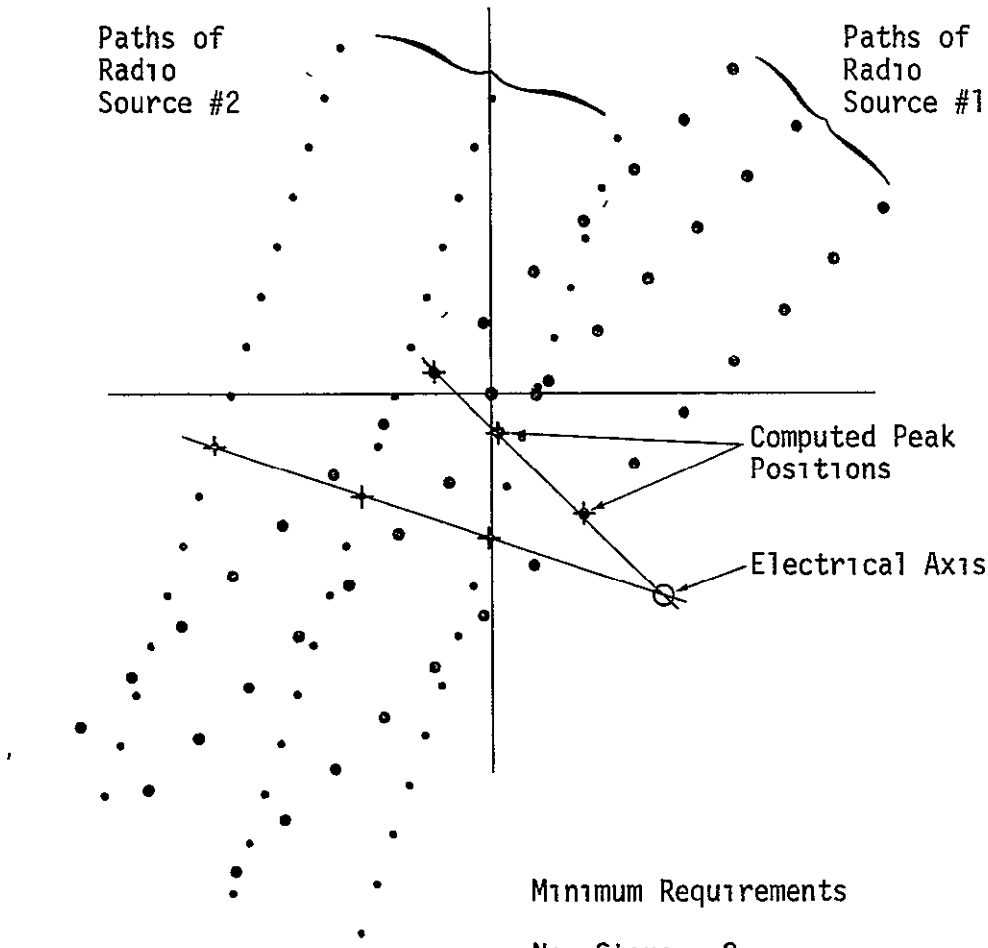

Minimum Requirements

No Stars	2
No Observations	3 or 4 passes per star
Observing Time	30-40 minutes (5 minutes per pass)

Figure 3

FIXED POSITION METHOD FOR

OBSERVING RADIO STARS

series of observations must be repeated using another radio star in a different portion of the sky to provide another line which passes through the electrical center These two lines should intersect at the electrical axis

Another approach to finding the electrical axis would be to use any single set of O-C's and to analytically compute a line normal to the path of the star If the direction of the antenna is not offset from the predicted star position for each set of observations, successive sets of O-C values would theoretically be equal In practice, a combination of the two approach could be used; for example, on two star passages the antenna setting could be set at the predicted directions so that the star passes through the field of view along the same track, and on two other passes the antenna settings could be offset so the star passes along different tracks

2 6 3 2 Single Axis Scan

In this method the antenna is pointed first at a position in the sky that is a little ahead of the computed star position One axis is held fixed and the star is then scanned manually back and forth with the other axis as shown in figure 4. As the antenna scans past the star, a variation in the voltage return is obtained The time of "peak" return is accepted as the instant at which the electrical axis either passed through or most nearly approached the position of the source The position of the non-fixed axis (the scanning axis) should differ in a systematic way from peak-to-peak, reflecting the apparent motion of the star

The direction that the antenna should have been pointing for the mechanical axis to point directly at the source can be determined by computing the position of the source at the time associated with each peak voltage return For each of these times, the O-C values are determined Theoretically all these O-C values should be the same for the axis in which the scanning is done since the electrical axis is considered as a point in some fixed relationship to the mechanical axis Therefore, when we fix the Y axis and scan in the X axis, we should get a series of points that lie on a line

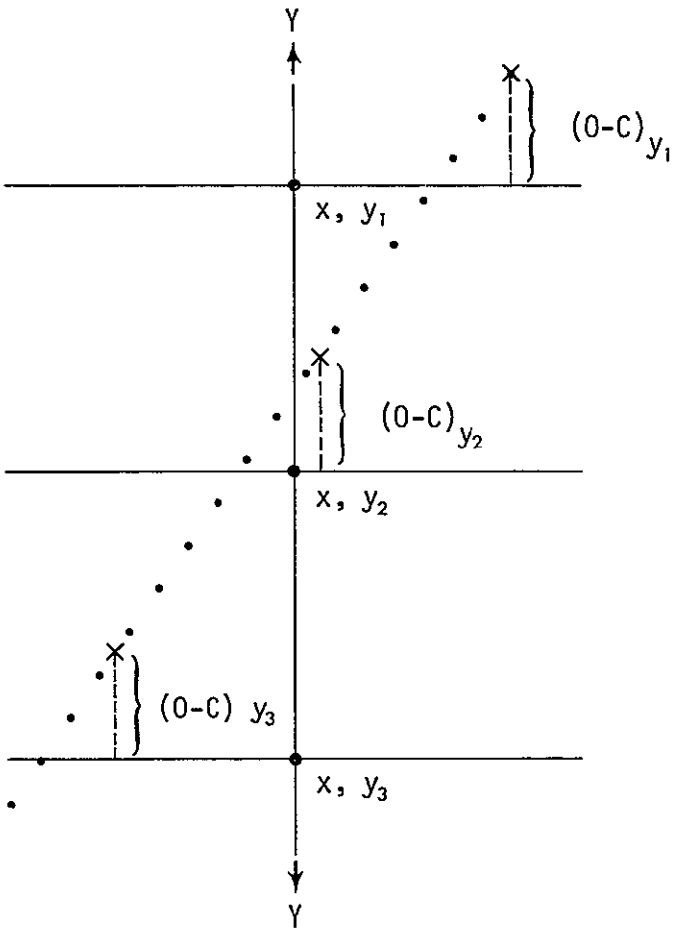

Minimum Requirements

No Stars 1
No Observations 8-10 scans per axis
Observing Time 10 minutes

Figure 4
SINGLE AXIS SCAN METHOD FOR
OBSERVING RADIO STARS

parallel to the X axis Also, when we scan in the X axis we should get a series of points that lie on a line parallel to the Y axis as shown in figure 4

2 6 3 3 Incremental Offsets

Basic to this method of observing is the capability of tracking the star sidereally This can be done with the antenna programmed directly or with a simulated tape drive Once the star is acquired using the predicted coordinates, offset angles are set in the Antenna Position Programmer at the console to move the antenna back and forth along each axis in order to locate the peak voltage The peak can be found by observing the graphic record (Beckman recorder) or the digital voltage readings Once this provisional peak is found, the sidereal drive holds the provisonal relationship of the mechanical to electrical axis so that the antenna is "riding" the peak From this position, systematic angle offsets at increments of $0^{o}05$ to $0^{o}1$ are applied to change the pointing of the antenna to either side of one axis while holding the other axis fixed At each offset position the signal voltages are recorded for several seconds together with the X and Y angle readings After taking a series of points through the peak, a similar series (line) of observations are then taken by offsetting the other axis about the provisional peak Observations are taken until two or three lines of points to either side of the provisional peak have been obtained for both axes as shown in figure 5

For each series of observations a mean time and angle is taken at each offset position and the O-C's computed This gives a series of O-C's for which corresponding voltage readings are available These voltage readings are then used to determine an adjusted peak for each series (line) of observations The peak voltage determined in this manner should, theoretically, lie on an O-C line perpendicular to the direction in which the angle offsetting was done The computed points will, of course, not form a straight line so a line is fitted to the points in both the X and Y directions The intersection of these lines will then be the adjusted electrical axis This adjusted value should be close to the provisional peak (within a half of the offset increment)

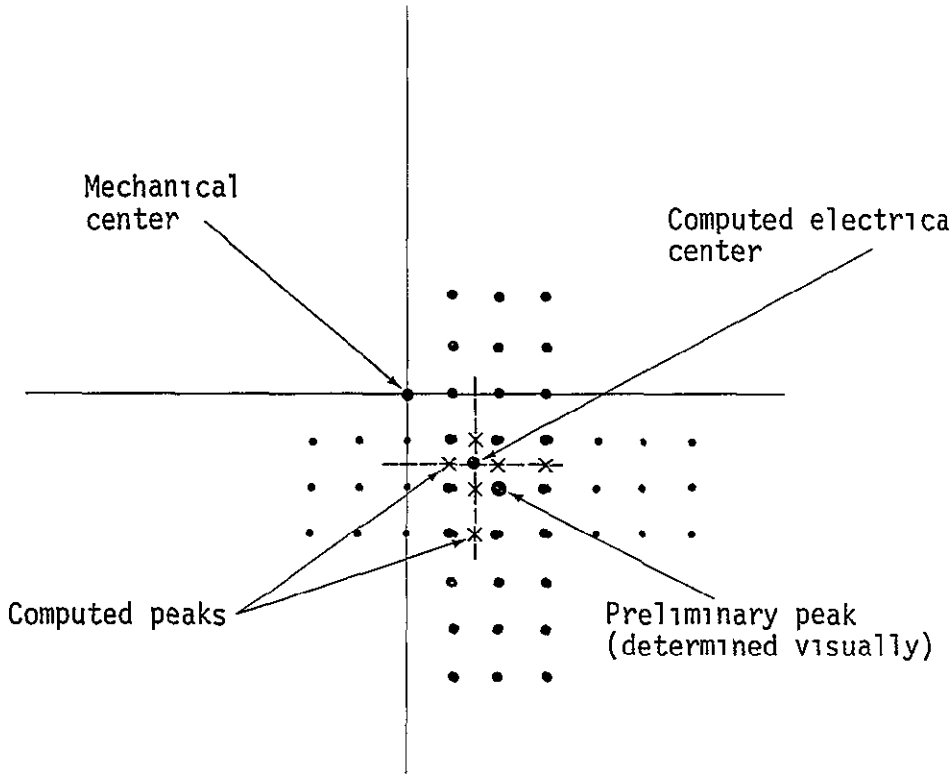

Minimum Requirements

No Stars	1
No. Observations	2-3 passes per axis (10-15 increments/ pass)
Observing Time	15 minutes
Programmed Track	Sidereal drive

Figure 5

INCREMENTAL OFFSET METHOD FOR OBSERVING RADIO STARS

2.6 4 Observational Data

As indicated in table 1 of appendix I, radio stars were observed on ten different days during the period 3 July through 4 October On several of these days it was found that the system noise level was very high and the time correlation for angle data was doubtful Consequently, no attempt was made to reduce observational data when this occurred

Table 4 of appendix I summarizes the useful observational data that were obtained on six different occasions This table lists the observing methods and experiments, and the radio sources observed As noted, procedures for recording the radio signals and angle data varied during the tests The early experiments on days no 185 and 198 used only the Beckman graph for recording the input signals The serial time code was displayed on the graphs so that these records could be correlated with the TDP printouts for the corresponding angle data Later in the test program site personnel were able to record the input signals from a digital voltmeter (dvm) with the data stored in the Univac 1218 computer A computer printout was then available listing the time, digital voltage readings, and corresponding X and Y angles As indicated in table 4, the digital voltage readings were available for days no. 206, 256, 277 and 278 For day 206, dvm readings were recorded at intervals of 2 or 4 second during the observation period Readings were intended for every 1 second interval but the computer program was not completely developed at this time On days 256 and 277, dvm readings were recorded and printed out at 1 second interval together with time and angle readings A computer program was also provided by site personnel to average the dvm readings over a 1 second time interval A printout of this was available for day 256 and 278 The 0.1 second dvm readings were not printed out for day 278 as the tapes were inadvertently erased before this was requested

Sample records of the radio star observations as received on the Beckman Dynograph and from the dvm computer printout are shown in appendix I These samples were annotated at the time of observation, supplemental notes have been added to clarify the data The sample records included in appendix I are the following

DVM Readings for Cassiopeia A Fixed Position Method
DVM Readings for Cassiopeia A Single Axis Scan
Single Axis Scan (Cassiopeia A)
Single Axis Scan (Cygnus A)
Single Axis Scan (3C400)
Incremental Offsets (Cassiopeia A)
Sector Scan (Cassiopeia A)
Raster Scan (Cassiopeia A)

2 7 ALSEP TRACKING

The ALSEP transponder which was left on the moon during the Apollo 11 mission was considered as a possible source for rf axis alignment The advantage of this source is that it can be autotracked by the 30-foot antennas, thereby providing a dynamic capability for calibrating the directional alignment of the electronic axis In addition, if suitable photographs of the moon could be taken through the antenna's optical system during autotrack, it would be possible to obtain a direct measure of the electronic-optical axis alignment

During the field tests several attempts were made to track the transponder on days when radio and optical stars were observed, but only on one occasion was ALSEP transmitting This occurred on the evening of August 28th During the autotrack period, photos of the moon were taken with the 35 mm camera, but they were of very poor quality An attempt was made, however, to reduce these photos and to measure the optical electronic alignment This is discussed in section 3 6

SECTION 3
RESULTS OF FIELD EXPERIMENTS

Prior to reducing the observational data, further studies were made to define mathematical formulas for the various calibration methods This effort was a continuation of the studies performed during the previous study phase and involved the following a) additional analysis of the star calibration model, b) development of analytical procedures for calibrating and using the spirit levels for tilt determination, and c) evaluation of astronomic versus geodetic coordinate references for angular calibrations These studies are summarized in appendix II and will be referred to in the discussions which follow

3 1 STAR SOLUTIONS

Various test solutions were made using optical star observations to evaluate the error model which was developed during the previous contract The purpose was to further check the validity of the observation and reduction procedures, as well as to derive an acceptable error model that could be used to calibrate any unified S-band antenna

Initially, we were looking for two main conditions (1) general agreement of results from different sets (samples) of observations, and (2) reasonable standard deviations of the derived coefficients. In addition, we wanted to be sure to account for all sources of significant systematic errors in the adopted error model

Test solutions were made for the star observations obtained for the following eight nights

1 May 1969 - 40 observations
15 May 1969 - 30 observations
26 June 1969 - 19 observations
18 July 1969 - 17 observations
1 August 1969 - 10 observations
7 August 1969 - 14 observations
29 August 1969 - 12 observations
4 October 1969 - 9 observations

In all cases an attempt was made to get the best distribution of the available stars Figures 6 through 13 show the actual distributions achieved for the given nights

The observations on May 1st and May 15th were divided into two groups (A and B) on each night On May 1st the groups contained 20 stars each, and on May 15th the groups contained 13 and 17 stars respectively Before observing the A group and between and A and B groups, the antenna was "leveled" to zenith by centering the level vials in the Y-wheelhouse and the encoder angles recorded

In all of the tabulations that follow, results are given for the A and B groups separately, as well as for the total (combined) distributions for the given night

3 1 1 Seven-coefficient Error Model

The seven coefficient model as developed in the first phase of this study was used as the starting model in the adjustment of the reduced star observations for the days given above (See appendix II C for the observation equations)

In the formulation of the seven-coefficient model the effect on the $d\alpha$ term due to antenna tilt was not included This was done under the assumption that the tilt would be small The purpose of making such an assumption was to allow the approximate determination of the values of both tilt components (η and ξ) at the time the observations were taken

Results of the solutions using the seven-coefficient model along with their error estimates (standard error) are given in table 2 As can be seen from this table, there is significant disagreement among the solutions Even for the A and B groups on nights of May 1st and 15th, the agreement is generally poor between the X encoder bias (Z_x) and the optical axis to Y axis lack of orthogonality (C) Ordinarily, the Z_x and C terms should be rather constant from night to night, much as the other terms are shown to be Some of the difference in the X encoder bias from one night of

(Cont'd on p 43

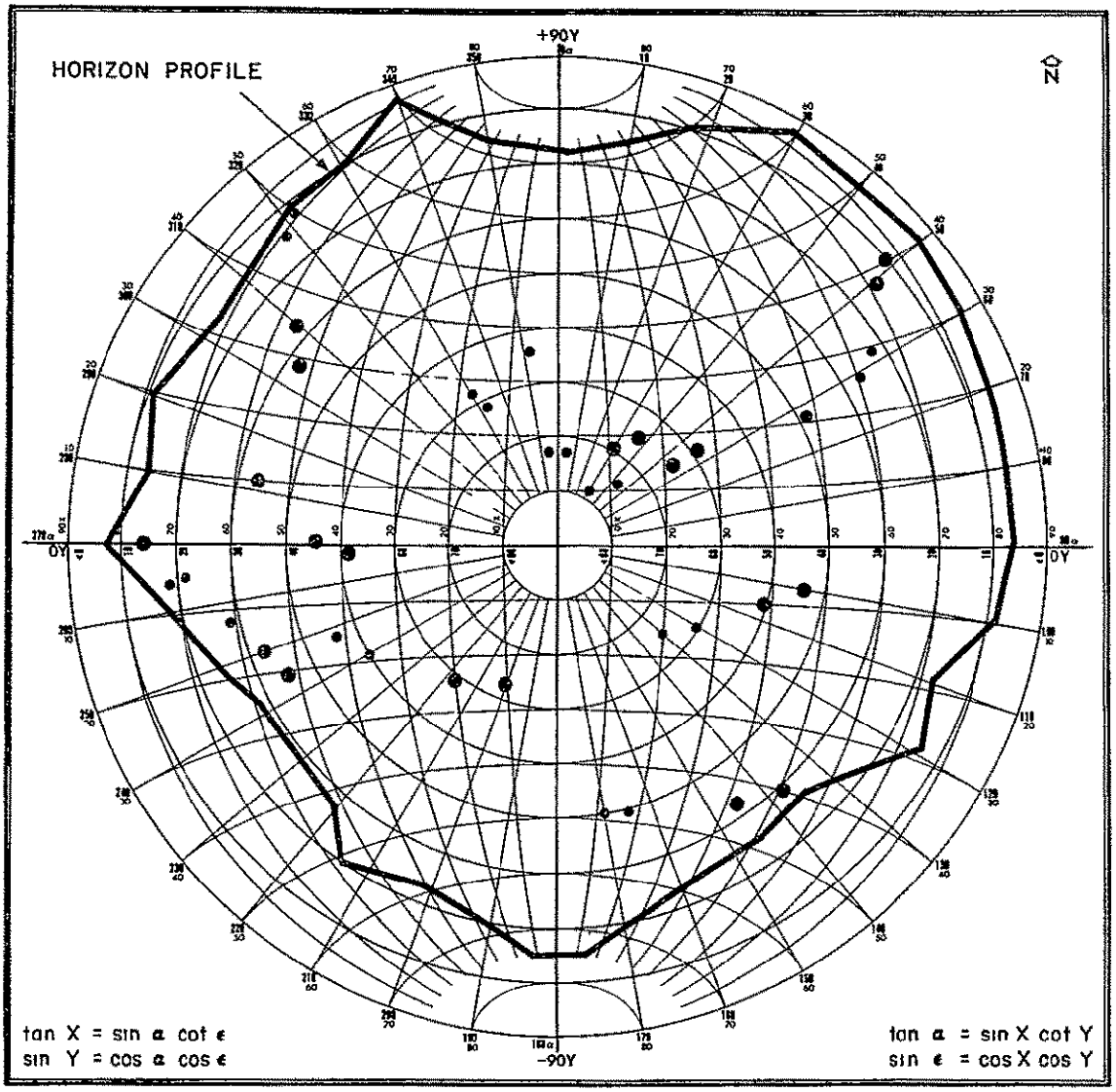

α-ε TO X Y CONVERSION GRAPH

- 1 st Set - 20 Obs. @ 2100 - 2200 hours
- 2nd Set - 20 Obs. @ 2300 - 2400 hours

Figure 6

STAR OBSERVATIONS - 1 MAY 1969

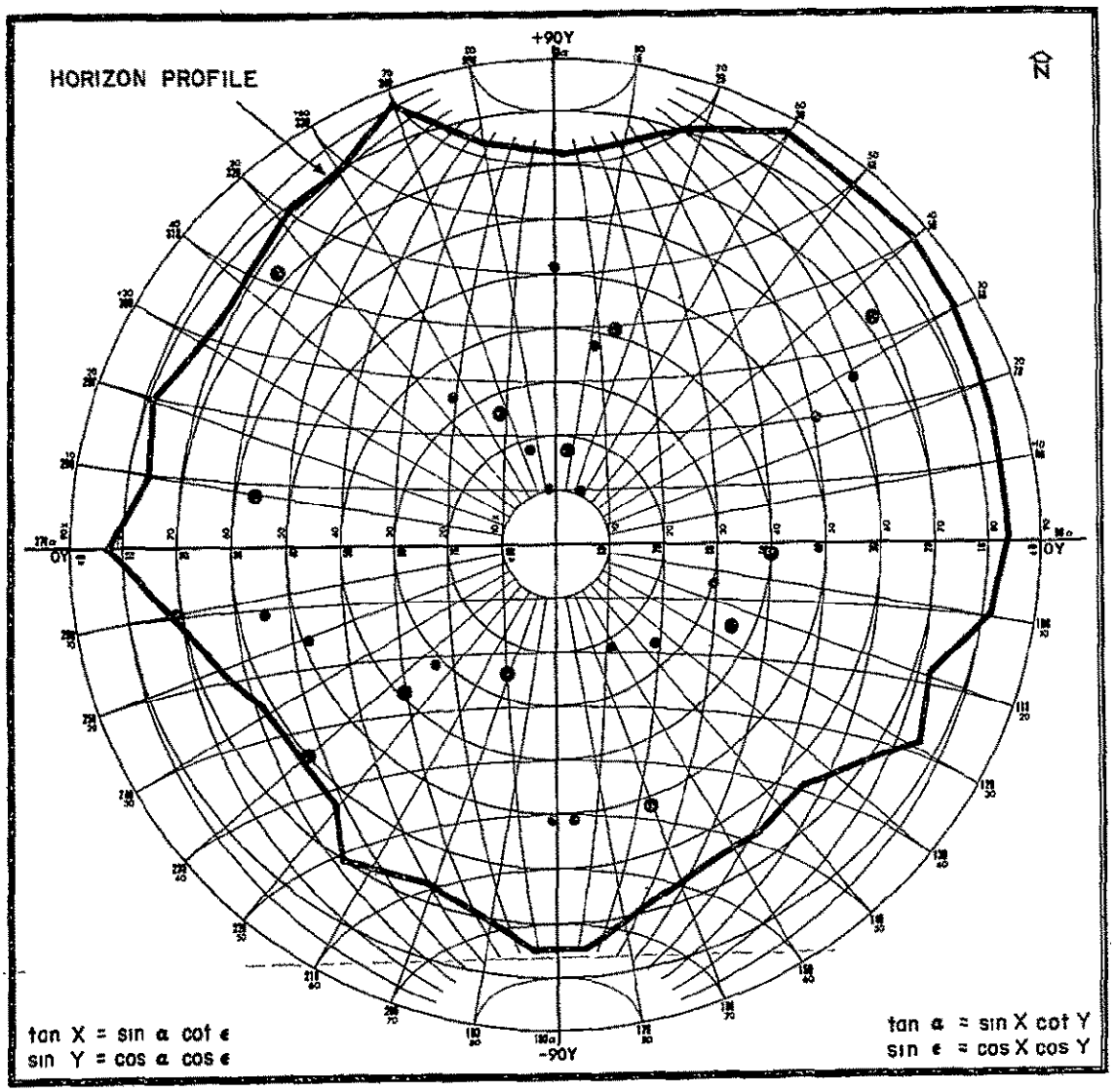

α-ε TO X-Y CONVERSION GRAPH

- 1 st Set - 13 Obs. @ 2130 - 2200 hours
- 2nd Set - 17 Obs. @ 2230 - 2330 hours

Figure 7

STAR OBSERVATIONS - 15 MAY 1969

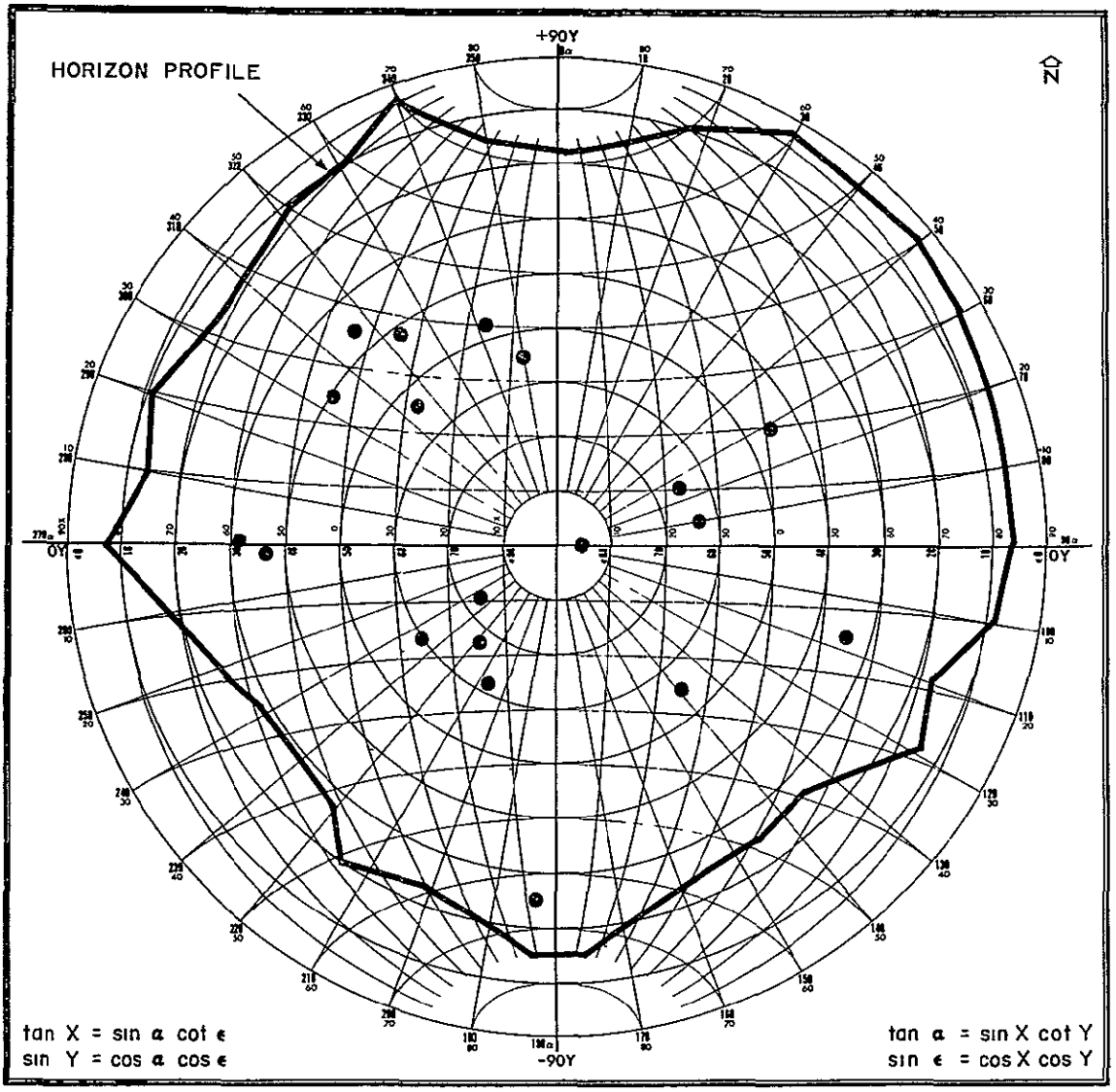

α-ε TO X Y CONVERSION GRAPH

19 Obs @ 2200 - 0130 hours

Figure 8

STAR OBSERVATIONS - 26/27 JUNE 1969

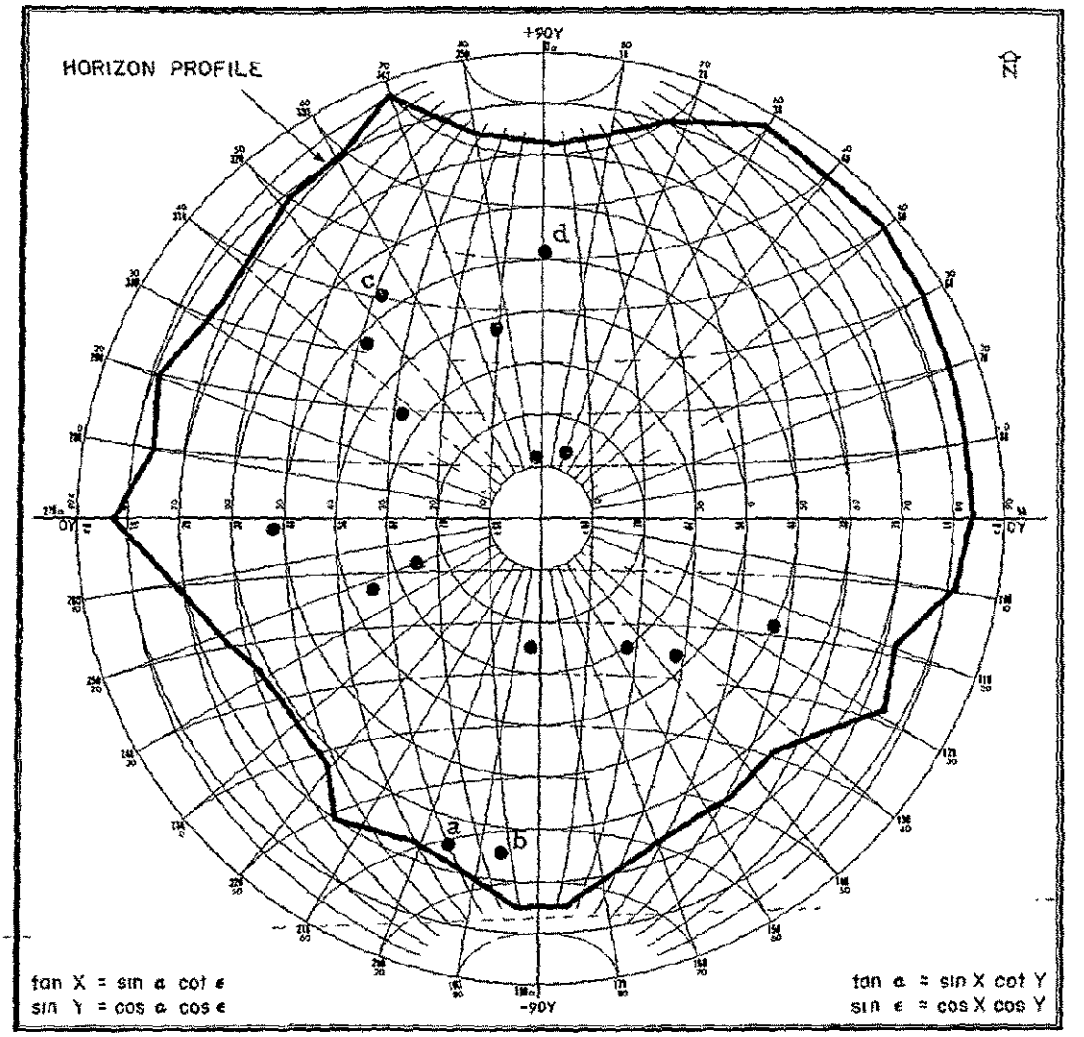

α-ε TO X-Y CONVERSION GRAPH

17 Obs @ 2200 - 2330 hours

a, b, c, d - obs deleted for correlation analysis (see table 3)

Figure 9

STAR OBSERVATIONS - 18 JULY 1969

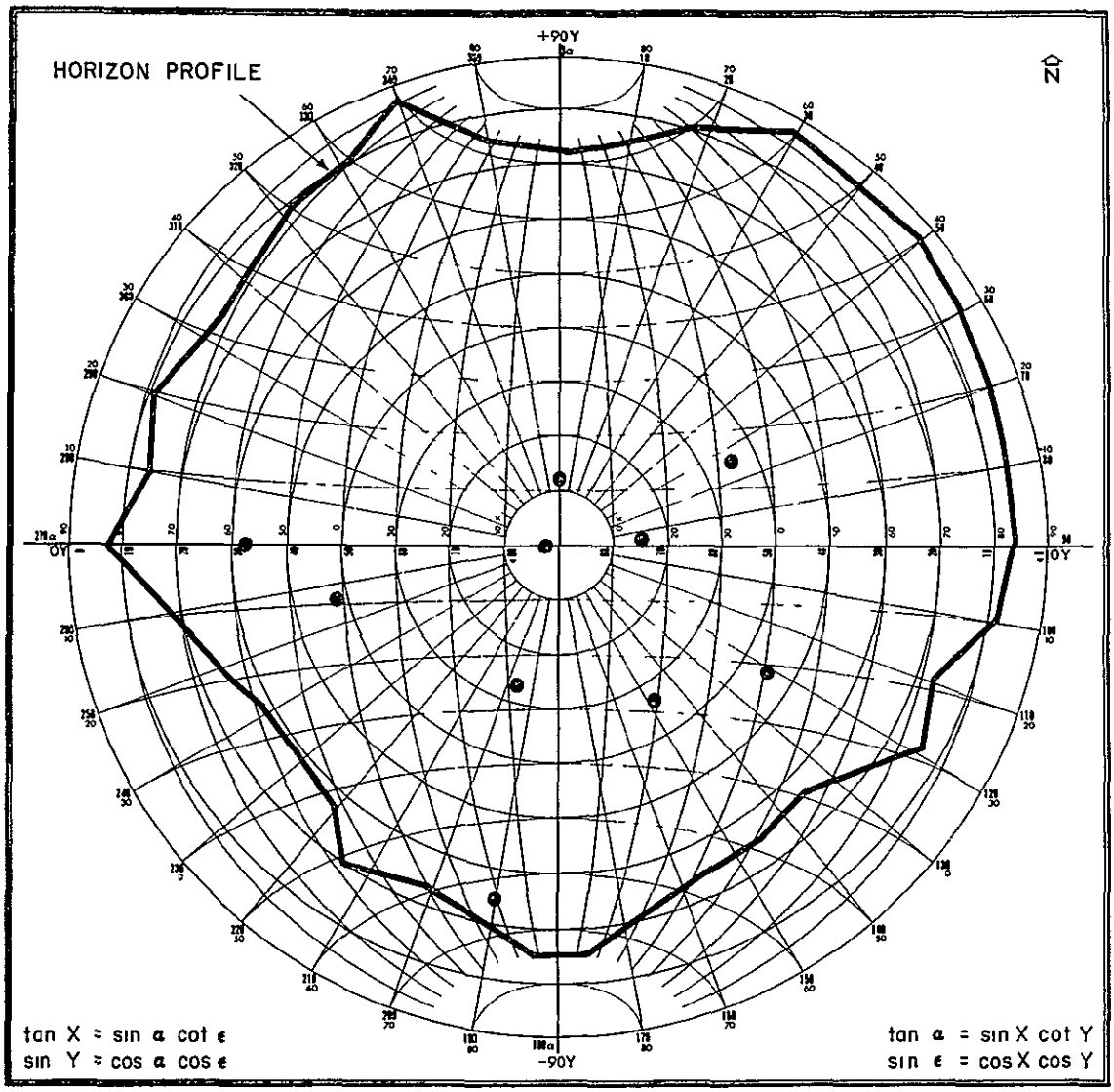

α-ε TO X Y CONVERSION GRAPH

10 Obs @ 2130 - 2300 hours

Figure 10

STAR OBSERVATIONS - 1 AUGUST 1969

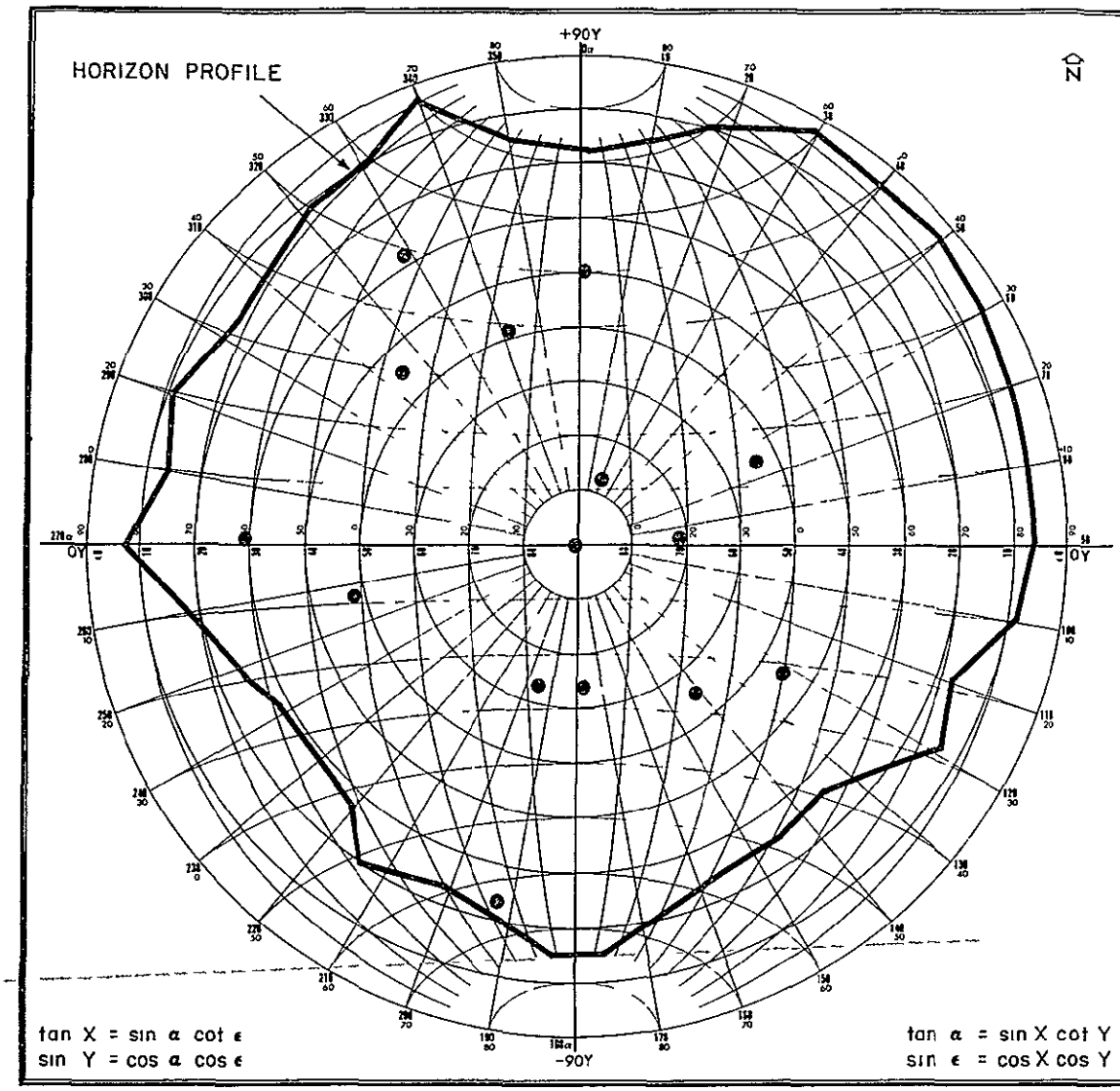

α-ε TO X Y CONVERSION GRAPH

14 Obs @ 2100 - 2300 hours

Figure 11

STAR OBSERVATIONS - 7 AUGUST 1969

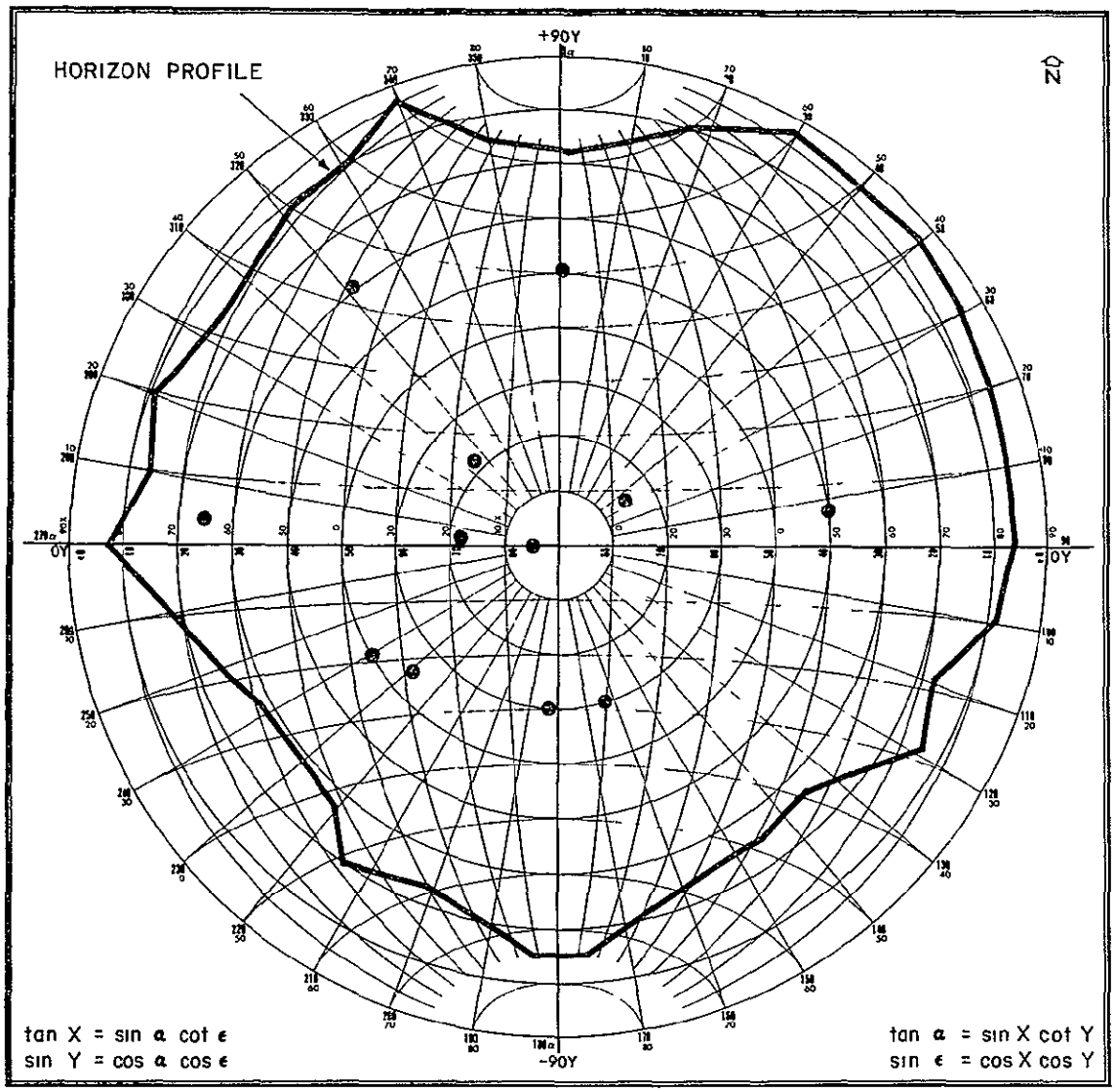

α-ε TO X Y CONVERSION GRAPH

12 Obs @ 2200 - 2300 hours

Figure 12

STAR OBSERVATIONS - 27 AUGUST 1969

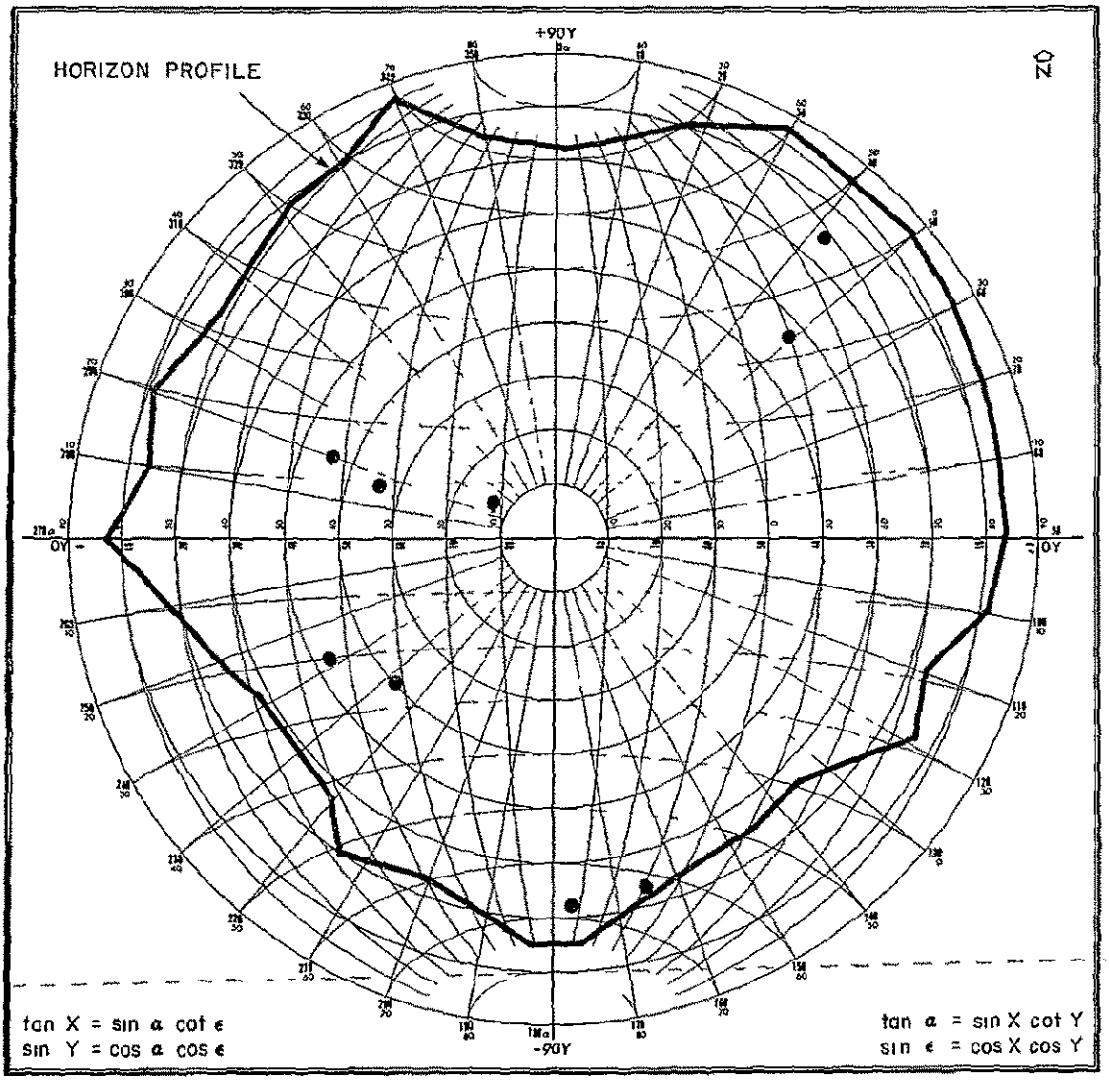

α-ϵ TO X Y CONVERSION GRAPH

9 Obs @ 2200 - 2300 hours

Figure 13

STAR OBSERVATIONS - 3 OCTOBER 1969

TABLE 2

STAR CALIBRATION RESULTS (7 coefficients)

DATE	1 MAY 1969			15 MAY 1969		
Sol / Coeff	122A 20 Obs	122B 20 Obs	122AB 40 Obs	136A 13 Obs	136B 17 Obs	136AB 30 Obs
Z_x	- 049°± 010	- 029°± 005	- 036°±.005	- 025°± 007	-.012°± 009	- 015°± 006
Z_y	004 ± 001	004 ± 001	004 ± 001	007 ± 001	007 ±.002	.007 ±.001
η	000 ± 002	- 001 ± 001	- 001 ± 001	- 003 ± 002	- 003 ±.003	- 003 ± 002
ξ	004 ± 002	003 ± 001	.003 ± 001	.003 ± 001	006 ± 003	005 ± 001
$d\alpha$	002 ± 001	003 ± 001	002 ± 001	002 ± 001	002 ± 003	002 ± 002
θ	- 003 ±.002	-.003 ± 001	- 003 ± 001	- 003 ± 002	-.004 ±.004	- 003 ± 002
C	022 ±.008	005 ± 004	010 ± 004	005 ± 006	006 ± 007	003 ± 005

Z_x = X-encoder bias
Z_y = Y-encoder bias
$d\alpha$ = azimuth misalignment
ξ = tilt component in the meridian (plus north)
η = tilt component in the prime vertical (plus east)
θ = X-axis to Y-axis lack of orthogonality
C = optical axis to Y-axis lack of orthogonality

TABLE 2 - (Cont'd)

STAR CALIBRATION RESULTS (7 coefficients)

DATE	26 JUNE 1969	18 JULY 1969	1 AUGUST 1969	7 AUGUST 1969	27 AUGUST 1969	4 OCTOBER 1969
Sol / Coeff	178 19 Obs	198 17 Obs	213 10 Obs	219 14 Obs	240 12 Obs	277 9 Obs
Z_x	020°± 004	042°± 005	088°±.010	.074°± 004	078°± 015	084°± 006
Z_y	003 ± 001	003 ± 002	004 ± 001	005 ± 001	001 ± 001	001 ± 001
η	- 004 ± 002	001 ± 002	005 ± 003	001 ± 002	- 004 ±.003	- 000 ± 004
ξ	004 ± 001	003 ± 002	001 ± 002	002 ± 002	000 ± 002	003 ± 002
$d\alpha$	005 ± 001	005 ± 003	002 ± 002	.002 ± 002	.001 ± 002	- 000 ± 002
Θ	- 002 ± 002	- 005 ± 003	.000 ± 006	-.005 ± 002	- 002 ± 004	-.006 ± 003
C	- 018 ± 003	- 017 ± 004	- 030 ±.010	- 016 ± 003	- 008 ±.012	011 ±.004

Z_x = X-encoder bias
Z_y = Y-encoder bias
$d\alpha$ = azimuth misalignment
ξ = tilt component in the meridian (plus north)
η = tilt component in the prime vertical (plus east)
Θ = X-axis to Y-axis lack of orthogonality
C = optical axis to Y-axis lack of orthogonality

observation to the next can be attributed to the drift in the X encoder (see section 3.2)

A thorough analysis of the observations and reductions did not produce any sources of error to account for large differences between the A and B solutions on the nights of May 1st and May 15th The distributions of the A and B groups were altered to be as similar as possible but still the results did not change significantly This analysis showed that the geometry of the observations alone was not the critical factor causing the difference This, of course, points up an apparent deficiency in the model itself

Table 2 shows, as has been noted before, that the correlation between the Z_x and C coefficients is very high The sum of the two terms (Z_x + C) is nearly constant when taken for the same night (the two A and B solutions along with their combined solutions) This sum is also reasonable on other nights when the X encoder drift is taken into account This condition of high interdependence is sensitive to the distribution of stars observed

An exercise to illustrate this high degree of correlation and the sensitivity of the solutions to the star distribution was done using the star distributions given in figure 9 Three different star distributions are considered in this figure 1) all 17 star observations, 2) a 15 star distribution (2 stars with large Y angles eliminated), and 3) a 13 star distribution (4 stars, all with large Y angles eliminated) The derived correlation matrices and a tabulation of results for each star distribution are given in table 3 As expected, the strongest determination of the model coefficients is obtained for the solution having the best distribution (all 17 stars) This is reflected in the standard deviations of the model coefficients, as well as the lowest of the three correlation coefficients (between Z_x and C), although the correlation is extremely high in all cases The deleted star observations were chosen to systematically weaken the 15 and 13 star solutions relative to the 17 star solution Again, this is reflected in the higher standard deviations on the model coefficients and the correlation coefficient between Z_x and C going to -1.0 in the 13 star distribution

TABLE 3

SOLUTIONS USING DIFFERENT STAR DISTRIBUTIONS

Coef	Z_x	Z_y	η	ξ	dα	o	C
Z_x	1 00	- 16	57	- 15	- 05	31	- 95
Z_y		1 00	- 10	69	31	- 12	14
η			1 00	02	- 09	18	- 39
ξ				1 00	05	16	14
dα					1 00	- 81	04
o						1 00	- 34
C							1 00

a) Correlation matrix - 17 stars

Coef	Z_x	Z_y	η	ξ	dα	o	C
Z_x	1 00	04	46	16	- 02	- 54	- 99
Z_y		1 00	- 06	67	30	- 17	- 06
η			1 00	14	- 04	- 07	- 37
ξ				1 00	11	- 07	- 17
dα					1 00	- 59	02
o						1 00	57
C							1 00

b) Correlation matrix - 15 stars

Coef	Z_x	Z_y	η	ξ	dα	o	C
Z_x	1 00	24	49	43	02	- 29	-1 00
Z_y		1 00	01	69	30	- 20	- 26
η			1 00	20	- 10	00	- 44
ξ				1 00	15	- 12	- 45
dα					1 00	- 61	- 03
o						1 00	30
C							1 00

c) Correlation matrix - 13 stars

Note See figure 9 for star distribution

Observations a and b removed for 15 star results

Observations a, b, c & d removed for 13 star results

Coef.	17 stars	15 stars	13 stars
Z_x	°042 ±°005	°040 ± 014	027 ± 025
Z_y	003 ± 002	003 ± 002	003 ± 002
η	001 ± 002	001 ± 003	002 ± 003
ξ	003 ± 002	002 ± 002	001 ± 003
dα	005 ± 003	005 ± 003	003 ± 003
o	- 005 ± 003	- 005 ± 004	- 003 ± 004
C	- 017 ± 004	- 015 ± 012	- 002 ± 022
correlation coef between Z_x & C	- 95	- 99	-1 00

d) Derived coefficients

This exercise demonstrates the necessity for making every effort to observe stars with large Y angles, and preferably near the meridian, when an optical calibration is to be attempted, in which it is desired to separate C from Z_x

Some indication of the strength of the approximate tilt terms can be gained by an inspection of the correlation The Z_y and ξ terms should be highly correlated and ideally, the Z_x and η terms should approach perfect correlation

3.1 2 Six-coefficient Error Model

In an attempt to gain insight into the effect on the solution caused by the high correlation between the Z_x and C, the same series of solutions with the C terms deleted from the model were run The results of these six-coefficient solutions are given in table 4

There is an obvious reason for not accepting the six-coefficient model a solution for either the Z_x or C coefficient alone gives a value that represents a combined effect of the two coefficients This, in effect, treats the influence of the non-orthogonality of the Y axis to optical axis as a constant, while it is formulated to have a systematic effect This explains the good agreement in Z_x between the A and B groups for May 1st and May 15th In fact, results would have been the same if we had chosen to delete the Z_x term and retained C

Table 5 was constructed to show the amount of error that could be introduced by using a value of $Z_x + C$, as determined in the six-coefficient solution, as opposed to a separate determination and application of these variables The table is based on known (assumed) values of C for targets having various Y angles It can be seen from the table that as long as the Y axis and optical axis are nearly orthogonal ($-^{\circ}010 < C < +^{\circ}010$), or the target is near the zenith, little error is introduced by applying the combined effect of Z_x and C as a constant

TABLE 4

STAR CALIBRATION RESULTS (6 coefficients)

DATE	1 MAY 1969			15 MAY 1969		
Sol / Coeff	122A 20 Obs	122B 20 Obs	122AB 40 Obs	136A 13 Obs	136B 17 Obs	136AB 30 Obs
Z_x	- 023°±.002	- 024°±.001	- 023°±.001	- 019°± 001	- 020°± 002	-.019°± 001
Z_y	.005 ±.001	.004 ±.001	004 ± 001	.007 ± 001	007 ± 002	007 ± 001
η	.000 ±.003	000 ± 001	.000 ± 001	- 003 ±.002	- 005 ± 003	-.004 ± 002
ξ	005 ±.002	004 ± 001	.004 ± 001	.004 ± 001	.006 ±.003	005 ± 001
$d\alpha$	.002 ±.001	.004 ±.001	.003 ± 001	.002 ±.001	.002 ± 003	002 ± 002
Θ	-.004 ±.002	-.003 ±.001	-.003 ±.001	- 003 ±.002	-.004 ±.004	-.003 ± 002

Z_x = X-encoder bias
Z_y = Y-encoder bias
$d\alpha$ = azimuth misalignment
ξ = tilt component in the meridian (plus north)
η = tilt component in the prime vertical (plus east)
Θ = X-axis to Y-axis lack of orthogonality

TABLE 4 - (Cont'd)

STAR CALIBRATION RESULTS (6 coefficients)

DATE	26 JUNE 1969	18 JULY 1969	1 AUGUST 1969	7 AUGUST 1969	27 AUGUST 1969	4 OCTOBER 1969
Sol. / Coeff	178 19 Obs	198 17 Obs	213 10 Obs	219 14 Obs	240 12 Obs	277 9 Obs
Z_x	-.004°± 002	019°± 002	058°± 003	.052°± 002	068°± 002	100°±.004
Z_y	002 ± 001	004 ± 002	005 ±.002	005 ±.002	001 ±.001	- 001 ±.002
η	- 008 ± 002	- 004 ±.003	004 ±.003	- 003 ±.003	- 006 ± 002	002 ± 005
ξ	.001 ± 002	004 ±.003	004 ±.003	003 ±.003	.000 ± 002	003 ± 003
$d\alpha$	004 ±.002	005 ±.003	002 ± 003	002 ± 003	001 ±.002	001 ± 002
θ	- 006 ± 002	- 009 ± 004	- 016 ± 004	- 006 ± 003	-.001 ± 003	- 003 ± 003

Z_x = X-encoder bias
Z_y = Y-encoder bias
$d\alpha$ = azimuth misalignment
ξ = tilt component in the meridian (plus north)
η = tilt component in the prime vertical (plus east)
θ = X-axis to Y-axis lack of orthogonality

TABLE 5

DIFFERENCES BETWEEN $Z_x + C$ AND $Z_x + C/\cos y$

Y-Angles

C Coefficient \ Y	10°	20°	30°	40°	50°	60°
01	°000	°001	°002	°003	°006	°010
02	000	001	003	006	011	020
03	000	002	005	009	017	030
04	001	003	006	012	022	040
05	001	003	008	015	028	050

The procedures for collimating the optical axis, as described in the previous study, should reduce or maintain the level of non-orthogonality of these two axes at a very low level, thus minimizing its effect on the observational data

3 1 3 Ten-coefficient Error Model

The six-variable model was rejected because of the magnitude of error that could be introduced (as shown in table 5) by the combined effect of Z_x + C This meant reintroducing the C variable, plus other variables to account for systematic errors which were affecting the results of the seven-coefficient model

A review of the seven coefficients relative to those suggested by Collins Radio Company and the one used by the Operations Evaluation Branch, Tracking and Data Systems Directorate, GSFC, revealed the most likely expressions to be added were those for structural deflection or sag Of the two approaches for formulating these expressions, the one used at GSFC is more straightforward and was the one selected Two variables (called A_5 and A_6) are used to allow for the total effect of sag in the X axis, while a single variable (called B_3) is used to express the effect of sag in the Y axis The designations of these terms are the same as those used by GSFC (See appendix II C)

The results of the solutions using this ten-variable model are given in table 6 This table shows that, for the most part, the results are quite reasonable when viewed relative to the previous tables The sum of the Z_x and C term is quite stable for a given night regardless of the solution (6, 7 or 10 variables) Results of the ten-variable model are the best of the three because of the overall consistency

The most significant variation noted for the ten-variable solution (table 6) is for the X bias term determined for the two sets of observations on May 15th This is attributed to the differences in the distribution of observations for the two groups This variation in the X bias is reflected in the C determination C is determined to be $0^{\circ}003$ for set A and $-0^{\circ}006$

TABLE 6

STAR CALIBRATION RESULTS (10 coefficients)

DATE	1 MAY 1969			15 MAY 1969		
Sol / Coeff	122A 20 Obs	122B 20 Obs	122AB 40 Obs	136A 13 Obs	136B 17 Obs	136AB 30 Obs
Z_X	-.026°± 010	- 027°± 004	- 031°± 004	- 023°± 004	- 012°± 004	- 015°± 005
Z_y	004 ± 001	004 ± 001	.004 ±.000	.007 ± 001	007 ± 001	007 ± 001
η	- 002 ± 002	- 001 ± 001	- 002 ± 001	- 004 ± 001	- 003 ±.001	- 004 ± 001
ξ	006 ± 001	003 ± 001	004 ± 001	004 ± 001	003 ± 001	005 ± 001
$d\alpha$	002 ± 001	003 ± 001	002 ± 001	.001 ± 001	003 ± 001	002 ±.001
Θ	- 003 ± 002	-.002 ± 001	- 003 ± 001	- 003 ± 001	- 004 ±.001	- 003 ± 001
C	*001 ± 009*	*003 ± 003*	*.006 ± 003*	*003 ± 003*	*- 006 ± 003*	*- 003 ± 004*
A_5	- 003 ± 011	009 ± 007	002 ± 005	- 004 ± 006	- 006 ± 026	- 008 ± 011
A_6	- 002 ±.012	- 012 ± 008	-.007 ± 006	000 ± 007	.003 ± 028	.004 ± 012
B_3	007 ± 003	006 ± 001	006 ± 001	003 ± 001	005 ± 001	008 ± 002

Z_X = X-encoder bias

Z_y = Y-encoder bias

$d\alpha$ = azimuth misalignment

ξ = tilt component in the meridian (plus north)

η = tilt component in the prime vertical (plus east)

Θ = X-axis to Y-axis lack of orthogonality

C = optical axis to Y-axis lack of orthogonality

A_5 = X directional sag (moment between X-axis and Y axis)

A_6 = X directional sag (moment between Y-axis and dish)

B_3 = Y directional sag

TABLE 6 - (Cont'd)

STAR CALIBRATION RESULTS (10 coefficients)

DATE	26 JUNE 1969	18 JULY 1969	1 AUGUST 1969	7 AUGUST 1969	27 AUGUST 1969	
Sol / Coeff.	178 19 Obs	198 17 Obs	213 10 Obs	219 14 Obs	240 12 Obs	
Z_x	.024°± 005	.040°± 006	097°± 020	.078°±.004	.082°±.007	
Z_y	.003 ±.001	003 ± 001	003 ± 001	004 ± 001	.001 ± 001	
η	- 003 ± 001	- 003 ± 002	004 ± 002	001 ± 001	-.004 ±.001	
ξ	.004 ± 001	002 ± 002	.001 ± 002	.002 ± 001	.001 ±.001	
$d\alpha$	004 ± 001	.005 ±.002	.002 ±.001	001 ± 001	001 ±.001	
Θ	-.002 ±.001	- 006 ± 003	.002 ±.004	-.005 ± 001	-.002 ±.002	
C	-.020 ±.004	- 015 ± 005	- 040 ± 019	- 019 ± 004	-.010 ± 005	
A_5	002 ± 018	001 ±.013	020 ± 038	.015 ± 008	.021 ± 008	
A_6	- 007 ± 018	- 007 ±.015	-.026 ±.040	- 023 ±.009	- 030 ± 009	
B_3	003 ±.001	001 ±.002	.004 ± 002	005 ± 001	007 ± 001	

Z_x = X-encoder bias
Z_y = Y-encoder bias
$d\alpha$ = azimuth misalignment
ξ = tilt component in the meridian (plus north)
η = tilt component in the prime vertical (plus east)
Θ = X-axis to Y-axis lack of orthogonality
C = optical axis to Y-axis lack of orthogonality
A_5 = X directional sag (moment between X-axis and Y axis)
A_6 = X directional sag (moment between Y-axis and dish)
B_3 = Y directional sag

for set B This is a significant difference in the derived C value, and points up the necessity for getting as good a distribution of observations as possible The value derived for C using the combined A and B sets of observations is $-0^{\circ}003$, and is believed to be a more representative value than either of the other two values The X encoder bias term of $-0^{\circ}015$ for the combined solution on May 15th is reasonable when compared with the value of $0^{\circ}031$ determined for the combined A and B solutions on May 1st Here again, the X encoder drift was taken into account

Of the three additional terms included in the ten-variable model (A_5, A_6 and B_3) that were not included in the seven-variable case, the B_3 term appears to be the only one that is determined with acceptable standard errors

Correlation matrices similar to the ones shown in table 3 were produced but are not given here They essentially showed coefficients similar to the previous ones in table 3 except for the A_5 and A_6 terms In all distributions tested these two terms were shown to be nearly perfectly correlated The correlation coefficients between A_5 and A_6 were -1 0 in all cases

3 1 4 Nine-coefficient Error Model

The fact that the A_5 and A_6 terms showed such high correlation, plus the fact that their standard deviations were excessively large compared to the values themselves, led us to use a model where the effect of X axis sag is not separated into two parts. Hence, a nine coefficient model was obtained by deleting the A_6 term

Samples of the results obtained using this model are given in table 7 As can be seen from these results, the main difference is in the standard deviations of the derived coefficients, although there are detectable improvements (more consistency) in some of the other values. These improvements indicate that an attempt to solve for both an A_5 and A_6 term had possibly exerted a negative influence on the ten-variable solutions

TABLE 7

STAR CALIBRATION RESULTS (9 coefficients)

Date	1 May 1969			15 May 1969	26 June 1969	18 July 1969
Sol / Coeff	122A	122B	122A&B	136B	178	198
Z_x	-°025± 008	-°031± 004	-°031± 004	-°012± 004	-°019± 003	°038± 005
Z_y	004± 001	004± 001	.004± 000	007± 001	003± 001	003± 002
η	- 002± 002	- 002± 001	002± 001	- 003± 001	003± 001	000± 002
ξ	006± 001	003± 001	005± 001	.003± 001	004± 001	002± 002
$d\alpha$	.002±.001	003± 001	002± 001	003± 001	004±.001	005± 002
θ	- 004± 002	- 003± 001	- 004± 001	- 004± 002	- 002± 001	- 006± 003
C	000± 007	006± 003	006± 003	006± 003	016± 002	- 013± 004
A_5	- 006± 001	- 002± 001	-.004± 001	- 003± 001	- 005± 001	- 005± 002
B_3	007± 003	006± 001	006± 001	.005± 001	003±.001	002± 002
σ_o	°003	°002	°003	°002	°002	°004

Z_x = X-encoder bias

Z_y = Y-encoder bias

$d\alpha$ = azimuth misalignment

ξ = tilt component in the meridian (plus north)

η = tilt component in the prime vertical (plus east)

θ = X-axis to Y-axis lack of orthogonality

C = optical axis to Y-axis lack of orthogonality

A_5 = X directional sag (moment between X-axis and Y axis)

B_3 = Y directional sag (moment between Y-axis and dish)

σ_o = standard error of a single observation

The nine-coefficient error model is sufficiently general to allow adequate determination of the various systematic errors That is, the effects of the systematic errors are reduced to the level of the pointing accuracy of the antenna As shown in table 7, the standard error of a single observation, σ_o, for the different solutions varies from 0^o002 to 0^o004 This value reflects the magnitude of the unknown errors in the observations

3 1 5 Adopted Error Model

The underlying philosophy behind this antenna calibration study has been to augment the directional accuracy of antenna tracking It was hoped that by monitoring various adjustments, orientation, and the tilt components of the antenna system, means would be available by which corrections could be applied to observations during a mission on a near real-time basis At the completion of this study, the Data Evaluation Branch, GSFC, indicated that they are not interested in separating η (east-west tilt) and Z_X (X encoder bias) Therefore, we have adopted an eight-coefficient error model for the field calibration manual, dropping the η term from the nine-coefficient model The effect on the observation equations (appendix II C) is to eliminate terms containing η and to change the ξ term from

$$\frac{\sin\alpha\cos\alpha\sec^2 e}{A} \quad \text{to} \quad \frac{\sin\alpha\cos\alpha}{A} \quad \text{in the dX equation,}$$

$$\frac{\tan e\cos^2\alpha}{\sqrt{A}} \quad \text{to} \quad \frac{\tan e}{\sqrt{A}} \quad \text{in the dY equation}$$

For an accepted set of observations, the difference between residuals computed using the eight- and nine-coefficient models for a given observation would rarely be as high as 0^o003 and in most cases would probably be 0^o001 or less A solution for the star distribution for May 1st (122B) was done using the eight-coefficient model A comparison of the corresponding residuals computed from the eight-and nine-coefficient models indicated that the largest change between residuals for this particular distribution was 0^o002 This occurred, as expected, on the observation with the highest

elevation angle ($76^{\circ}.5$) The average difference between residuals was $0^{\circ}0007$

If in the future it becomes desirable to have accurate angular data for spacecraft tracking, particularly to permit single station tracking, then certainly a closer monitoring of the attitude of the antenna structure takes on greater significance. At present, there is no assurance that the X encoder bias is a constant, in fact all indications are that there is a considerable drift.

It is not essential that the axis bias terms be zero when the rf axis is in the zenith, but it is essential that these terms are constant, particularly the X term, or can be made to be constant. This will permit greater flexibility in monitoring antenna tilt, due either to diurnal heating or long range causes If the ultimate in directional accuracy is to be attained, certainly the approach should not be plagued with drifting encoder biases.

3 2 ANALYSIS OF LEVEL READINGS

3.2 1 Stability of Angle Encoders and Antenna Structure

As previously mentioned, the X angle encoder was found to be drifting constantly during the test program. This was suspected in the second month when consistent changes in both Y wheelhouse level and optical target observations were noted An inspection of the level readings in table 3 of appendix I indicates the approximate amount of drift that occurred in the X encoder The first level readings were taken on 29 April At this time the X encoder was reading $-0^{\circ}018$ At the end of the field tests, on 4 October, the angle reading was $0^{\circ}107$ Thus, over a five month period the angle readings showed a change of $0^{\circ}.125$ During the first two months the drift rate appeared to be constant at about $0^{\circ}.0005$ per day At the time of the Apollo 11 mission, when the antenna was monitored daily, the drift rate seemed to increase to about $0^{\circ}.002$ per day After the mission the rate of drift seemed to return to the earlier value for the remainder of the tests.

A verification of the X encoder drift was made by using the results of the optical star solutions to compute values for the X level readings These values were compared with the observed level readings and plotted as shown in figure 14 This figure reflects the drift rates noted above and shows there is close agreement in the differential values of the computed and observed angles As indicated, the values of the observed angles are consistently larger (in the plus direction) than the computed angles This difference is a measure of the angular misalignment between the optical axis and the plane of the level vials. (See para 3.2 2)

The cause of the X encoder drift is not known at this time From available test results it cannot be determined whether the drift rate is constant. Indications are that it changed during the Apollo mission, but there are not sufficient data to verify this. Since noting this drift effect, project personnel have been informed that this problem has occurred in the past at the Canary Islands and Corpus Christi sites.

As was noted in the previous study, the antenna structure appears to be affected by solar heating Level observations obtained in the earlier tests showed that there were pronounced changes in the X and Y level readings from 0800 to 2400 hours amounting to almost $0^{\circ}02$ in X and $0^{\circ}01$ in Y. Also, there were day-to-day variations in both X and Y readings of about $0.^{\circ}01$. These were maximum during the daylight hours when temperat changes and differential heating effects were maximum

During this test phase level readings were obtained mostly in the evening hours On three occasions, 15 May, 21 July and 22 July, readings were obtained from morning through evening as shown in figure 15 For 15 May, a clear sunny day with ambient temperatures varying about 30°F, the X level reading varied over a range of $0^{\circ}014$ On 21 and 22 July, the diurnal variations in the X reading averaged only about $0.^{\circ}004$. These small diurnal changes can probably be attributed to the weather conditions as on both days there was total cloud cover with ambient temperatures not varying more than 15° F.

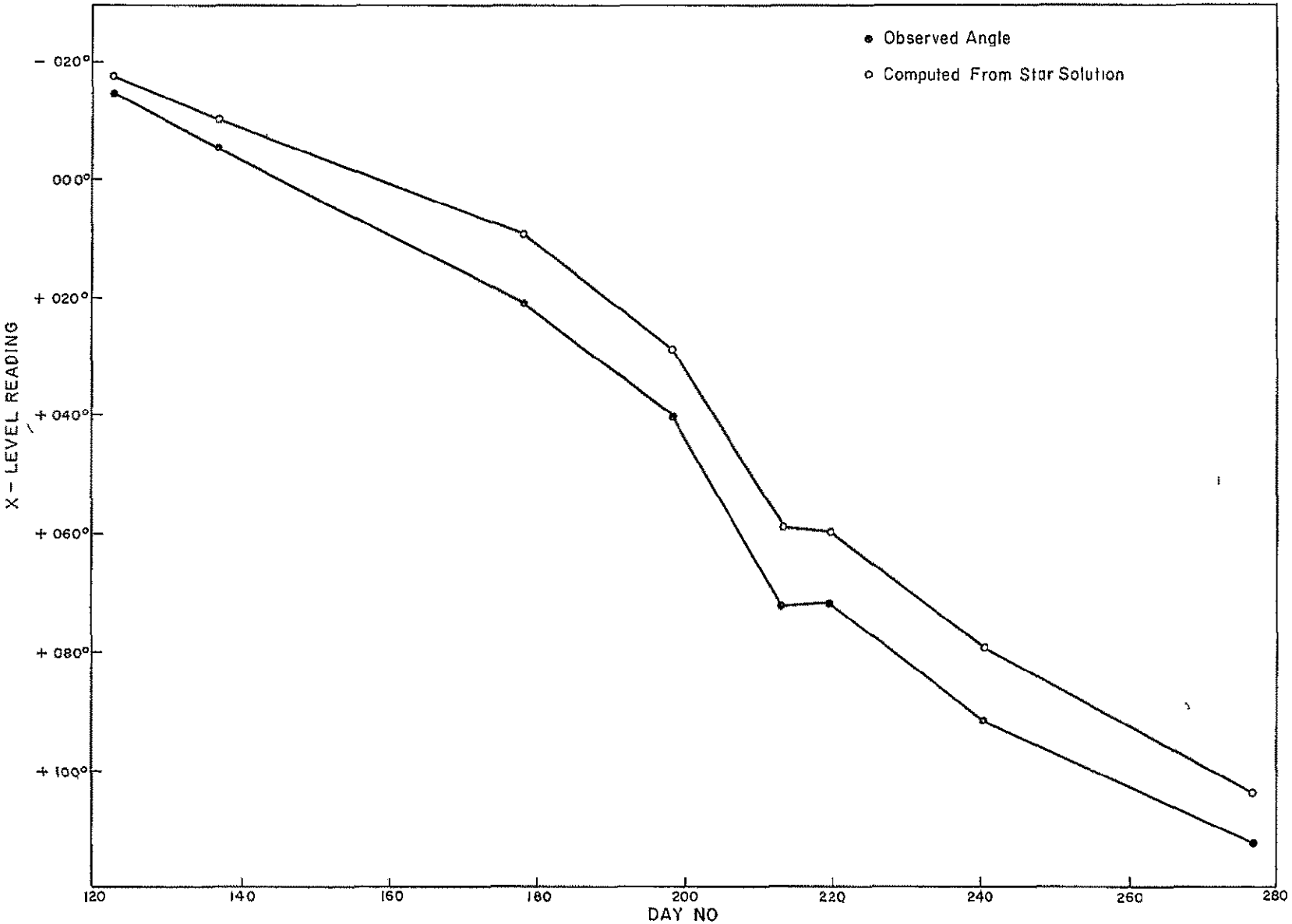

Figure 14

OBSERVED AND COMPUTED X-ANGLE LEVEL READINGS

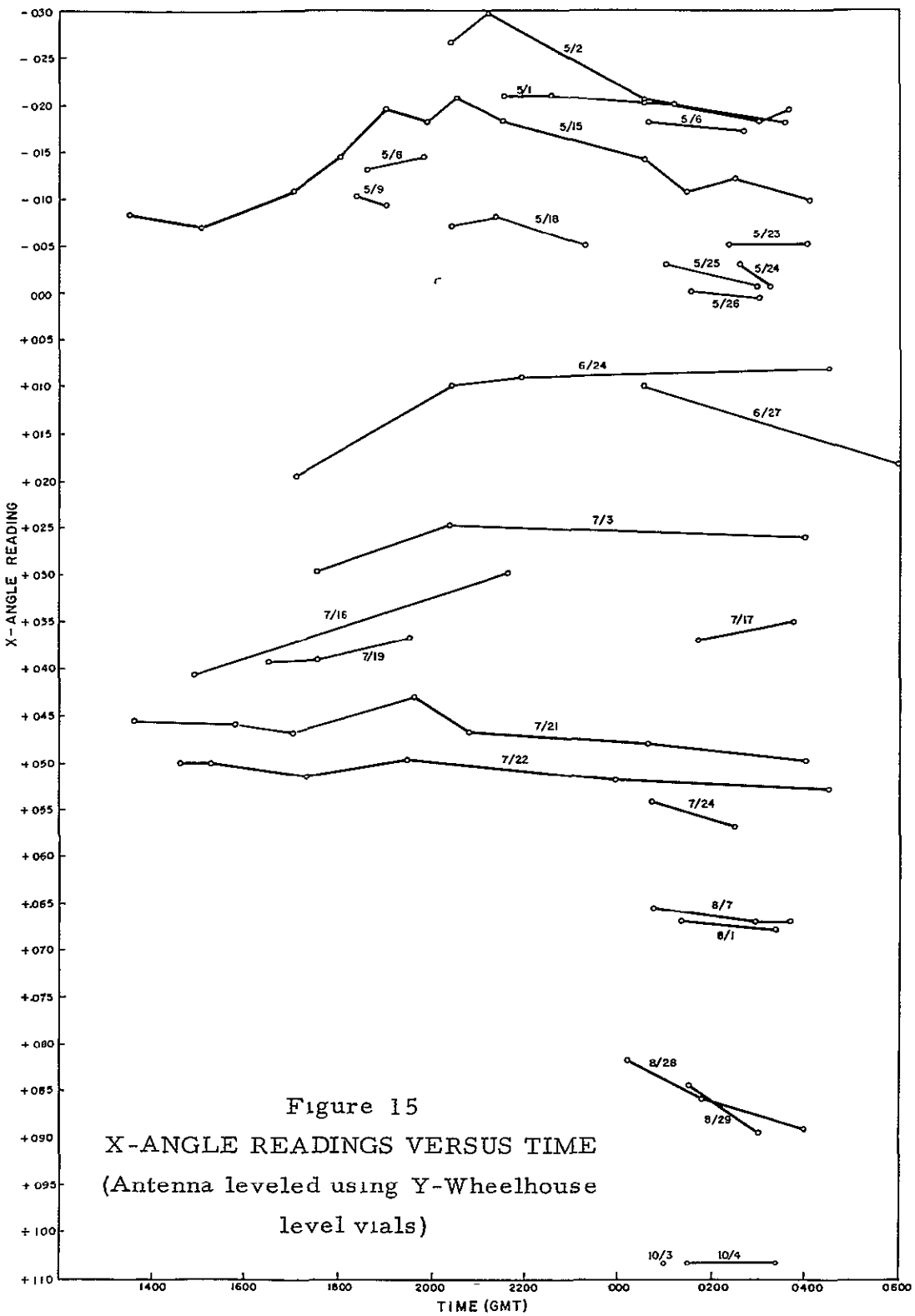

Figure 15

X-ANGLE READINGS VERSUS TIME

(Antenna leveled using Y-Wheelhouse level vials)

A graph of the Y level readings versus time is shown in figure 16 No attempt was made to separate the daily readings since they seldom varied more than $0^{\circ}002$ to $0^{\circ}003$ The day-to-day readings are seen to vary over a range of $0^{\circ}01$ about a mean value of approximately $+0^{\circ}.005$. The mean of the observations reflects the small Z_y bias terms that were obtained from the star solutions in the previous section

It seems evident from these and the previous test results that the diurnal changes in the X and Y readings must be monitored or allowed for empirically by experimental data if X and Y angles of much better than $0^{\circ}.01 - 0^{\circ}02$ are to be expected

3 2 2 Application of Spirit Levels for Tilt Determination

Ideally, the X and Y encoder bias should be zero and the axes of the Y-wheelhouse levels parallel to lines defining the centers of rotation of the X and Y axes If such a condition existed, the determination of the two tilt components, η and ξ, of the antenna would be a simple matter. Adopting the convention that a positive tilt is a "lean" of the antenna to the east and north respectively, we have $\eta = -L_x$ and $\xi = -L_y$ in which L_x and L_y are the X and Y encoder readings when the bubbles of the Y wheelhouse spirit levels are centered by rotating the antenna to the zenith

If the encoder bias is not zero but is Z_x and Z_y, we then have

$$\eta = Z_x - L_x \text{ and } \xi = Z_y - L_y$$

Further, if the spirit levels are not in adjustment but their errors, in relation to X and Y axes, are E_x and E_y (plus, east or north end up) then

$$\eta = Z_x + E_x - L_x \text{ and } \xi = Z_y + E_y - L_y$$

(see equations (3) and (4) appendix II. B)

Finally, as long as the Z and E terms stay constant, we can monitor the tilt by changes in L_x and L_y, and the sums, $\eta + L_x$, and $\xi + L_y$ will be

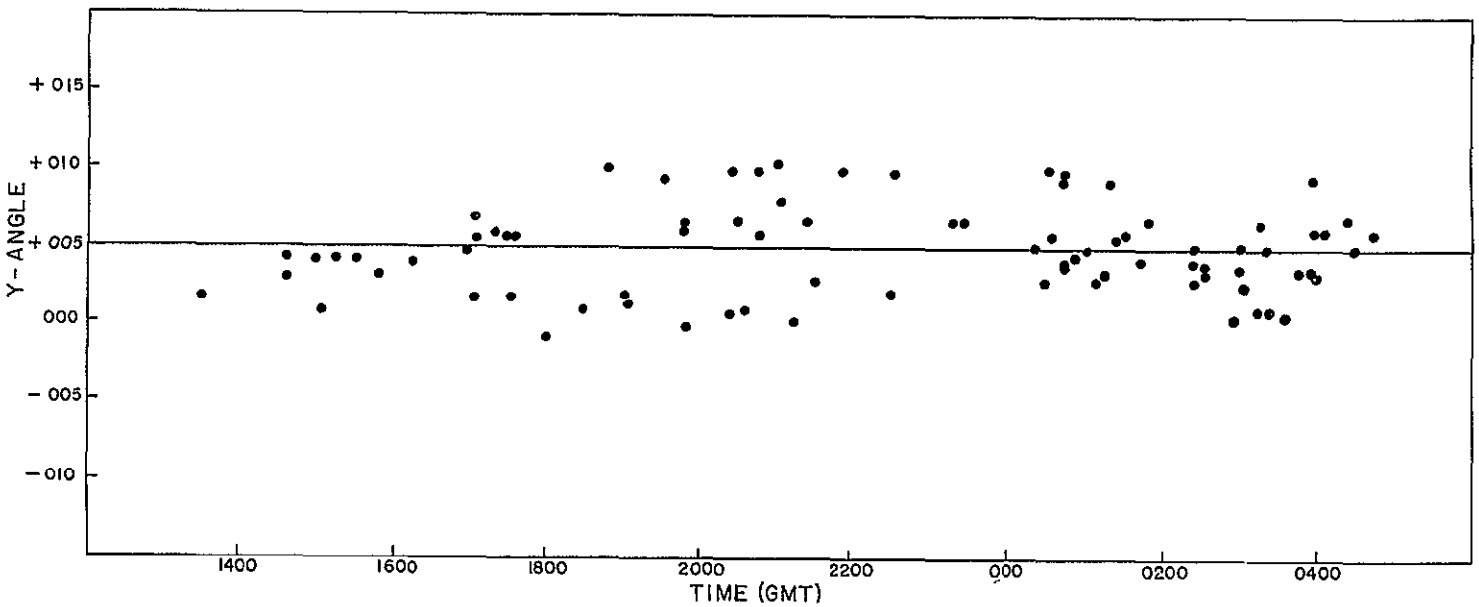

Figure 16

Y-ANGLE LEVEL READINGS VERSUS TIME

PERIOD 1 MAY - 4 OCTOBER 1969

constant. If we once determine what these sums are, we can not only monitor tilt changes, but also determine their absolute values from L_x and L_y

But here we are plagued with the vagaries of the spirit level adjustments and encoder biases If these slowly drift or change, and the effects of tilt and diurnal heating are of the same order, we will be unable to separate their different effects

Values for E_x and E_y, the misalignment errors in the spirit levels with respect to the X and Y axes, were derived using results of the nine-coefficient star solutions listed in table 7. Values for E_x varied from $-.^{\circ}005$ to $+.^{\circ}010$ and those for E_y from $-^{\circ}001$ to $+^{\circ}007$. In both cases the range of values is within the combined standard error of the solutions and the level readings As expected, the E_y values are somewhat more stable than the E_x values due to the instability of the X encoder.

3.3 COMPARISON OF TILT DETERMINATION BY OPTICAL TARGETS WITH SPIRIT LEVELS

Tests conducted during the previous study phase showed there was close agreement between relative changes in level readings and antenna tilt determined by optical target observations. The tests results indicated that the spirit levels can be used to monitor differential changes in the antenna tilt over short periods of time, whereas the optical targets can be used to determine absolute tilt components, η and ξ, in conjunction with periodically determined star calibrations.

Figure 17 shows a comparison of optical target tilt solutions and X and Y level readings obtained during this test period As indicated in the figure, there is excellent agreement in the differential changes of the computed tilt components and the level readings When the systematic difference (bias) of approximately $-0^{\circ}020$ in the X level readings and $+0.^{\circ}007$ in the Y level readings are removed, the X and Y encoder readings provide accurate measurements of the absolute tilt of the antenna For completeness, it should be mentioned here that the antenna is leveled to the gravity vector, not to the spheroid normal For details related to this problem, see Appendix II A

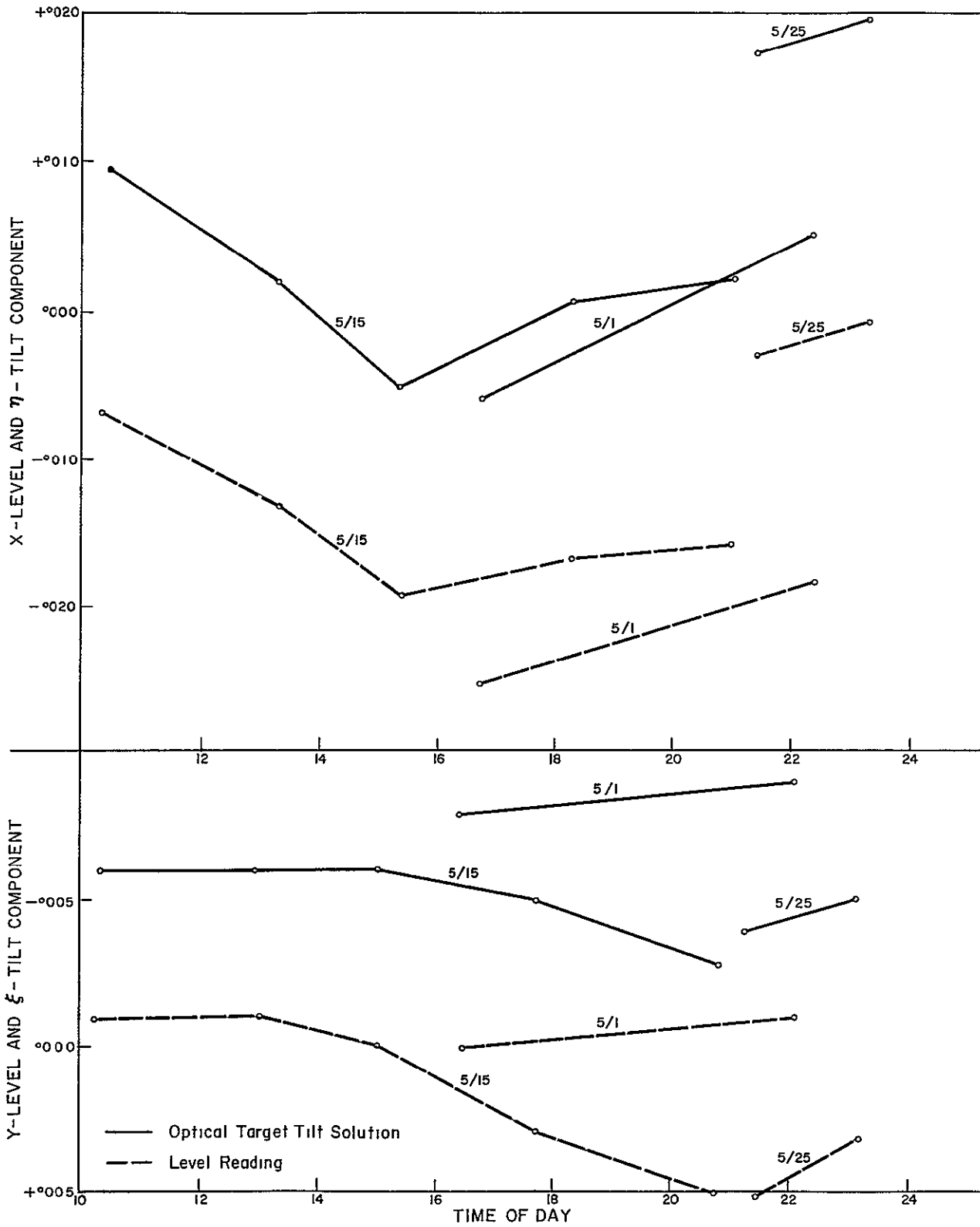

Figure 17

COMPARISON OF X AND Y LEVEL READINGS AND OPTICAL TARGET TILT SOLUTION

3 4 ANALYSIS OF RF AND OPTICAL BORESIGHTING

During the period from April 29 through May 26, 1969, repeated checks of the collimation of the S-band antenna were made for both the rf and optical axes, using the targets on the collimation tower Only RHC polarization was checked for the rf collimation.

When the antenna is facing the collimation tower, $X \approx 86^{\circ}$ and $Y \approx 68^{\circ}$, thus a ΔX is substantially a change in elevation and a ΔY is a change in azimuth Inasmuch as a change in atmospheric refraction and multipath conditions have a marked effect on vertical angles and very little on horizontal angles, the ranges and fluctuations in the X component of both rf and optical collimation are much greater than in the Y component (see table 8) The Y values are quite steady throughout the entire period, particularly for the optical collimation

In the rf collimation tests, over the period of about 4 weeks, there is a definite indication that, for some reason, the X encoder readout was reducing numerically by about $0^{\circ}06$ or $0^{\circ}.07$ whereas the same trend was obtained in the X encoder readout in the optical test, but only to the extent of about $0^{\circ}.02$. This latter value closely approximates the amount of encoder drift that occurred over this time period.

If we remove the drift of the X encoder indicated by the optical collimation from that indicated by the rf collimation we have a residual of about $0^{\circ}.04$ that might be assigned as an outside uncertainty in rf collimation determination by this method This could indicate a one sigma error of about $0^{\circ}02$, at least for RHC polarization

The surveyed value for the optical target was $0^{\circ}.001$ over the collimation test average for X and $0^{\circ}.010$ under the test value for Y The differences between rf and optical X and Y values, roughly $0^{\circ}.03$ and $0^{\circ}.07$, could be due to some error in the relative location of the optical and rf targets, but more likely is due to lack of parallelism of the rf and optical axes.

The two right hand columns of table 8 list the individual determinations of angular differences, in X and Y, between the rf and optical boresighting

TABLE 8

COMPARISON OF RF AND OPTICAL BORESIGHTING

Date	Hours	RF Autotrack (RHC)		Optical Target		Angular Difference	
		X	Y	X	Y	ΔX	ΔY
4/29	2215	-86°459	68°085	-86°475	68°155	-0°016	0°070
4/30	1740	461	085	473	155	012	070
	2035	450	084	470	152	020	076
	2245	461	084	466	151	005	076
5/1	1625	457	083	468	159	011	076
	2055	440	082	461	155	021	073
	2240	408	081	454	154	.046	076
5/8	1510	440	105	466	160	026	055
5/15	1745	428	088	461	155	033	067
	2050	427	090	463	153	046	063
	2115	433	090	461	156	028	066
5/22	2230	425	086	453	156	028	070
5/24	2235	388	096	452	155	064	062
5/25	2115	419	095	453	154	036	059
	2250	426	093	448	151	022	058
5/26	2145	383	090	448	152	056	062
	2300	388	090	447	152	061	062
Mean		-86°429	68°088	-86°460	86°154	-0°031	0°067
					σ =	0°017	0°007
					σ_m=	0°004	0°002

Survey values of optical target X = - 86°461, Y = + 68°144

in the sense, optical minus rf The means of $-0.^{\circ}031$ and $0.^{\circ}067$, for ΔX and ΔY, have standard deviations of $0^{\circ}004$ and $0^{\circ}002$ respectively with $0.^{\circ}017$ and $0.^{\circ}007$ standard deviations of a single observation The larger errors in ΔX are due to the greater fluctuation in the rf observations

3.5 ANALYSIS OF RADIO STAR OBSERVATIONS

Radio stars were observed on six different occasions during the period 3 July through 4 October (day nos. 185-278). (See table 4, appendix I). Procedures for recording the signals varied from use of the Beckman Dynograph to a computer printout of digital voltage readings with time and corresponding X and Y angle readings Observations obtained on days no 185, 198 and 206 using the single axis scanning technique were reduced, but results were erratic with the O-C values varying over a range of $0^{\circ}1$ - $0^{\circ}2$. These large variations were attributed to two factors· the antenna scanning rates were too high ($0^{\circ}1$ - $0.^{\circ}2$/second) to achieve any reasonable degree of precision, and it was very difficult to obtain accurate time correlation between the graphical record of the signal voltages and X and Y angles from the TDP printouts. These early tests pointed up the need for recording angle readings at a higher sample rate, for reducing the rate at which the radio source is scanned, and for having a computer printout of voltages and angle readings accurately correlated with time to within ± 0.1 second

Observations for days no. 256, 277 and 278 provide the only useful data for evaluating the different observing techniques The analysis of these observations is given below but it will be seen that results are inconclusive, and that a considerable amount of additional testing must be done before the capabilities of the various observing techniques can be fully assessed

3.5.1 Data Reduction Procedures

The large amount of data obtained by sampling the digital voltmeter at 0.1 second intervals indicated a need to reduce the amount of data to be handled during the early stages of developing reduction procedures and to devise a method of smoothing the data It was realized that once the

reduction techniques were established, data handling would be a simple matter to automate on the on-site computer

With this in mind, the digital voltage recordings at 0 1 second intervals were handled so as to produce average values at one second intervals It is assumed that any errors in this process are in the voltage readings, not in the timing Inasmuch as only a single instant of time, that of the peak voltage and the associated X and Y readings, is sought, this method of smoothing is admissible

The above procedure produced a series of points which had to be analyzed to find the time associated with the peak voltage To do this a second-degree polynomial was used to determine the best fitting parabola, the vertex of which provided a convenient means for computing the time corresponding to the peak voltage reading Since a full series of voltages over the antenna's directional pattern more closely approximates the Gaussian curve, only points near the maximum signal level were used Figure 18 shows a sample radio signal recording with the smoothed data points and the associated parabola This figure shows most of the signal returns for the scan, not just points near the maximum voltage level In this case a semblance of the Gaussian curve is discernible

When the radio signals were sufficiently strong, as in figure 18, the curve fitting procedure determined the time of peak within about a half second For the single axis scanning method, where the scan rate was usually around $0^{\circ}06$ per second, the error could amount to about $0^{\circ}03$ in the X or Y readings, therefore, the O-C values can be expected to show this kind of variation. In those cases where the signals are weaker and the graph shows a less distinct peak, the curve fitting procedure can give much poorer results, for this reason, a closer look at both the digital and graphical records were made in many instances, particularly for the Cygnus A and 3C400 measurements A graphical technique using the total signal return over the entire scan was used on several occasions to determine the time of peak

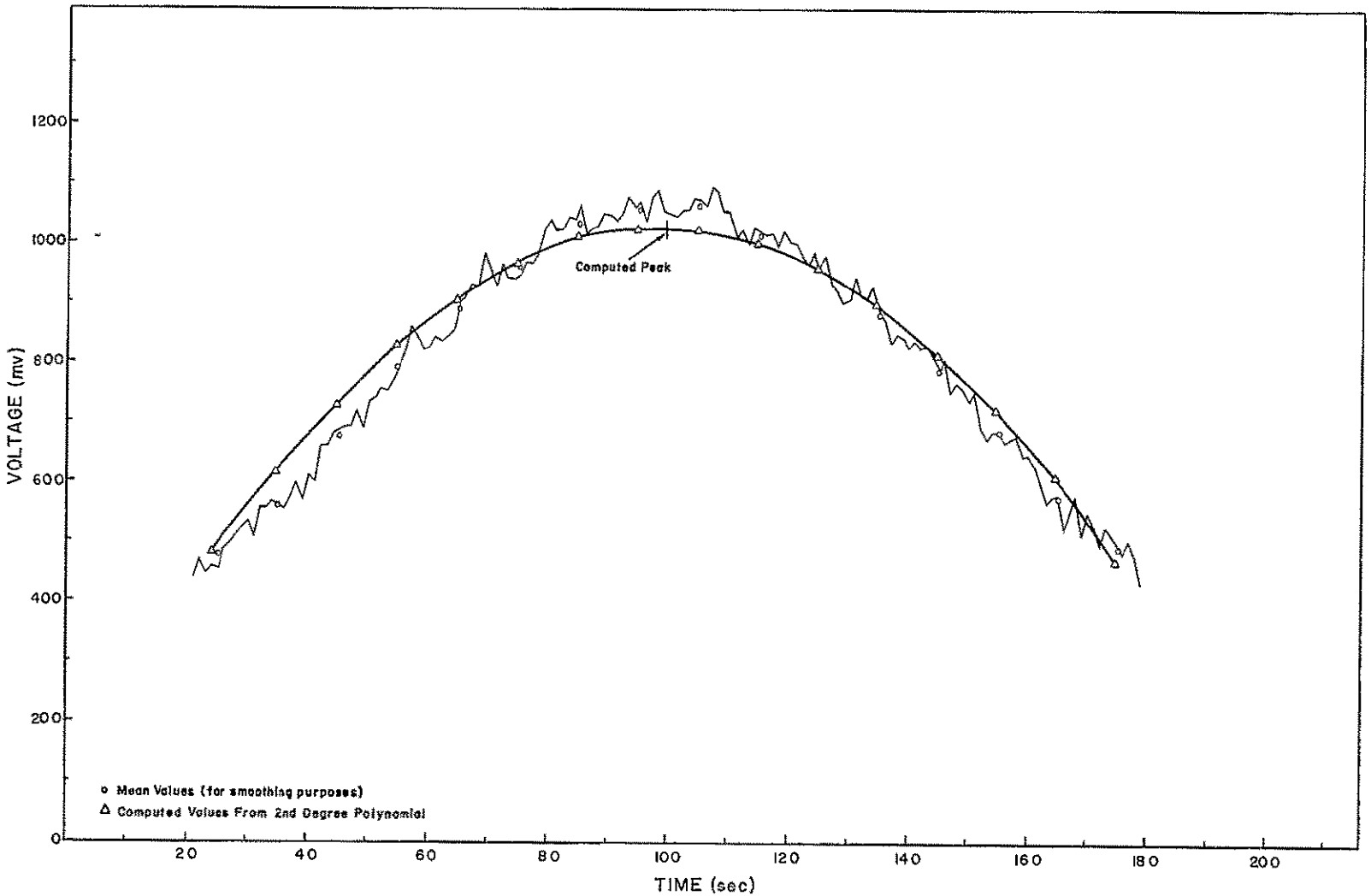

Figure 18

OBSERVED VOLTAGE READINGS AND

COMPUTED CURVE FIT

(Cassiopeia A-Single Axis Scanning)

Using the procedure described above, the "peak" time of all the voltage readings obtained from the scanning and fixed position observing methods were determined From each computed instant of time the adopted ephemeri was used to compute the angular directions to the radio stars These values were then compared with the observed X and Y angle readings to obtain O-C values. In computing the pointings to the radio star, corrections for atmospheric refractions were handled in accordance with the procedures in appendix IV

3.5.2 Results of Fixed Position Method

Observations of Cassiopeia A, Cygnus A, and 3C400 were obtained on days no 256 and 277 by the fixed position method. Each of the radio sources was observed three times. The observations of 3C400 on day 277 were not reduced because the voltage readings were too weak to define the time when maximum signals occurred

For the reduced observations, it was found that the time of occurrence of the maximum voltage varied significantly for each star passage For example, for Cassiopeia A on day no. 277, the observed (computed) times of maximum voltage for the three star passages differed from the predicted times by +26 seconds, +100 seconds and -30 seconds This in turn introduced large variations in the X and Y angle O-C values. The reason for the large time differences is unknown and cannot be explained by the small angle offsets that were introduced so that the star would pass through the antenna field of view on slightly different tracks

The fact that there were large and unexplained differences in the results indicates some weakness in the observing method. In all cases, the received signal voltages developed a very flat curve along which it is difficult to determine (either graphically or by curve fitting) the time of peak voltage to better than about 5 - 10 seconds But there is another factor that might explain a large part of the difficulty The voltage differences along the curve are so very small that it does not seem unreasonable that the high noise level of the system might influence the received signals to an extent to grossly offset the apparent peak voltages.

The observations obtained were too meager and uncertain to provide a definitive assessment Considerably more experimentation will be required before the merits of this method can be determined.

3.5.3 Results of Single Axis Scan Method

Table 9 summarizes results obtained with the single axis scan method for Cassiopeia A, Cygnus A, and 3C400 on day nos. 256 and 277 The upper portion of the table shows the X_{o-c} and Y_{o-c} values for each of the reduced scans and the mean for each series of scans. The number of scans obtained for each radio source varied on both days, with usually 7-10 scans per axis being observed. Scanning rates of approximately $0^{\circ}.05$ per second were used on both days. All the scans were not reduced, particularly for Cygnus A and 3C400, because the recorded voltage readings were either too weak or too noisy to determine the peak voltage time with any certainty As might be expected, the O-C values for Cassiopeia A provide the most consistent results owing to the relatively high signal to noise ratio.

The lower portion of the table shows the computed angular differences between the rf and the adjusted mechanical axes. The star calibration corrections were obtained from the results of the star observations. The large difference in the X axis correction for the two days is due mainly to the drift effect of the X angle encoder which also affected the first term Thus the differences are reasonably undisturbed

The results for Cassiopeia A and Cygnus A are reasonably consistent and indicate that the angular misalignment between the rf and adjusted mechanical axis, ΔX and ΔY, averages about $0^{\circ}.030$ and $-0^{\circ}060$, respectively Results for source 3C400 are not expected to agree with these values because as noted earlier, its spatial coordinates (right ascension and declination) are only approximately known. However, the results obtained from 3C400 on both days tend to be in agreement within about $0^{\circ}.03$.

3.5.4 Results of Incremental Offsetting

Observations of Cassiopeia A were made on day nos. 277 and 278 using the incremental offset techniques. Four sets of observations were made on

TABLE 9

RESULTS OF RADIO STAR OBSERVATIONS

SINGLE AXIS SCAN METHOD

Cassiopeia A		Cygnus A		3C400	
Day 256		Day 256		Day 256	
Xo-c	Yo-c	Xo-c	Yo-c	Xo-c	Yo-c
°112	-°066	°158	-°065	-°205	-°265
113	- 053	093	- 064	-.208	- 265
115	-.083	098	- 050	- 184	- 256
111	- 063	.088	- 073*		- 248*
104	-.063	133*	- 034		
110	- 055				
125	- 035				
mean 113	-.060	.114	- 057	- 199	- 258
Day 277		Day 277		Day 277	
Xo-c	Yo-c	Xo-c	Yo-c	Xo-c	Yo-c
°129	-°064	°126	-°126	-°210*	-°281
161	- 037	163	- 058	- 179	- 279
.075	-.035	093	- 070	- 157*	- 185
162	- 068	141	-.058		- 217
145			-.090		- 241
					- 233
mean 134	- 051	.131	- 080	- 182	- 223
		*based on graphic record			

Angular Differences (rf-adjusted mechanical) = mean - correction (star calib)

$\Delta X = \bar{x} - Cx$, $\Delta Y = \bar{y} - Cy$

	Day 256	
ΔX= 113- 081= °032	ΔX= 114-.084= °030	ΔX=- 199- 084=-°283
ΔY=- 060- 001=-.061	ΔY=- 057- 001=-.056	ΔY=- 258-.001=- 259
	Day 277	
ΔX= 134- 097= °037	ΔX= 131- 098= °033	ΔX=- 182- 098=-°280
ΔY=- 051- 004=- 055	ΔY=- 080+ 002=- 078	ΔY=- 223+ 002=- 221

both days, but because of problems with the computer, only two sets of observations were successfully obtained on each day On day 277, the two successful sets of observations were made with offset increments of $0^{\circ}2$, while those for day 278 were made with offset increments of $0^{\circ}1$ It is noted that each set of observations consisted only of a single line of offset points for each axis through the provisional peak signal and not 2 or 3 lines of points per axis as recommended in section 2 6 3.3 and figure 5

In reducing these observations, the time of the peak voltage return was not critical as it was in the previous two methods Curve fitting techniques were used as before to obtain the peak signal return, but in this case maximum voltage readings were computed as a function of the incremental offsets

Figure 19 is a graph representing this procedure and indicates the insensitivity of the voltmeter to small increments in the vicinity of the peak. The small changes in the voltage readings near the peak, for the $0^{\circ}1$ increments shown, indicate that Cassiopeia A is not detected as a point source but as a small area in the sky

Results of the observations in terms of the angular difference between the electronic and adjusted mechanical axes, are tabulated as follows

Day	Obs	ΔX	ΔY
277	1st set	$^{\circ}087$	$-^{\circ}205$
	2nd set	- 061	- 078
288	1st set	091	- 071
	2nd set	- 048	015

It is readily apparent that results are inconsistent and vary over a wide range of values. It is realized that there is some weakness introduced in the method by using large incremental offsets ($0^{\circ}1$ and $0^{\circ}2$), but this fact alone does not explain the wide variation in the results

More observations and analysis are necessary to evaluate this observing technique as a means for locating the electrical axis of the antenna

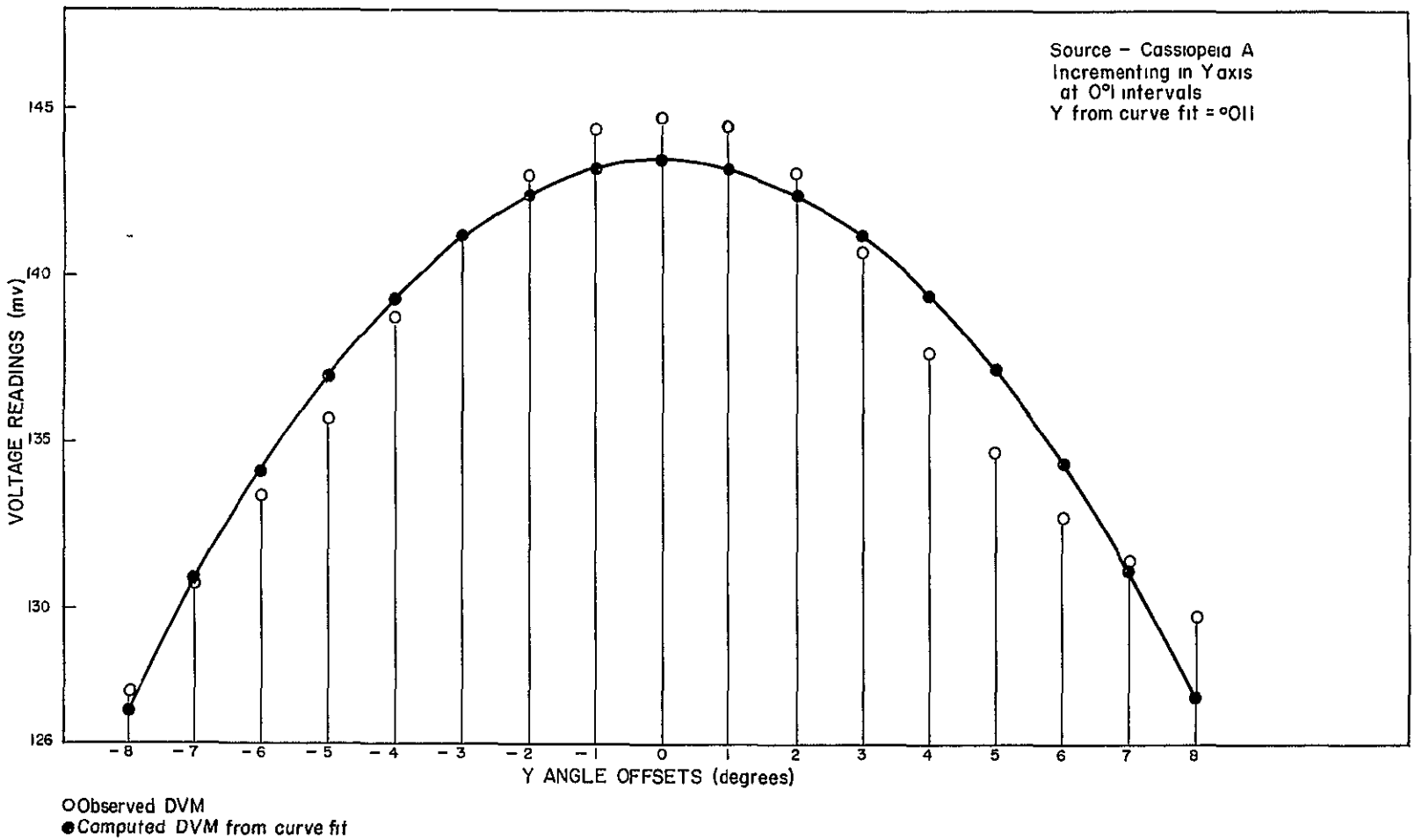

Figure 19

OBSERVED VOLTAGES AND COMPUTED CURVE FIT

INCREMENTAL OFFSET METHOD

3.5 5 Analysis of Other Observing Schemes

Several other techniques for observing Cassiopeia A were tried using the star track program on days no. 277 and 278. This included sector scanning and directional offsetting The sector and raster scans were done at the slowest possible scan rate for the automatic program modes, which was $0^{o}5$ per second. The directional offsets were used in an attempt to manually peak-up on the maximum signal by observing the Beckman Dynograph recordings. With this technique, a directional offset is applied to the Antenna Position Programmer to override the star track drive and to move the antenna so it is not pointing directly at the source The antenna is then manually moved back, by reducing the servo-error signal, until the radio source's peak voltage level is visually observed. This was repeated from cardinal directions.

Observations from the sector and raster scans were only partially reduced because the initial results were found to be very inconsistent The scan rates are much too high for either of these scanning modes to be of any value for aligning the antenna's electric axis

Results of the peaking-up method with the directional offsets were also too erratic to be of any value. This method is somewhat similar to the incremental offset method, except that no attempt was made with the latter to obtain the maximum signal directly Since the incremental angle offsets would be more sensitive for this purpose, the peak-up method could be considered an alternate approach for the incremental offset technique discussed above If any further work is to be done in this area, it would be desirable to use the incremental offsets to peak-up directly by observing the digital voltmeter rather than the Beckman recorder, and to repeat this a number of times to test the repeatability of the method

3 6 RESULTS OF ALSEP OBSERVATIONS

As noted earlier in section 2 7, an attempt was made on several occasions to autotrack the ALSEP transponder A successful track was

obtained on the evening of August 28th (day no 241), and at this time photographs of the moon were taken. Thus, an effort was made to use the ALSEP transponder for both rf-mechanical axes alignment and rf-optical axes alignment It is recognized that these limited observations can only provide an indication of the potential application of ALSEP for rf axis alignment.

The ALSEP track was reduced by the Data Evaluation Branch, GSFC, and observed minus computed values (O-C's) for the X and Y angles were determined. The mean X_{o-c} for the track was $+0^{\circ}09$ and the mean Y_{o-c} was $-0^{\circ}05$ These values were considered to represent the misalignment errors between the electronic axis and the uncalibrated mechanical axes Angular corrections for the mechanical axis were obtained using the derived coefficients from the star calibration solution for August 27th Applying these corrections to the X and Y values, the angular differences, ΔX and ΔY, between the electronic and adjusted mechanical axes were found to be $\pm 0.^{\circ}02$ and $-0^{\circ}05$, respectively It is noted that these values are in close agreement with the results of the observations of Cassiopeia A using the single axis scanning method for day numbers 256 and 277 (see table 9).

The photographs of the moon were only marginally successful The video picture was good but the 35 mm film records were either overexposed or poorly processed. Seven photo frames which provided a fair delineation of the moon were evaluated The objective in using the photos was to measure the angle difference between the center of the reticle of the TV picture and the apparent location of ALSEP Since the antenna was autotracking ALSEP at the time the photographs were taken, this angle should represent the rf to optical axes misalignment which should be equal to the ΔX and ΔY values mentioned above The main difficulty with the photos was that they were of such poor quality that the Apollo 11 landing site could not be determined with any reasonable degree of certainty With good photos it should be possible to spot the location of ALSEP on the photos within $\pm 0^{\circ}010$

Results of the photo measurements are given in the following table where dx and dy represent the angular differences between the rf and optical axes

Exposure No	Time	dx	dy
5123	$2^h\ 34^m\ 42^s$	^{o}005	-^{o}046
5149	2 35 42	.005	- 025
5157	2 36 00	.005	- 065
5182	2 37 00	002	- 018
5192	2 37 24	005	- 065
5248	2 49 12	005	- 070
5252	2 49 24	015	- 025
	mean	^{o}.006	-^{o}.045

These values are found to be in reasonable agreement with the X and Y values from ALSEP autotrack data and the results of the radio star single axis scanning method Also there is fair agreement between these values and the boresight measurements listed in table 8.

3 7 COMPARISON OF RESULTS OF RF ALIGNMENT METHODS

Since it is the rf and not the mechanical or optical axis that is involved in tracking spacecraft, all other calibrations and alignments are really steps toward rf alignment. The approach then is, through use of the optical axis and a star shot program, to determine all errors in the antenna attitude, optical and mechanical axes alignments, encoder biases, etc The problem then is reduced to relating the rf axis to the system This is done by directly relating the rf to the optical axis, as in the boresight tower or in the ALSEP photographic method, or indirectly by radio observations corrected by the angular differences shown at the bottom of table 9.

Table 10 is a convenient listing of the results of rf axis alignments by the several methods, all reduced, for comparison purposes, to the optical-rf axes relationship expressed in ΔX and ΔY The agreements are generally within the standard deviations which favor the boresight tower method However, this is about the ultimate capability for the boresight tower method, whereas the others have gone through only a preliminary testing

TABLE 10

COMPARISON OF RF AXIS ALIGNMENT USING DIFFERENT OBSERVING TECHNIQUES

	Cassiopeia A		Cygnus A	
Using Celestial Radio Sources	ΔX	ΔY	ΔX	ΔY
Single Axis Scan Method				
Day 256	°032 ±°01	-°061 ±°02	°030 ±°03	-°056 ±°01
Day 277	.037 ± 03	- 055 ± 02	.033 ± 03	- 078 ± 03
Using ALSEP Transponder		ΔX	ΔY	
ALSEP (autotrack)		°020 ±°02	-°050 ±°02	
ALSEP (photos)		006 ±.01	- 045 ±.02	
Using Boresight Tower		ΔX	ΔY	
Mean value over day nos 120-147		031 ±.02	-.067 ± 01	

ΔX, ΔY = angular differences between rf axis and adjusted mechanical axis (rf to optical axis relationship)

Admittedly the data employed in this analysis are rather meager and not conclusive, but at the same time they strongly point up the potential of rf axis alignment by celestial sources There can be little doubt that such a method, when developed, will be far superior in accuracy to the boresight tower method with its obvious limitations

SECTION 4
CONCLUSIONS AND RECOMMENDATIONS

Based on the studies performed under this contract, and the investigations conducted during the previous contract, the following conclusions and recommendations are made

4 1 CONCLUSIONS

In general, it is believed that the calibration procedures which were developed and tested under this study program will be capable of determining the static angular alignment of the 30-foot antenna system within an accuracy of $\pm 0^{\circ}025$ (standard deviation). The capabilities of the various calibration and alignment techniques are noted as follows·

Star Solutions. To obtain an optimum solution for a star calibration model composed of eight or nine error coefficients, as defined in section 3 1, a total of approximately 20 to 25 star shots are required If they are uniformly distributed both in azimuth and elevation, the error coefficients should be determined within a standard deviation not exceeding $\pm 0^{\circ}004$ and a standard deviation of a single observation, σ_o, of $\pm 0^{\circ}003$

Y-Wheelhouse Spirit Levels These levels afford an excellent means of monitoring changes in antenna tilt, particularly when due to diurnal heating effects In conjunction with star and ground target observation, these level readings (X and Y encoder readouts when bubbles are centered) can determine absolute tilt values within approximately $\pm 0^{\circ}003$

Optical Ground Targets. These targets are useful for determining antenna tilt independently of the spirit levels and checking antenna orientation However, they cannot replace the star shot program for complete calibration of the antenna Advantages include day and night use under all weather conditions, which is of particular value during an actual mission

RF and Optical Boresighting Tests at Goddard indicate that, despit multipath problems, the direction of the rf axis can be determined by boresighting on the collimation tower, along with the optical axis, within a maximum error of about $\pm 0^{\circ}04$ and a standard error of $\pm 0^{\circ}02$. Most of this is in the vertical plane. Conditions vary at othe S-band antenna locations and only local tests will resolve boresight limitations

Celestial Radio Source Data resulting from observation on radio stars to collimate the rf axis are not sufficient to form a definitive statement on the accuracy of the method At the same time, however there was enough experimentation to indicate a distinct possibility of developing techniques that will not only permit a much needed chec on rf boresighting on a nearby collimation tower, but should definitely yield higher accuracies Experience indicates that a strong radio source, such as Cassiopeia A, yields better results The lack of mai strong radio stars with sufficient positional accuracy is a present limitation An overall assessment of accuracy obtained by experimen with the single axis scanning method is about $\pm 0^{\circ}03$ as the standard deviation of rf axis collimation

ALSEP Tracking Results from the limited observations of ALSEP were encouraging The rf to mechanical relationship can be obtained from a series of autotracks of the ALSEP package, in turn, these values can be reduced to give the calibrated mechanical (optical) to rf relationship In addition, if reasonable quality photographs of the moon are taken at the time of tracking, a check on this method of observing can be achieved Based on the limited observations analyze it appears that ALSEP transponders could be used to determine the rf axis within a directional accuracy of about $\pm 0^{\circ}02$ (standard deviation)

4 2 RECOMMENDATIONS

As a result of the work performed under this study program the following recommendations are offered

Alignment Manual The field manual, "Operation Manual for Angular Alignment and Static Calibration of Unified S-Band 30-Foot Antenna," written under this contract should be issued for use at all antenna sites. A careful utilization of the procedures outlined in this manual should improve directional pointing accuracy of all antennas

Spirit Levels Because of the ease with which the Y-wheelhouse spirit levels can be used to monitor antenna attitude, it is recommended that serious consideration be given the installation of additional sets of bubbles, or similar devices. Two additional sets of bubbles, installed at other places within the Y-wheelhouse would provide standards to run periodic checks against The three sets of bubbles would then provide a reliable source to determine encoder bias or to re-set the encoders after overhaul Also, it is recommended that an appropriate covering be installed for the existing level vials to protect them from being damaged or knocked out of adjustment This covering should surround the platform on which the vials are placed and not be connected to it

Optical Targets. When terrain conditions permit, ground optical targets should be installed around the antennas. Such targets would be useful in providing a stable standard reference in detecting such biases as encoder drift effects. Existing permanent structures, such as finials of lighthouses, can also be used for this purpose.

External RF Alignment. Further field testing should be made to evaluate the capabilities of celestial radio sources and

ALSEP transponders for rf axis collimation For radio stars, investigations should include tests to determine the optimum system configuration for detecting and recording radio signals, and to develop further the observing and reduction methods that were considered under this study

If the history of scientific measurements has taught us anything it is that the requirement for accuracy has invariably increased over the years, and usually by at least an order of magnitude It is quite possible that this may apply to the accuracy of observations for direction to the spacecraft Thus the procedures and modifications recommended above, and in particular the inherent accuracy of rf axis collimation by celestial sources, takes on added importance, the latter should be vigorously pursued experimentally to assure ultimate practical results

REFERENCES

[1] Proceedings of the Apollo Unified S-Band Technical Conference held at GSFC July, 1965 Report No. NASA SP-87

[2] Preliminary Erection Procedure for Unified S-Band 30-Foot X-Y Antenna, Collins Radio Co , 16 October 1964

[3] Final Acceptance Test Procedures for GSFC 30-Foot Antenna System, Revision B Volume I Test Procedures, Collins Radio Co , 1 June 1966

[4] Use of Optical Targets for Geodetic Orientation of C-Band Radar, Geonautics, Inc , November 1968 Contract NAS 5-10638

APPENDIX I
SUMMARY OF OBSERVATIONAL DATA

A summary of the field test data obtained during this contract is presented herein together with some sample recordings of the celestial radio sources

Table 1 provides a log of the different observations obtained during the test program

Table 2 lists the stars included in the eight sets of observations which were used in calibrating the mechanical axis The star distributions for each night are given in section 3 1 of the report (figures 6-13)

Table 3 provides a tabulation of the X and Y level readings together with corresponding temperatures and pressures

Table 4 summarizes the observational data obtained from the celestial radio sources indicating the methods of recording

Table 5 and 6 provide samples of the computer printout of the radio star observations for the fixed position and single axis scanning methods

Figures 1 through 6 are samples of the graphical recordings of the different radio sources using the various observing techniques

TABLE 1

FIELD TESTS DATA OBTAINED FOR

USB ANTENNA ALIGNMENT STUDIES

DATE	TIME (local)	OBSERVATIONS					REMARKS
		Level Vials	Optical Targets	Optical Stars	Radio Stars	rf Bore-sighting	
29 April	2100	x				x	
	2230	x					
30 April	1730	x	x			x	
	2030	x	x			x	
	2100	x		x		x	8 star obs
	2330	x	x			x	
1 May	1600	x	x			x	
	1700	x					
	2030	x	x			x	
	2230	x		x		x	40 star obs
	2330	x		x			
6 May	2200	x	x			x	
8 May	1430	x				x	
	1530	x	x				
9 May	1030	x				x	
15 May	0930	x	x			x	
	1100	x				x	
	1300	x	x			x	
	1400	x				x	
	1500	x	x			x	
	1600	x					
	1630						
	1730	x	x			x	
	2030	x	x			x	
	2130	x		x		x	30 star obs
	2230	x		x			
	2400	x				x	
18 May	1630	x	x			x	Apollo 10 track #1
	1730	x				x	
20 May	1400	x	x			x	Apollo 10 track #2
	1500	x					

TABLE 1

FIELD TESTS DATA OBTAINED FOR

USB ANTENNA ALIGNMENT STUDIES

(Continued)

DATE	TIME (local)	OBSERVATIONS					REMARKS
		Level Vials	Optical Targets	Optical Stars	Radio Stars	rf Bore-sighting	
22 May	1000	x					Apollo 10 tracks #3, 4, & 5
	2200	x	x			x	
	2400	x					
23 May	2200	x	x			x	Apollo 10 tracks #6 & 7 Photos of moon obtained during track #7 (poor quality)
	2300	x				x	
24 May	2100	x	x			x	Apollo 10 tracks #8 & 9
	2300	x	x				
25 May	2130	x	x	x		x	Apollo 10 tracks #10 & 11 5 star obs. (visibility poor)
	2300	x				x	
24 June	1700	x	x				Radio stars attempted
	2000	x					
	2100	x	x				
	2400	x	x				
26 June	2030	x					Radio stars attempted
	2300	x		x			
27 June	0100	x		x			19 star obs
30 June	2200						Radio stars attempted
2 July	2000						Radio stars attempted.
3 July	1330	x	x				Sun, Cassiopeia A, and Cygnus A observed (Only peak voltage timed)
	1630	x	x		x		
	2300	x	x	x	x		
8 July	2200				x		Cass A observed - high noise level

TABLE 1

FIELD TESTS DATA OBTAINED FOR

USB ANTENNA ALIGNMENT STUDIES

(Continued)

DATE	TIME (local)	OBSERVATIONS					REMARKS
		Level Vials	Optical Targets	Optical Stars	Radio Stars	rf Bore-sighting	
11 July	2000				x		Cass A observed - high noise level
12 July	2300				x		Cass A observed wit TTY 6 sec tape
16 July	1100	x	x			x	Apollo 11 track #1
	1700	x	x			x	Apollo 11 track #2
	2100	x		x			Apollo 11 track #3
	2200	x					
	2400			x	x		19 star obs. Cass A observed with 1 sec TDY printout.
17 July	2000	x					Apollo 11 track #4
18 July	1630	x					Apollo 11 track #5
	1730	x				x	Apollo 11 track #6
	1900	x				x	Apollo 11 track #7
19 July	1230	x					Apollo 11 track #8
	1330	x					
	1500	x					Apollo 11 track #9
21 July	1680	x					Apollo 11 track #10
22 July	0930	x	x				
	1030	x	x				
	1130	x	x				
	1300	x	x				
	1500	x	x				
	1630	x	x				
	2000	x	x			x	Apollo tracks #11,
	2400	x	x				12 and 13
23 July	1000	x	x				
	1100	x	x				Apollo track #14
	1200	x	x				
	1300	x	x				
	1500	x	x				

TABLE 1

FIELD TESTS DATA OBTAINED FOR

USB ANTENNA ALIGNMENT STUDIES (Continued)

DATE	TIME (local)	OBSERVATIONS					REMARKS
		Level Vials	Optical Targets	Optical Stars	Radio Stars	rf Bore-sighting	
	1900	x	x				
	2400	x					
24 July	2030	x			x		Apollo tracks #15 & 16, Cass A & Cygnus A with 6 sec TTY printout
	2300	x					
	2400	x					
31 July	2100	x		x			10 star obs
6 Aug	2030	x		x			14 star obs
	2300	x					
	2400	x					
27 Aug	2030	x					
	2200	x		x			12 star obs
	2400	x					
28 Aug	2130	x		x		x	ALSEP track with photos of moon
	2400	x					
3 Sept	2100				x		Cass A with 6 sec TTY printout
12 Sept	2000				x		Cass A, Cygnus A, & 3C400, with digital voltages @ 2- 4 sec
3 Oct	2100	x			x		Cass A, Cygnus A, & 3C400, with digital voltages @ 1 sec
4 Oct	2100	x		x	x		Cass A, Cygnus A, & 3C400, with DVM @ 1 sec , 9 optical star obs

TABLE 2

STARS OBSERVED FOR USB ANTENNA CALIBRATION TESTS

NAME	MAGNITUDE	DATE							
		5 MAY	15 MAY	27 JUNE	18 JULY	1 AUG	7 AUG.	27 AUG	3 OCT
Betelgeuse	0 1	x							
Vega	0 1	x	x	x	x	x	x	x	x
Arcturus	0.2	x	x	x	x	x	x	x	
Capella	0 2	x	x						x
Procyon	0.5	x	x						
Altaır	0.9			x	x	x	x	x	x
Antares	1 2			x	x	x	x		
Pollux	1 2	x							
Spıca	1.2	x	x						
Deneb	1 3		x	x		x	x	x	x
Fomalhaut	1.3								x
Regulus	1 3	x	x						
Alıoth	1 7	x	x	x	x		x	x	
Alkaıd	1 9	x	x	x	x				
Dubhe	1 9	x	x	x	x		x		
Mırfak	1 9								x
Polarıs	2 1		x		x		x	x	
Rasalhague	2 1			x	x	x	x	x	
Alphard	2 2		x						
Alpheratz	2 2							x	
Denebola	2 2		x						
Kochab	2 2		x	x	x		x		
Alphecca	2 3		x	x	x				
Eltanın	2 4		x		x	x		x	

TABLE 3

ANTENNA LEVEL DATA FOR PERIOD 4/29/69 - 10/4/69

DATE	DAY NO.	HOUR (GMT)	X-ANGLE (degrees)	Y-ANGLE (degrees)	TEMP (deg C)	PRESSURE (in Hg)
29 April	120	0040	- 018	004	16 0	29 88
		0240	- 017	003	14 0	29 90
29 April	120	2130	- 021	003	14.8	29 99
		2230	- 021	.002		
1 May	121	0030	-.020	003	11 0	30 04
		0110	-.020	003		
		0325	- 018	.001	10 0	30 04
1 May	121	2020	- 024	001	20 0	30 10
		2110	- 027	000	21.0	30 11
2 May	122	0030	- 021	003	14 5	30 11
		0250	- 018	001	9 5	30 15
		0340	- 019	001	8 6	30 15
6 May	126	0145	- 016	007	17 0	29 82
8 May	128	1840	- 013	010	25 5	29 80
		1942	-.014	007	24 5	29 80
9 May	129	1435	- 013	005	18 3	
15 May	135	1335	- 008	002	17 3	30 20
		1505	- 007	001	19 0	30 20
		1700	- 011	002	20.8	30.20
		1800	- 014	- 001	21 0	30 19
		1900	- 019	002	22 4	30 17
		1950	- 018	000	25 0	30 16
		2030	- 021	001	26 5	30 16
		2135	- 018	003	29 0	30 16
16 May	136	0032	- 014	005	17 1	30 17
		0125	- 011	006	16 0	30 18
		0220	- 012	003	15 4	30.20
		0404	- 010	003	13.2	30.21
18 May	138	2020	- 007	007	27 0	30 04
		2120	- 008	007	27 0	30 04
		2315	- 005	007	23 5	30 05
20 May	140	1820	- 010	.001	28 8	29 85
		1905	- 009	002	29.0	29 85

TABLE 3

ANTENNA LEVEL DATA FOR PERIOD 4/29/69 - 10/4/69

(Continued)

DATE	DAY NO.	HOUR (GMT)	X-ANGLE (degrees)	Y-ANGLE (degrees)	TEMP (deg C)	PRESSURE (in Hg)
23 May	143	0225	-.005	005	16 5	30 08
		0405	- 005	003	14 0	30 10
24 May	144	0230	- 003	004		
		0320	- 001	005	18 0	30.04
25 May	145	0105	- 003	005	17.2	29 92
		0255	- 001	.003	14 5	29 92
26 May	146	0140	000	.004	18 0	29 85
		0250	.001	004	18 0	29 88
24 June	175	1710	.019	007	32 4	29 74
		2020	010	010	35 4	29 75
		2150	.011	.010	35 0	29 74
25 June	176	0025	012	007	24 2	29.75
27 June	178	0030	010	010	24 5	30 05
		0340	016	006	21 5	30.06
		0545	018	005	20 7	30 06
3 July	184	1730	.030	002	32 3	29 86
		2020	025	010	35 4	29 85
4 July	185	0405	026	006	17 4	29 92
12 July	193	2255	025	004	24.8	29 74
16 July	197	1450	041	004	31 0	30 13
		1525	041	004	31.0	30 13
		2140	.030	010	33 5	30 06
17 July	198	0148	.037	.007	25 1	30.08
		0345	035	008	24.0	30 08
18 July	199	0040	033	010	29 5	30 01
18 July	199	2100	034	011		
		2235	035	010		
19 July	200	1630	.040	006	35 0	30 06
		1730	039	006	34.5	29 98
		1930	037	009	31 5	29 95

TABLE 3

ANTENNA LEVEL DATA FOR PERIOD 4/29/69 - 10/4/69

(Continued)

DATE	DAY NO.	HOUR (GMT)	X-ANGLE (degrees)	Y-ANGLE (degrees)	TEMP. (deg C)	PRESSURE (in Hg)
20 July	201	2100	039	.008	30 3	29 87
21 July	202	1340	046		29 8	29 93
		1435	046	003	26 5	29 95
		1545	046	003	29 5	29 94
		1650	.047	.004	29 3	29 92
		1940	.043	006	30 0	29 91
		2045	047	006	27 0	29 91
22 July	203	0040	048	006	24 0	29.94
		0410	051	006		
22 July	203	1435	.050	004	30 0	29 96
		1520	.050	004	29 5	29 98
		1615	051	004	30 0	29 96
		1720	052	006	31 8	29 95
		1925	050	006	31.0	29 92
		2325	052	.006	24.0	29 93
23 July	204	0430	.053	005	22 0	29 93
24 July	205	0045	054	.003	22 0	29 85
		0230	057	003		
1 Aug	213	0120	067	009		
		0320	068	007		
7 Aug	219	0040	066	009	22 0	29 95
		0300	067	.005	20.0	29 98
		0340	067	006	20 0	29 98
28 Aug	240	0025	.082	005	18 0	30 15
		0140	087	004	16.5	30 17
		0400	088	003	13 5	30 18
29 Aug	241	0130	084	006	19.0	30 20
		0305	089	003	17 0	30 20
3 Oct	276	0045	107	.004		
4 Oct	277	0115	107	.002	14.0	30 10
		0315	107	.000	14 0	30 15

TABLE 4

OBSERVATIONAL DATA FOR RADIO STAR EXPERIMENTS

DAY	OBSERVATION METHOD OR EQUIPMENT	RECORDED DATA	
		RADIO SIGNALS	X AND Y ANGLES
185	Single Axis Scans @ 1/2°/sec--Cass A & Cygnus A	Beckman graph with serial time code	TDP slow speed (6 sec)
198	Single Axis Scans @ 1/8°/sec--Cass A & Cygnus A	Beckman graph with serial time code.	TDP high speed (1 sec)
206	Single Axis Scans @ 1/8-1/2°/sec--Cass A & Cygnus A	Beckman graph and digital voltmeter (dvm) readings every 2- 4 sec	Computer p/o every 2- 4 sec
256	Fixed Position--Cass A, Cygnus A; & 3C400	Beckman graph and dvm readings every 1 sec	Computer p/o every .1 sec.
277	Fixed Position--Cass A, Cygnus A, & 3C400 Single Axis Scans--Cass, Cygnus A, & 3C400 Incremental Offsets (.2°)--Cass A (APP tape) "Peaking Up" (3° offsets)--Cass A (APP tape) Sector Scan (1/2°--N,S,E & W)--Cass A (APP tape) Raster Scan (1/2° & 1° N-S & E-W)--Cass A (APP tape)	Beckman graph and dvm readings every .1 sec.	Computer p/o every 1 sec
278	Incremental Offsets (1°)--Cass (APP tape) Sector Scan (1/2°--N,S,E & W)--Cass A (APP tape) Raster Scan (1/2° N-S & E-W)--Cass A (APP tape)	Beckman graph and dvm readings (1 sec avg)	Computer p/o every 1 sec

TABLE 5

DVM READINGS FOR CASSIOPEIA A

FIXED POSITION METHOD

GMT	X	Y	DVM
256:02:04:14.4	+23.5141	+25.3193	01044
256:02:04:15.4	+23.5141	+25.3193	01054
256:02:04:16.4	+23.5141	+25.3193	01057
256:02:04:17.4	+23.5141	+25.3193	01048
256:02:04:18.4	+23.5141	+25.3193	01049
256.02:04:19.4	+23.5141	+25.3193	01056
256:02:04:20.4	+23.5141	+25.3193	01061
256:02:04:21.4	+23.5141	+25.3193	01058
256:02:04:22.4	+23.5141	+25.3193	01069
256:02:04:23.4	+23.5141	+25.3193	01068
256:02:04:24.4	+23.5141	+25.3193	01065
256:02:04:25.4	+23.5141	+25.3193	01071
256:02:04:26.4	+23.5141	+25.3193	01072
256:02:04:27.4	+23.5141	+25.3193	01071
256:02:04:28.4	+23.5141	+25.3193	01063
256:02:04:29.4	+23.5141	+25.3193	01072
256:02:04:30.4	+23.5141	+25.3193	01079
256:02:04:31.4	+23.5141	+25.3193	01087
256:02:04:32.4	+23.5141	+25.3193	01082
256:02:04:33.4	+23.5141	+25.3193	01092
256:02:04:34.4	+23.5141	+25.3193	01090
256:02:04:35.4	+23.5141	+25.3193	01104
256:02:04:36.4	+23.5141	+25.3193	01109
256:02:04:37.4	+23.5141	+25.3193	01102
256:02:04:38.4	+23.5141	+25.3193	01116
256:02:04:39.4	+23.5141	+25.3193	01131
256:02:04:40.4	+23.5141	+25.3193	01143
256:02:04:41.4	+23.5141	+25.3193	01142
256:02:04:42.4	+23.5141	+25.3193	01144
256:02:04:43.4	+23.5141	+25.3193	01153
256:02:04:44.4	+23.5141	+25.3193	01156
256:02:04:45.4	+23.5141	+25.3193	01168
256:02:04:46.4	+23.5141	+25.3193	01177
256:02:04:47.4	+23.5141	+25.3193	01175
256:02:04:48.4	+23.5141	+25.3193	01182
256:02:04:49.4	+23.5141	+25.3193	01188
256:02:04:50.4	+23.5141	+25.3193	01205
256:02:04:51.4	+23.5141	+25.3193	01208
256:02:04:52.4	+23.5141	+25.3193	01204
256:02:04:53.4	+23.5141	+25.3193	01194
256:02:04:54.4	+23.5141	+25.3193	01212
256:02:04:55.4	+23.5141	+25.3193	01214
256:02:04:56.4	+23.5141	+25.3193	01214
256:02:04:57.4	+23.5141	+25.3193	01228
256:02:04:58.4	+23.5141	+25.3193	01222
256:02:04:59.4	+23.5141	+25.3193	01235
256:02:05:00.4	+23.5141	+25.3193	01244
256:02:05:01.4	+23.5141	+25.3193	01250
256:02:05:02.4	+23.5141	+25.3193	01254
256:02:05:03.4	+23.5141	+25.3193	01261

Average of 10 readings over 1 second interval

Table 5 (Cont'd)

GMT	X	Y	DVM
256:02:05:04.4	+23.5141	+25.3193	01276
256:02:05:05.4	+23.5141	+25.3193	01281
256:02:05:06.4	+23.5141	+25.3193	01275
256:02:05:07.4	+23.5141	+25.3193	01280
256:02:05:08.4	+23.5141	+25.3193	01288
256:02:05:09.4	+23.5141	+25.3193	01291
256:02:05:10.4	+23.5141	+25.3193	01289
256:02:05:11.4	+23.5141	+25.3193	01277
256:02:05:12.4	+23.5141	+25.3193	01285
256:02:05:13.4	+23.5141	+25.3193	01292
256:02:05:14.4	+23.5141	+25.3193	01291
256:02:05:15.4	+23.5141	+25.3193	01294
256:02:05:16.4	+23.5141	+25.3193	01292
256:02:05:17.4	+23.5141	+25.3193	01300
256:02:05:18.4	+23.5141	+25.3193	01305
256:02:05:19.4	+23.5141	+25.3193	01295
256:02:05:20.4	+23.5141	+25.3193	01307
256:02:05:21.4	+23.5141	+25.3193	01308
256:02:05:22.4	+23.5141	+25.3193	01316
256:02:05:23.4	+23.5141	+25.3193	01326
256:02:05:24.4	+23.5141	+25.3193	01330
256:02:05:25.4	+23.5141	+25.3193	01329
256:02:05:26.4	+23.5141	+25.3193	01338
256:02:05:27.4	+23.5141	+25.3193	01343
256:02:05:28.4	+23.5141	+25.3193	01343
256:02:05:29.4	+23.5141	+25.3193	01350
256:02:05:30.4	+23.5141	+25.3193	01354
256:02:05:31.4	+23.5141	+25.3193	01369
256:02:05:32.4	+23.5141	+25.3193	01370
256:02:05:33.4	+23.5141	+25.3193	01363
256:02:05:34.4	+23.5141	+25.3193	01370
256:02:05:35.4	+23.5141	+25.3193	01366
256:02:05:36.4	+23.5141	+25.3193	01374
256:02:05:37.4	+23.5141	+25.3193	01338
256:02:05:38.4	+23.5141	+25.3193	01377
256:02:05:39.4	+23.5141	+25.3193	01386
256:02:05:40.4	+23.5141	+25.3193	01388
256:02:05:41.4	+23.5141	+25.3193	01387
256:02:05:42.4	+23.5141	+25.3193	01344
256:02:05:43.4	+23.5141	+25.3193	01369
256:02:05:44.4	+23.5141	+25.3193	01361
256:02:05:45.4	+23.5141	+25.3193	01368
256:02:05:46.4	+23.5141	+25.3193	01373
256:02:05:47.4	+23.5141	+25.3193	01372
256:02:05:48.4	+23.5141	+25.3193	01375
256:02:05:49.4	+23.5141	+25.3193	01372
256:02:05:50.4	+23.5141	+25.3193	01389
256:02:05:51.4	+23.5141	+25.3193	01378
256:02:05:52.4	+23.5141	+25.3193	01387
256:02:05:53.4	+23.5141	+25.3193	01372

Table 5 (Cont'd)

GMT	X	Y	DVM	
256:02:05:54.4	+23.5141	+25.3193	01370	
256:02:05:55.4	+23.5141	+25.3193	01368	
256:02:05:56.4	+23.5141	+25.3193	01357	
256:02:05:57.4	+23.5141	+25.3193	01363	
256:02:05:58.4	+23.5141	+25.3193	01351	
256:02:05:59.4	+23.5141	+25.3193	01351	
256:02:06:00.4	+23.5141	+25.3193	01358	
256:02:06:01.4	+23.5141	+25.3193	01353	
256:02:06:02.4	+23.5141	+25.3193	01344	
256:02:06:03.4	+23.5141	+25.3193	01349	
256:02:06:04.4	+23.5141	+25.3193	01358	
256.02:06:05.4	+23.5141	+25.3193	01414	
256:02:06:06.4	+23.5141	+25.3193	01511	
256:02:06:07.4	+23.5141	+25.3193	01443	
256:02:06:08.4	+23.5141	+25.3193	01391	
256:02:06:09.4	+23.5141	+25.3193	01392	
256:02:06:10.4	+23.5141	+25.3193	01378	
256:02:06:11.4	+23.5141	+25.3193	01379	
256:02:06:12.4	+23.5141	+25.3193	01379	
256:02:06:13.4	+23.5141	+25.3193	01370	
256:02:06:14.4	+23.5141	+25.3193	01370	
256:02:06:15.4	+23.5141	+25.3193	01375	
256:02:06:16.4	+23.5141	+25.3193	01376	
256:02:06:17.4	+23.5141	+25.3193	01376	
256:02:06:18.4	+23.5141	+25.3193	01372	← Computed time of peak voltage by curve 02 06 19 1
256:02:06:19.4	+23.5141	+25.3193	01385	
256:02:06:20.4	+23.5141	+25.3193	01379	
256:02:06:21.4	+23.5141	+25.3193	01373	
256:02:06:22.4	+23.5141	+25.3193	01381	
256:02:06:23.4	+23.5141	+25.3193	01393	
256:02:06:24.4	+23.5141	+25.3193	01393	
256:02:06:25.4	+23.5141	+25.3193	01390	
256:02:06:26.4	+23.5141	+25.3193	01403	
256:02:06:27.4	+23.5141	+25.3193	01402	
256:02:06:28.4	+23.5141	+25.3193	01393	
256:02:06:29.4	+23.5141	+25.3193	01411	
256:02:06:30.4	+23.5141	+25.3193	01368	
256:02:06:31.4	+23.5141	+25.3193	01403	
256:02:06:32.4	+23.5141	+25.3193	01403	
256:02:06:33.4	+23.5141	+25.3193	01393	
256:02:06:34.4	+23.5141	+25.3193	01406	
256:02:06:35.4	+23.5141	+25.3193	01403	
256:02:06:36.4	+23.5141	+25.3193	01407	
256:02:06:37.4	+23.5141	+25.3193	01405	
256:02:06:38.4	+23.5141	+25.3193	01399	
256:02:06:39.4	+23.5141	+25.3193	01390	
256:02:06:40.4	+23.5141	+25.3193	01399	
256:02:06:41.4	+23.5141	+25.3193	01402	
256:02:06:42.4	+23.5141	+25.3193	01400	
256:02:06:43.4	+23.5141	+25.3193	01405	

Table 5 (Cont'd)

GMT	X	Y	DVM
256:02:06:44.4	+23.5141	+25.3193	01394
256:02:06:45.4	+23.5141	+25.3193	01397
256:02:06:46.4	+23.5141	+25.3193	01391
256:02:06:47.4	+23.5141	+25.3193	01370
256:02:06:48.4	+23.5141	+25.3193	01394
256:02:06:49.4	+23.5141	+25.3193	01375
256:02:06:50.4	+23.5141	+25.3193	01392
256:02:06:51.4	+23.5141	+25.3193	01374
256:02:06:52.4	+23.5141	+25.3193	01378
256:02:06:53.4	+23.5141	+25.3193	01366
256:02:06:54.4	+23.5141	+25.3193	01363
256:02:06:55.4	+23.5141	+25.3193	01364
256:02:06:56.4	+23.5141	+25.3193	01365
256:02:06:57.4	+23.5141	+25.3193	01366
256:02:06:58.4	+23.5141	+25.3193	01359
256:02:06:59.4	+23.5141	+25.3193	01349
256:02:07:00.4	+23.5141	+25.3193	01343
256:02:07:01.4	+23.5141	+25.3193	01336
256:02:07:02.4	+23.5141	+25.3193	01329
256:02:07:03.4	+23.5141	+25.3193	01315
256:02:07:04.4	+23.5141	+25.3193	01297
256:02:07:05.4	+23.5141	+25.3193	01303
256:02:07:06.4	+23.5141	+25.3193	01292
256:02:07:07.4	+23.5141	+25.3193	01292
256:02:07:08.4	+23.5141	+25.3193	01285
256:02:07:09.4	+23.5141	+25.3193	01268
256:02:07:10.4	+23.5141	+25.3193	01277
256:02:07:11.4	+23.5141	+25.3193	01271
256:02:07:12.4	+23.5141	+25.3193	01257
256:02:07:13.4	+23.5141	+25.3193	01259
256:02:07:14.4	+23.5141	+25.3193	01248
256:02:07:15.4	+23.5141	+25.3193	01243
256:02:07:16.4	+23.5141	+25.3193	01246
256:02:07:17.4	+23.5141	+25.3193	01240
256:02:07:18.4	+23.5141	+25.3193	01237
256:02:07:19.4	+23.5141	+25.3193	01226
256:02:07:20.4	+23.5141	+25.3193	01235
256:02:07:21.4	+23.5141	+25.3193	01233
256:02:07:22.4	+23.5141	+25.3193	01233
256:02:07:23.4	+23.5141	+25.3193	01229
256:02:07:24.4	+23.5141	+25.3193	01236
256:02:07:25.4	+23.5141	+25.3193	01234
256:02:07:26.4	+23.5141	+25.3193	01227
256:02:07:27.4	+23.5141	+25.3193	01237
256:02:07:28.4	+23.5141	+25.3193	01239
256:02:07:29.4	+23.5141	+25.3193	01245
256:02:07:30.4	+23.5141	+25.3193	01243
256:02:07:31.4	+23.5141	+25.3193	01239
256:02:07:32.4	+23.5141	+25.3193	01235
256:02:07:33.4	+23.5141	+25.3193	01239

Table 5 (Cont'd)

GMT	X	Y	DVM
256:02:07:34.4	+23.5141	+25.3193	01239
256:02:07:35.4	+23.5141	+25.3193	01235
256:02:07:36.4	+23.5141	+25.3193	01235
256:02:07:37.4	+23.5141	+25.3193	01228
256:02:07:38.4	+23.5141	+25.3193	01227
256:02:07:39.4	+23.5141	+25.3193	01221
256:02:07:40.4	+23.5141	+25.3193	01218
256:02:07:41.4	+23.5141	+25.3193	01221
256:02:07:42.4	+23.5141	+25.3193	01223
256:02:07:43.4	+23.5141	+25.3193	01227
256:02:07:44.4	+23.5141	+25.3193	01216
256:02:07:45.4	+23.5141	+25.3193	01212
256:02:07:46.4	+23.5141	+25.3193	01208
256:02:07:47.4	+23.5141	+25.3193	01215
256:02:07:48.4	+23.5141	+25.3193	01218
256:02:07:49.4	+23.5141	+25.3193	01214
256:02:07:50.4	+23.5141	+25.3193	01209
256:02:07:51.4	+23.5141	+25.3193	01214
256:02:07:52.4	+23.5141	+25.3193	01211
256:02:07:53.4	+23.5141	+25.3193	01216
256:02:07:54.4	+23.5141	+25.3193	01214
256:02:07:55.4	+23.5141	+25.3193	01199
256:02:07:56.4	+23.5141	+25.3193	01196
256:02:07:57.4	+23.5141	+25.3193	01200
256:02:07:58.4	+23.5141	+25.3193	01196
256:02:07:59.4	+23.5141	+25.3193	01174
256:02:08:00.4	+23.5141	+25.3193	01170
256:02:08:01.4	+23.5141	+25.3193	01168
256:02:08:02.4	+23.5141	+25.3193	01173
256:02:08:03.4	+23.5141	+25.3193	01172
256:02:08:04.4	+23.5141	+25.3193	01166
256:02:08:05.4	+23.5141	+25.3193	01155
256:02:08:06.4	+23.5141	+25.3193	01145
256:02:08:07.4	+23.5141	+25.3193	01141
256:02:08:08.4	+23.5141	+25.3193	01140
256:02:08:09.4	+23.5141	+25.3193	01126
256:02:08:10.4	+23.5141	+25.3193	01133
256:02:08:11.4	+23.5141	+25.3193	01126
256:02:08:12.4	+23.5141	+25.3193	01114
256:02:08:13.4	+23.5141	+25.3193	01111
256:02:08:14.4	+23.5141	+25.3193	01106
256:02:08:15.4	+23.5141	+25.3193	01114
256:02:08:16.4	+23.5141	+25.3193	01108
256:02:08:17.4	+23.5141	+25.3193	01099
256:02:08:18.4	+23.5141	+25.3193	01091
256:02:08:19.4	+23.5141	+25.3193	01089
256:02:08:20.4	+23.5141	+25.3193	01085
256:02:08:21.4	+23.5141	+25.3193	01075
256:02:08:22.4	+23.5141	+25.3193	01057
256:02:08:23.4	+23.5141	+25.3193	01065

TABLE 6
DVM READINGS FOR CASSEIOPEIA A
SINGLE AXIS SCAN METHOD

GMT	X	Y	DVM
256:03:34:35.2	+11.4936	+21.0107	00676
256:03:34:35.3	+11.4951	+21.0107	00681
256:03:34:35.4	+11.4965	+21.0107	00681
256:03:34:35.5	+11.5012	+21.0107	00679
256:03:34:35.6	+11.5012	+21.0107	00693
256:03:34:35.7	+11.5061	+21.0107	00727
256:03:34:35.8	+11.5087	+21.0107	00712
256:03:34:35.9	+11.5095	+21.0107	00709
256:03:34:36.0	+11.5151	+21.0107	00733
256:03:34:36.1	+11.5151	+21.0107	00742
256:03:34:36.2	+11.5185	+21.0100	00727
256:03:34:36.3	+11.5227	+21.0100	00717
256:03:34:36.4	+11.5227	+21.0100	00728
256:03:34:36.5	+11.5273	+21.0107	00705
256:03:34:36.6	+11.5302	+21.0107	00746
256:03:34:36.7	+11.5314	+21.0107	00708
256:03:34:36.8	+11.5363	+21.0107	00755
256:03:34:36.9	+11.5375	+21.0100	00746
256:03:34:37.0	+11.5390	+21.0100	00763
256:03:34:37.1	+11.5446	+21.0100	00760
256:03:34:37.2	+11.5446	+21.0100	00782
256:03:34:37.3	+11.5480	+21.0107	00787
256:03:34:37.4	+11.5527	+21.0107	00769
256:03:34:37.5	+11.5527	+21.0107	00778
256:03:34:37.6	+11.5561	+21.0107	00783
256:03:34:37.7	+11.5603	+21.0107	00757
256:03:34:37.8	+11.5603	+21.0107	00767
256:03:34:37.9	+11.5651	+21.0107	00764
256:03:34:38.0	+11.5671	+21.0107	00776
256:03:34:38.1	+11.5678	+21.0100	00785
256:03:34:38.2	+11.5727	+21.0100	00805
256:03:34:38.3	+11.5754	+21.0107	00813
256:03:34:38.4	+11.5761	+21.0107	00824
256:03:34:38.5	+11.5815	+21.0107	00813
256:03:34:38.6	+11.5822	+21.0107	00798
256:03:34:38.7	+11.5852	+21.0107	00807
256:03:34:38.8	+11.5891	+21.0107	00813
256:03:34:38.9	+11.5898	+21.0107	00783
256:03:34:39.0	+11.5939	+21.0107	00831
256:03:34:39.1	+11.5974	+21.0107	00802
256:03:34:39.2	+11.5974	+21.0107	00837
256:03:34:39.3	+11.6030	+21.0100	00815
256:03:34:39.4	+11.6042	+21.0100	00838
256:03:34:39.5	+11.6064	+21.0100	00822
256:03:34:39.6	+11.6110	+21.0100	00875
256:03:34:39.7	+11.6125	+21.0107	00851
256:03:34:39.8	+11.6152	+21.0107	00873
256:03:34:39.9	+11.6193	+21.0107	00885
256:03:34:40.0	+11.6201	+21.0107	00848
256:03:34:40.1	+11.6242	+21.0107	00855

Scanning in X axis at about 0°025/sec Y axis fixed

Table 6 (Cont'd)

GMT	X	Y	DVM
256:03:34:40.2	+11.6276	+21.0107	00827
256:03:34:40.3	+11.6276	+21.0107	00860
256:03:34:40.4	+11.6330	+21.0107	00860
256:03:34:40.5	+11.6359	+21.0107	00832
256:03:34:40.6	+11.6364	+21.0107	00852
256:03:34:40.7	+11.6420	+21.0107	00893
256:03:34:40.8	+11.6435	+21.0107	00898
256:03:34:40.9	+11.6462	+21.0107	00917
256:03:34:41.0	+11.6511	+21.0107	00910
256:03:34:41.1	+11.6516	+21.0107	00918
256:03:34:41.2	+11.6550	+21.0107	00894
256:03:34:41.3	+11.6591	+21.0107	00923
256:03:34:41.4	+11.6599	+21.0107	00890
256:03:34:41.5	+11.6647	+21.0107	00905
256:03:34:41.6	+11.6674	+21.0107	00911
256:03:34:41.7	+11.6689	+21.0107	00925
256:03:34:41.8	+11.6743	+21.0107	00946
256:03:34:41.9	+11.6757	+21.0100	00937
256:03:34:42.0	+11.6770	+21.0100	00912
256:03:34:42.1	+11.6826	+21.0100	00930
256:03:34:42.2	+11.6833	+21.0100	00924
256:03:34:42.3	+11.6867	+21.0100	00930
256:03:34:42.4	+11.6909	+21.0100	00939
256:03:34:42.5	+11.6914	+21.0107	00953
256:03:34:42.6	+11.6962	+21.0107	00944
256:03:34:42.7	+11.6989	+21.0107	00934
256:03:34:42.8	+11.6997	+21.0107	00930
256:03:34:42.9	+11.7053	+21.0107	00949
256:03:34:43.0	+11.7072	+21.0107	00960
256:03:34:43.1	+11.7094	+21.0107	00966
256:03:34:43.2	+11.7141	+21.0107	00973
256:03:34:43.3	+11.7148	+21.0100	01016
256:03:34:43.4	+11.7189	+21.0100	00976
256:03:34:43.5	+11.7224	+21.0100	00978
256:03:34:43.6	+11.7231	+21.0100	00985
256:03:34:43.7	+11.7285	+21.0107	00973
256:03:34:43.8	+11.7307	+21.0107	00982
256:03:34:43.9	+11.7319	+21.0107	00965
256:03:34:44.0	+11.7375	+21.0107	00977
256:03:34:44.1	+11.7382	+21.0107	00997
256:03:34:44.2	+11.7402	+21.0100	00990
256:03:34:44.3	+11.7458	+21.0100	01010
256:03:34:44.4	+11.7458	+21.0100	01004
256:03:34:44.5	+11.7500	+21.0100	01029
256:03:34:44.6	+11.7539	+21.0100	01018
256:03:34:44.7	+11.7539	+21.0100	01005
256:03:34:44.8	+11.7595	+21.0100	01032
256:03:34:44.9	+11.7614	+21.0107	01009
256:03:34:45.0	+11.7629	+21.0107	01029
256:03:34:45.1	+11.7678	+21.0107	01000

Table 6 (Cont'd)

GMT	X	Y	DVM
256:03:34:45.2	+11.7690	+21.0107	01000
256:03:34:45.3	+11.7724	+21.0107	00990
256:03:34:45.4	+11.7766	+21.0107	01010
256:03:34:45.5	+11.7766	+21.0107	01022
256:03:34:45.6	+11.7814	+21.0100	01026
256:03:34:45.7	+11.7841	+21.0100	01051
256:03:34:45.8	+11.7856	+21.0100	01063
256:03:34:45.9	+11.7910	+21.0100	01068
256:03:34:46.0	+11.7917	+21.0100	01060
256:03:34:46.1	+11.7951	+21.0100	01042
256:03:34:46.2	+11.8000	+21.0100	01059
256:03:34:46.3	+11.8000	+21.0100	01026
256:03:34:46.4	+11.8041	+21.0100	01048
256:03:34:46.5	+11.8076	+21.0107	01075
256:03:34:46.6	+11.8083	+21.0107	01058
256:03:34:46.7	+11.8129	+21.0107	01056
256:03:34:46.8	+11.8159	+21.0100	01069
256:03:34:46.9	+11.8171	+21.0100	01084
256:03:34:47.0	+11.8227	+21.0100	01073
256:03:34:47.1	+11.8239	+21.0100	01072
256:03:34:47.2	+11.8254	+21.0100	01090
256:03:34:47.3	+11.8308	+21.0107	01103
256:03:34:47.4	+11.8308	+21.0107	01090
256:03:34:47.5	+11.8349	+21.0107	01081
256:03:34:47.6	+11.8391	+21.0107	01089
256:03:34:47.7	+11.8391	+21.0107	01075
256:03:34:47.8	+11.8447	+21.0100	01088
256:03:34:47.9	+11.8466	+21.0100	01061
256:03:34:48.0	+11.8474	+21.0100	01068
256:03:34:48.1	+11.8527	+21.0100	01088
256:03:34:48.2	+11.8542	+21.0100	01090
256:03:34:48.3	+11.8569	+21.0100	01094
256:03:34:48.4	+11.8610	+21.0107	01088
256:03:34:48.5	+11.8618	+21.0107	01109
256:03:34:48.6	+11.8671	+21.0107	01046
256:03:34:48.7	+11.8693	+21.0107	01098
256:03:34:48.8	+11.8713	+21.0107	01085
256:03:34:48.9	+11.8769	+21.0107	01120
256:03:34:49.0	+11.8776	+21.0100	01094
256:03:34:49.1	+11.8818	+21.0107	01105
256:03:34:49.2	+11.8852	+21.0107	01099
256:03:34:49.3	+11.8857	+21.0100	01142
256:03:34:49.4	+11.8920	+21.0107	01104
256:03:34:49.5	+11.8933	+21.0107	01111
256:03:34:49.6	+11.8962	+21.0107	01117
256:03:34:49.7	+11.9016	+21.0107	01113
256:03:34:49.8	+11.9016	+21.0107	01134
256:03:34:49.9	+11.9057	+21.0107	01141
256:03:34:50.0	+11.9106	+21.0100	01109
256:03:34:50.1	+11.9106	+21.0107	01117

Table 6 (Cont'd)

GMT	X	Y	DVM
256:03:34:50.2	+11.9160	+21.0107	01127
256:03:34:50.3	+11.9187	+21.0100	01084
256:03:34:50.4	+11.9194	+21.0107	01122
256:03:34:50.5	+11.9262	+21.0107	01113
256:03:34:50.6	+11.9270	+21.0107	01112
256:03:34:50.7	+11.9296	+21.0107	01151
256:03:34:50.8	+11.9353	+21.0107	01128
256:03:34:50.9	+11.9353	+21.0107	01124
256:03:34:51.0	+11.9394	+21.0107	01155
256:03:34:51.1	+11.9436	+21.0107	01117
256:03:34:51.2	+11.9440	+21.0107	01126
256:03:34:51.3	+11.9497	+21.0107	01132
256:03:34:51.4	+11.9523	+21.0107	01071
256:03:34:51.5	+11.9538	+21.0107	01137
256:03:34:51.6	+11.9592	+21.0107	01088
256:03:34:51.7	+11.9599	+21.0107	01113
256:03:34:51.8	+11.9633	+21.0107	01121
256:03:34:51.9	+11.9682	+21.0107	01113
256:03:34:52.0	+11.9689	+21.0107	01130
256:03:34:52.1	+11.9731	+21.0107	01114
256:03:34:52.2	+11.9765	+21.0107	01126
256:03:34:52.3	+11.9777	+21.0107	01129
256:03:34:52.4	+11.9833	+21.0107	01140
256:03:34:52.5	+11.9846	+21.0107	01147
256:03:34:52.6	+11.9875	+21.0107	01145
256:03:34:52.7	+11.9929	+21.0107	01138
256:03:34:52.8	+11.9929	+21.0107	01116
256:03:34:52.9	+11.9970	+21.0107	01121
256:03:34:53.0	+12.0012	+21.0107	01126
256:03:34:53.1	+12.0019	+21.0107	01127
256:03:34:53.2	+12.0065	+21.0107	01122
256:03:34:53.3	+12.0095	+21.0107	01166
256:03:34:53.4	+12.0107	+21.0107	01160
256:03:34:53.5	+12.0170	+21.0107	01143
256:03:34:53.6	+12.0175	+21.0107	01159
256:03:34:53.7	+12.0205	+21.0107	01136
256:03:34:53.8	+12.0258	+21.0107	01130
256:03:34:53.9	+12.0258	+21.0100	01112
256:03:34:54.0	+12.0307	+21.0100	01111
256:03:34:54.1	+12.0341	+21.0107	01122
256:03:34:54.2	+12.0349	+21.0107	01112
256:03:34:54.3	+12.0402	+21.0107	01125
256:03:34:54.4	+12.0417	+21.0107	01155
256:03:34:54.5	+12.0444	+21.0107	01149
256:03:34:54.6	+12.0493	+21.0107	01139
256:03:34:54.7	+12.0500	+21.0107	01144
256:03:34:54.8	+12.0546	+21.0107	01130
256:03:34:54.9	+12.0581	+21.0107	01167
256:03:34:55.0	+12.0588	+21.0107	01137
256:03:34:55.1	+12.0644	+21.0100	01131

Computed time of peak voltage by curve fit
03·34 52 7

Table 6 (Cont'd)

GMT	X	Y	DVM
256:03:35:00.2	+12.2153	+21.0107	01025
256:03:35:00.3	+12.2182	+21.0107	01014
256:03:35:00.4	+12.2194	+21.0107	00996
256:03:35:00.5	+12.2243	+21.0107	00979
256:03:35:00.6	+12.2263	+21.0107	00994
256:03:35:00.7	+12.2285	+21.0107	01000
256:03:35:00.8	+12.2338	+21.0100	01001
256:03:35:00.9	+12.2346	+21.0100	01022
256:03:35:01.0	+12.2373	+21.0100	00984
256:03:35:01.1	+12.2421	+21.0107	00997
256:03:35:01.2	+12.2429	+21.0107	00991
256:03:35:01.3	+12.2478	+21.0107	00973
256:03:35:01.4	+12.2512	+21.0107	01003
256:03:35:01.5	+12.2512	+21.0107	00989
256:03:35:01.6	+12.2573	+21.0107	00980
256:03:35:01.7	+12.2587	+21.0107	00958
256:03:35:01.8	+12.2607	+21.0107	00979
256:03:35:01.9	+12.2663	+21.0107	00974
256:03:35:02.0	+12.2668	+21.0107	00984
256:03:35:02.1	+12.2702	+21.0100	00974
256:03:35:02.2	+12.2744	+21.0100	00962
256:03:35:02.3	+12.2751	+21.0100	00996
256:03:35:02.4	+12.2800	+21.0100	00972
256:03:35:02.5	+12.2827	+21.0107	00987
256:03:35:02.6	+12.2834	+21.0107	00985
256:03:35:02.7	+12.2888	+21.0107	00957
256:03:35:02.8	+12.2902	+21.0107	00926
256:03:35:02.9	+12.2922	+21.0107	00933
256:03:35:03.0	+12.2978	+21.0107	00940
256:03:35:03.1	+12.2978	+21.0100	00962
256:03:35:03.2	+12.3020	+21.0100	00952
256:03:35:03.3	+12.3061	+21.0100	00956
256:03:35:03.4	+12.3061	+21.0100	00939
256:03:35:03.5	+12.3115	+21.0100	00982
256:03:35:03.6	+12.3129	+21.0107	00910
256:03:35:03.7	+12.3156	+21.0107	00934
256:03:35:03.8	+12.3205	+21.0107	00930
256:03:35:03.9	+12.3205	+21.0107	00921
256:03:35:04.0	+12.3251	+21.0107	00907
256:03:35:04.1	+12.3286	+21.0100	00872
256:03:35:04.2	+12.3293	+21.0107	00879
256:03:35:04.3	+12.3342	+21.0100	00868
256:03:35:04.4	+12.3361	+21.0100	00906
256:03:35:04.5	+12.3383	+21.0107	00875
256:03:35:04.6	+12.3432	+21.0100	00870
256:03:35:04.7	+12.3444	+21.0100	00870
256:03:35:04.8	+12.3466	+21.0107	00880
256:03:35:04.9	+12.3520	+21.0107	00899
256:03:35:05.0	+12.3520	+21.0100	00887
256:03:35:05.1	+12.3562	+21.0107	00891

Table 6 (Cont'd)

GMT	X	Y	DVM
256:03:34:55.2	+12.0664	+21.0100	01139
256:03:34:55.3	+12.0678	+21.0107	01104
256:03:34:55.4	+12.0739	+21.0107	01102
256:03:34:55.5	+12.0754	+21.0107	01090
256:03:34:55.6	+12.0773	+21.0107	01107
256:03:34:55.7	+12.0830	+21.0107	01127
256:03:34:55.8	+12.0834	+21.0107	01104
256:03:34:55.9	+12.0876	+21.0107	01128
256:03:34:56.0	+12.0917	+21.0107	01106
256:03:34:56.1	+12.0917	+21.0107	01130
256:03:34:56.2	+12.0974	+21.0107	01114
256:03:34:56.3	+12.0993	+21.0100	01103
256:03:34:56.4	+12.1015	+21.0100	01089
256:03:34:56.5	+12.1069	+21.0107	01107
256:03:34:56.6	+12.1076	+21.0100	01104
256:03:34:56.7	+12.1110	+21.0100	01107
256:03:34:56.8	+12.1159	+21.0107	01082
256:03:34:56.9	+12.1159	+21.0107	01092
256:03:34:57.0	+12.1206	+21.0107	01098
256:03:34:57.1	+12.1240	+21.0107	01078
256:03:34:57.2	+12.1247	+21.0107	01099
256:03:34:57.3	+12.1303	+21.0107	01117
256:03:34:57.4	+12.1315	+21.0107	01137
256:03:34:57.5	+12.1348	+21.0107	01127
256:03:34:57.6	+12.1391	+21.0107	01111
256:03:34:57.7	+12.1391	+21.0107	01079
256:03:34:57.8	+12.1455	+21.0107	01061
256:03:34:57.9	+12.1467	+21.0107	01062
256:03:34:58.0	+12.1489	+21.0107	01055
256:03:34:58.1	+12.1542	+21.0107	01059
256:03:34:58.2	+12.1550	+21.0100	01067
256:03:34:58.3	+12.1599	+21.0100	01102
256:03:34:58.4	+12.1625	+21.0100	01054
256:03:34:58.5	+12.1633	+21.0107	01079
256:03:34:58.6	+12.1694	+21.0107	01077
256:03:34:58.7	+12.1701	+21.0107	01055
256:03:34:58.8	+12.1735	+21.0107	01043
256:03:34:58.9	+12.1777	+21.0107	01066
256:03:34:59.0	+12.1784	+21.0107	01016
256:03:34:59.1	+12.1831	+21.0100	01020
256:03:34:59.2	+12.1857	+21.0100	01046
256:03:34:59.3	+12.1872	+21.0100	01006
256:03:34:59.4	+12.1928	+21.0107	01039
256:03:34:59.5	+12.1940	+21.0107	01030
256:03:34:59.6	+12.1962	+21.0107	01039
256:03:34:59.7	+12.2016	+21.0107	01053
256:03:34:59.8	+12.2023	+21.0107	01025
256:03:34:59.9	+12.2058	+21.0107	01019
256:03:35:00.0	+12.2099	+21.0107	01022
256:03:35:00.1	+12.2114	+21.0107	01090

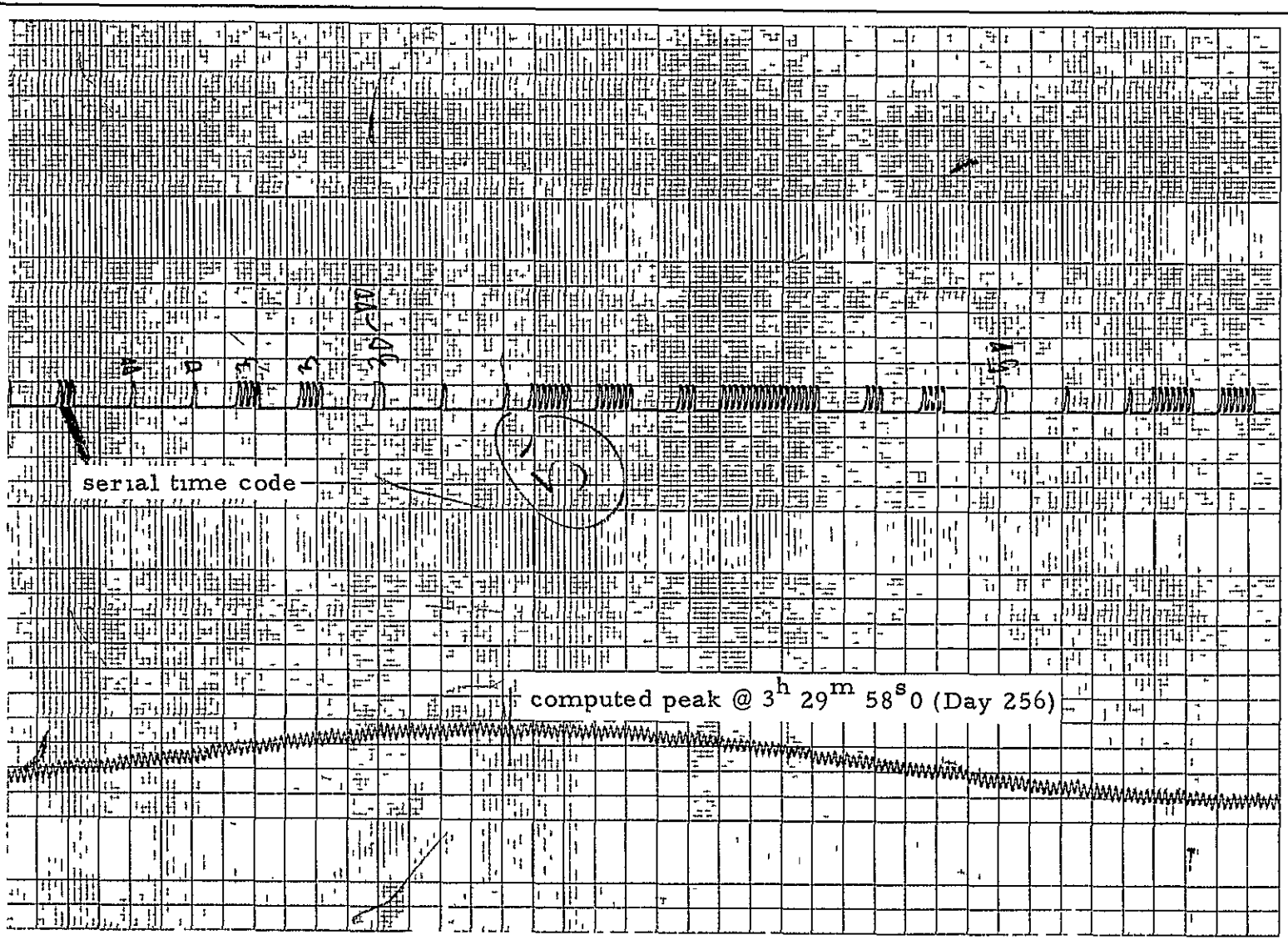

Figure 1

SINGLE AXIS SCAN OF CASSIOPEIA A - Y AXIS SCANNING @ 1/16°/SEC.

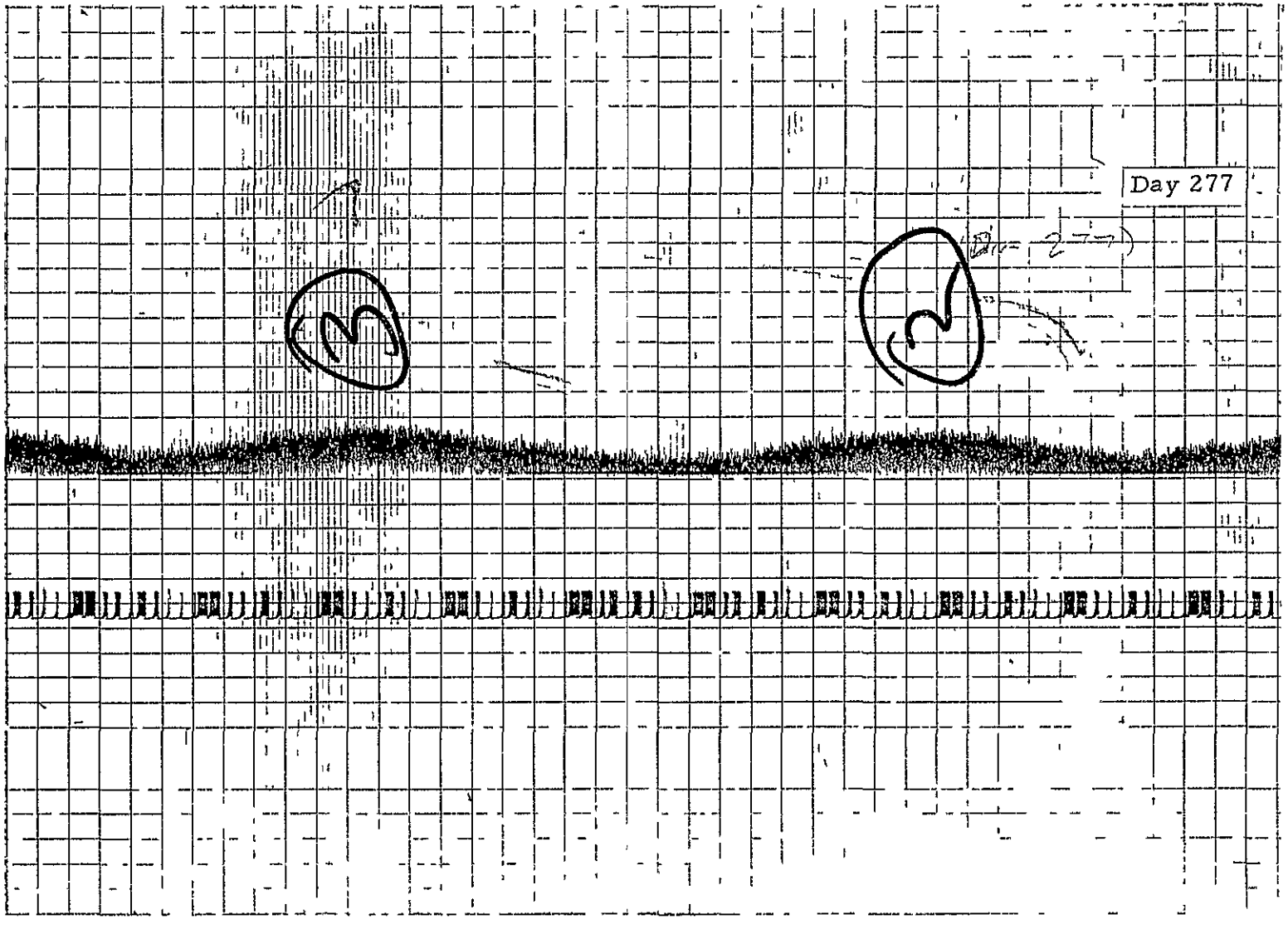

Figure 2

SINGLE AXIS SCAN OF CYGNUS A - X AXIS SCANNING @ 1/4°/SEC

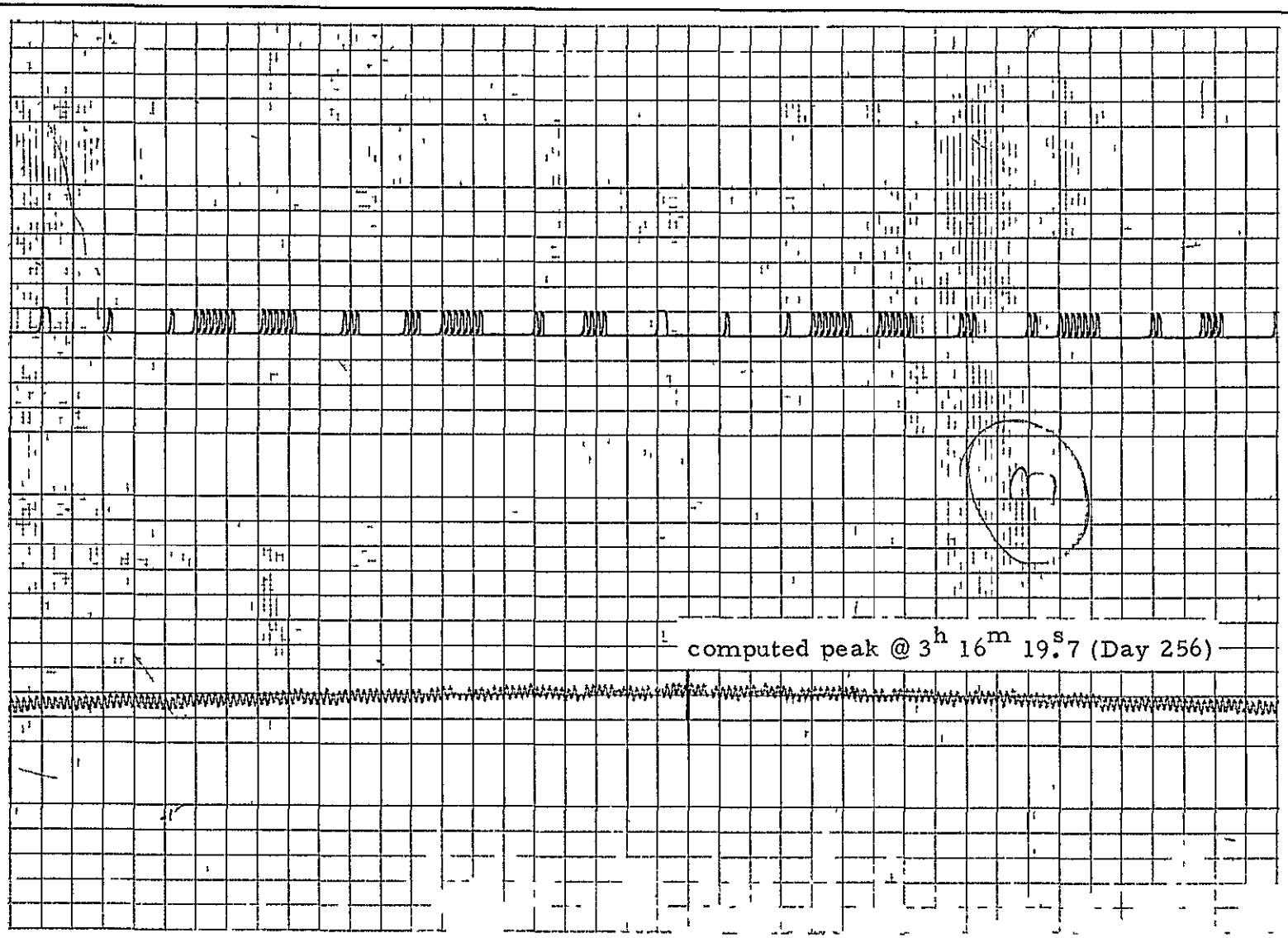

Figure 3

SINGLE AXIS SCAN OF 3C400 - Y AXIS SCANNING @ 1/16°/SEC.

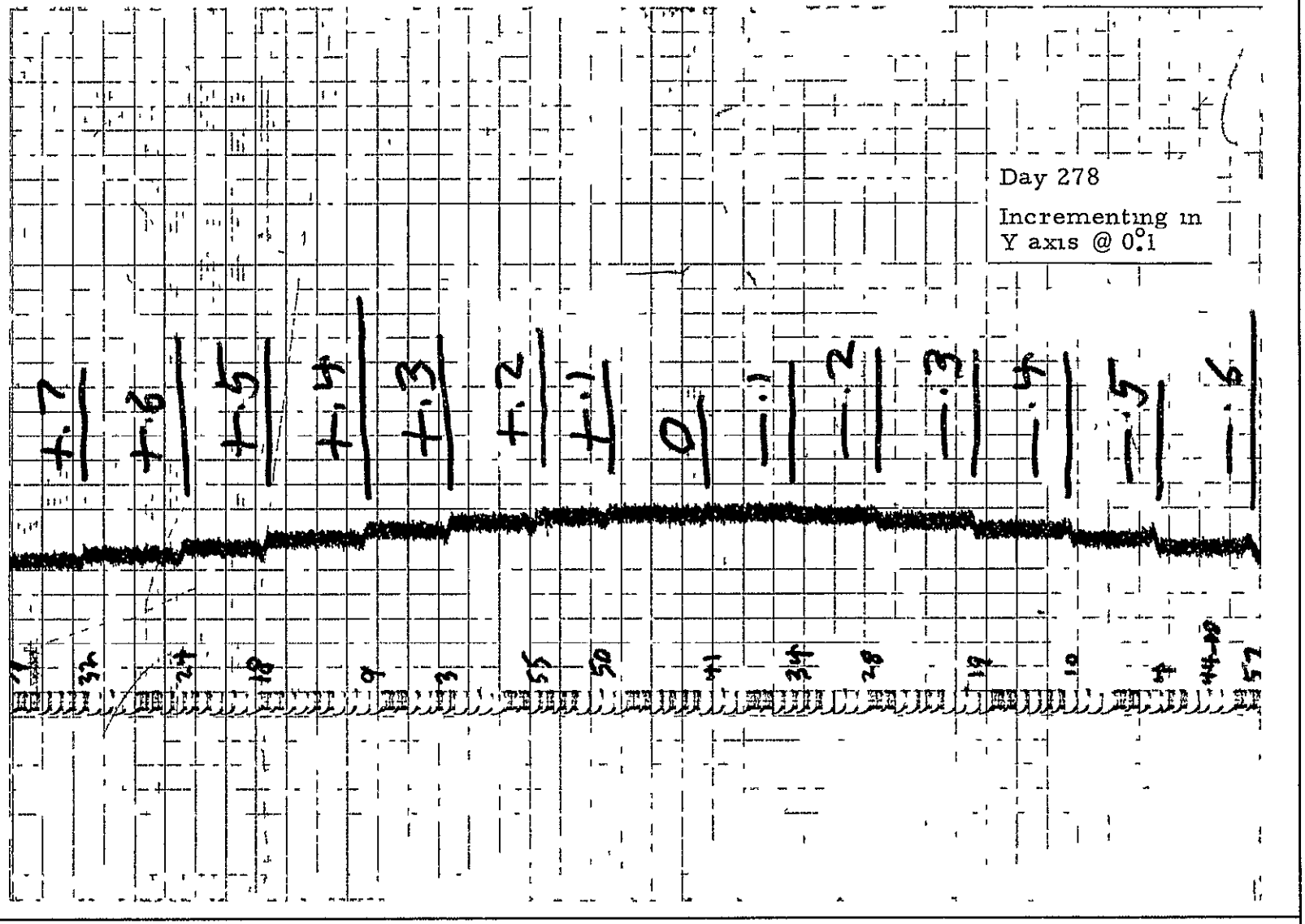

Figure 4

INCREMENTAL OFFSET OF CASSIOPEIA A

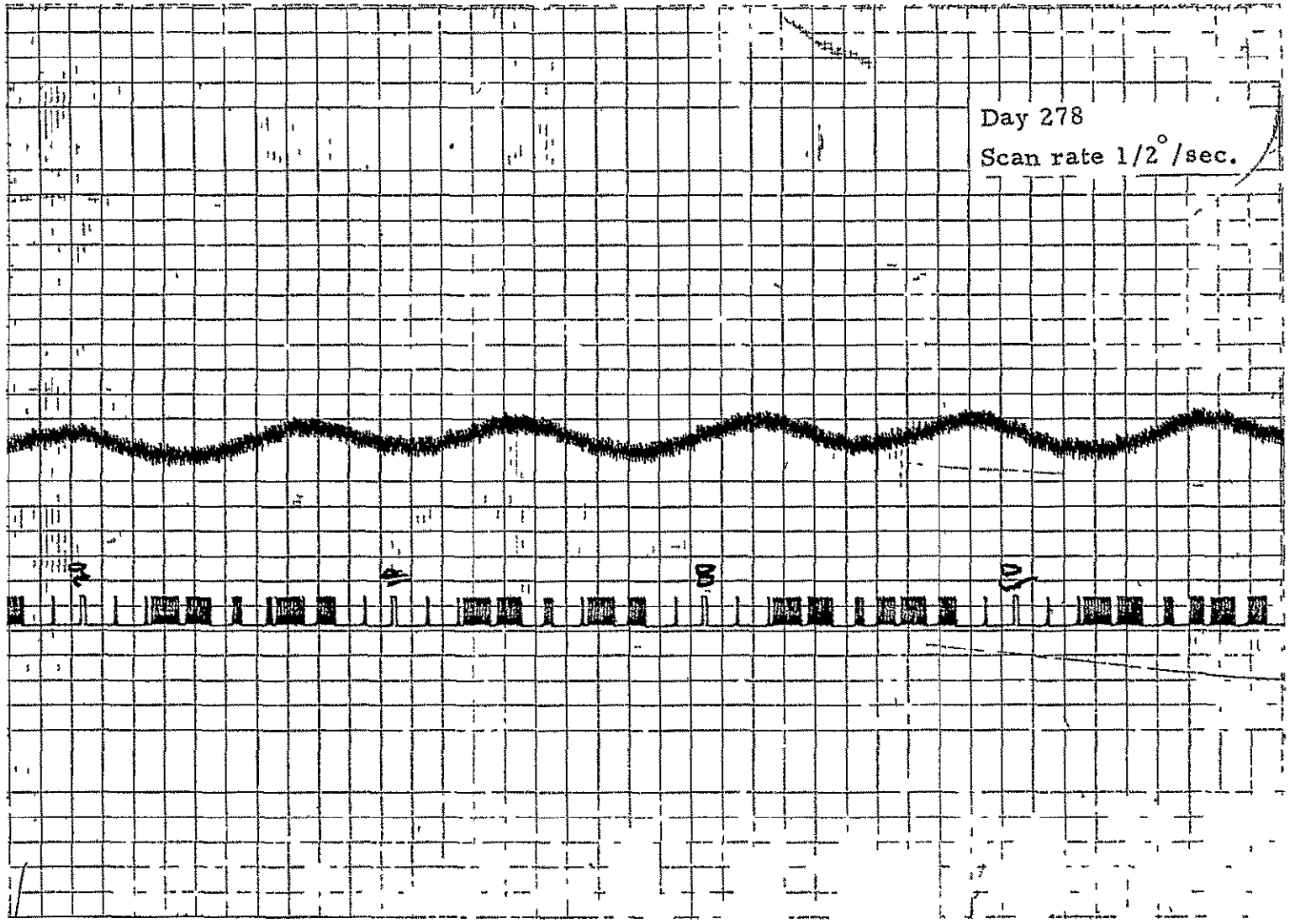

Figure 5

RASTER SCAN OF CASSIOPEIA A

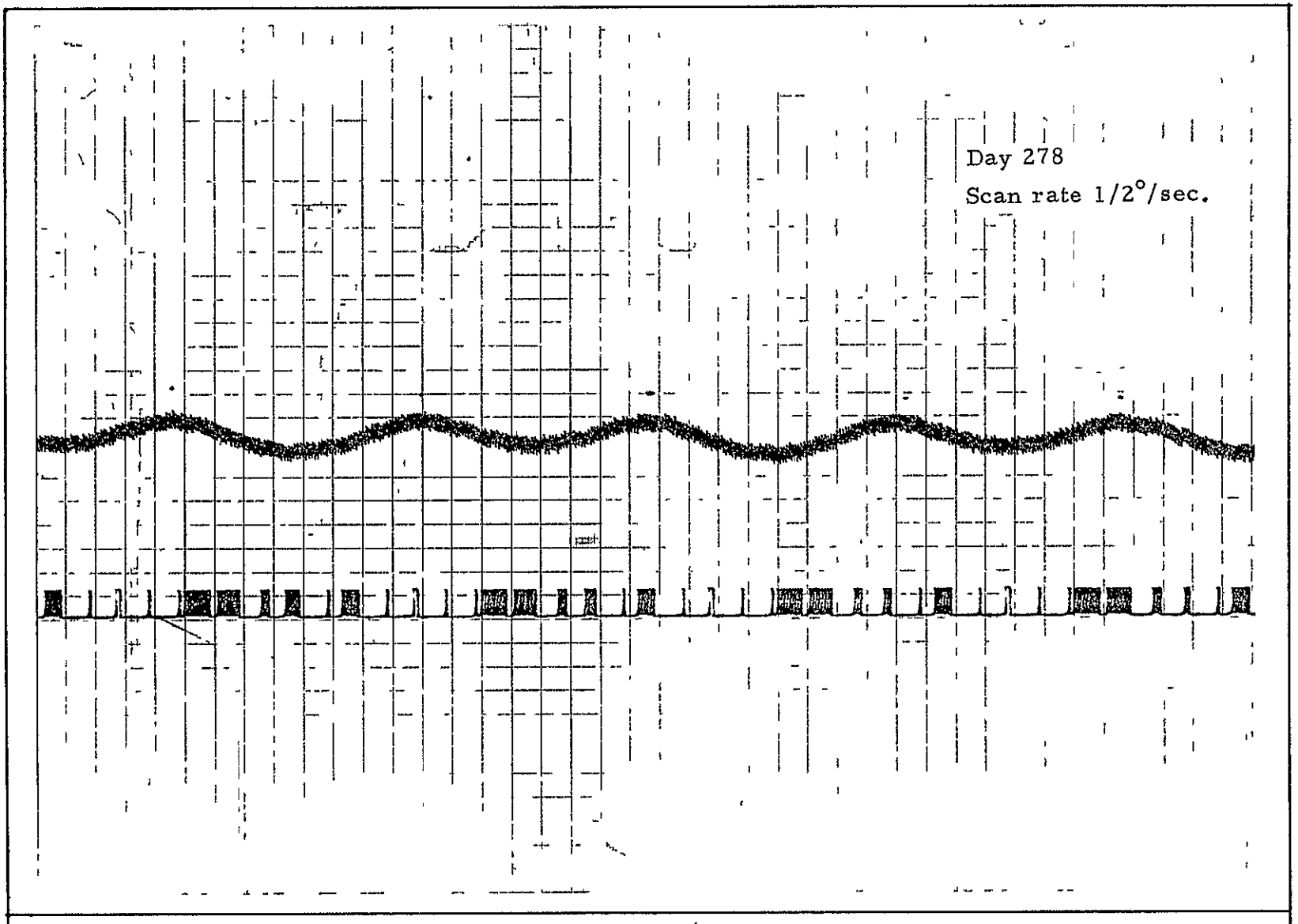

Figure 6

SECTOR SCAN OF CASSIOPEIA A

APPENDIX II
ANALYSIS OF CALIBRATION TECHNIQUES

A EFFECT OF ASTRONOMIC POSITION ON X & Y ANGLES

The surveyed position of the antenna is generally termed "geodetic" and is based on some geodetic datum Ideally the antenna should be "leveled" to the geodetic position This is to say that the X- and Y- axes of the antenna should be perpendicular to the spheroid at the station, not parallel to the gravity vector, and in 0° and 90° geodetic azimuth, respectively For example, if we assume a worldwide network of antennas tracking an artificial satellite and the positions of these antennas are coordinated on a world geodetic datum, then we would expect the antenna X- and Y- angles to refer to the geodetic zenith and horizon

For very practical reasons the antennas are leveled to the gravity vector which contains the astronomic zenith and is a measure of the astronomic position To be consistent, the X- and Y- axes should be in 0° and 90° astronomic azimuths, respectively The antenna so leveled and oriented will measure what might be called "astronomic" angles In order to correct to the geodetic framework, we need to know the tilt components in the meridian and prime vertical These may be determined from the differences between the astronomic latitudes and longitudes and their geodetic counterparts and define what is known as the deflection of the vertical The meridian component of the tilt (ξ) is astro minus geodetic latitude ($\phi_a - \phi_g$) and when plus the geodetic zenith is to the south of the astronomic The prime vertical component (η) is astro minus geodetic longitude (east) multiplied by the cosine of the latitude $[(\lambda_a - \lambda_g) \cos \phi]$ and when plus the geodetic zenith is to the west of the astronomic

What is needed then to determine these tilt components, and therefore the corrections to obtain the "geodetic" X- and Y-angles, is the astronomic position of the tracking antenna This can easily be obtained to an accuracy of 1 to 2 seconds of arc (0°0003 to 0°0005) at little expense Having these and the adopted geodetic positions, the tilt components, ξ and η, are determined

In triangulation this same problem of the deflection of the vertical arises since the observed angles are referred to the gravity vector and not, as they should be, to the spheroid normal The horizontal angles are not seriously affected because of the small elevation angles But at times, in the most precise work, both horizontal and vertical directions are corrected The corrections to horizontal directions and vertical angles are, respectively

$$d\alpha = - (\xi \sin \alpha - \eta \cos \alpha) \tan \epsilon \qquad (1)$$

$$d\epsilon = - (\xi \cos \alpha + \eta \sin \alpha) \qquad (2)$$

where α is azimuth from the north and ϵ is elevation angle. The definitions, including the signs of ξ and η, have already been given

What is really needed are expressions giving the corrections to the observed X- and Y- angles, which are referenced to the astronomic framework,to convert them to the geodetic framework, or at least to assess the effect of the deflections of the vertical on the X - Y system.

In terms of α and ϵ we have

$$\tan X = \sin \alpha \cot \epsilon \qquad (3)$$

$$\sin Y = \cos \alpha \cos \epsilon \qquad (4)$$

and in terms of X and Y we have

$$\tan \alpha = \sin X \cot Y \qquad (5)$$

$$\sin \epsilon = \cos X \cos Y \qquad (6)$$

Differentiating (3) we get

$$\sec^2 X \; dX = \cos \alpha \cot \epsilon \, d\alpha - \sin \alpha \csc^2 \epsilon \; d\epsilon$$

Substituting (1) and (2) for $d\alpha$ and $d\epsilon$ we have

$$\begin{aligned} dX &= \cos^2 X \left[(\cos \alpha \cot \epsilon) (- \xi \sin \alpha + \eta \cos \alpha) \tan \epsilon \right. \\ &\qquad \left. + (\sin \alpha \csc^2 \epsilon) (+ \xi \cos \alpha + \eta \sin \alpha) \right] \\ &= \cos^2 X \left[- \xi \sin \alpha \cos \alpha (1 - \csc^2 \epsilon) + \eta \cos^2 \alpha + \eta \sin^2 \alpha \right. \\ &\qquad \left. + \eta \sin^2 \alpha \cot^2 \epsilon \right] \\ &= \cos^2 X \left(\xi \sin \alpha \cos \alpha \cot^2 \epsilon + \eta + \eta \sin^2 \alpha \cot^2 \epsilon \right) \end{aligned}$$

But $\eta + \eta \sin^2 \alpha \cot^2 \epsilon = \eta + \eta \tan^2 X = \eta \sec^2 X$

and $\sin\alpha\cos\alpha\cot^2\epsilon = \frac{\sin\alpha\cos\epsilon\ \cos\alpha\cos\epsilon}{\sin^2\epsilon} = \frac{\sin X\cos Y\sin Y}{\cos^2 X\ \cos^2 Y}$

$$= \frac{\sin X\tan Y}{\cos^2 X}$$

Finally, $\underline{\underline{dX = +\xi\sin X\tan Y + \eta}}$ (7)

Differentiating (4) we get

$$\cos Y\, dY = -\sin\alpha\cos\epsilon\, d\alpha - \cos\alpha\sin\epsilon\, d\epsilon$$

Substituting (1) and (2) for $d\alpha$ and $d\epsilon$ and rearranging we have

$$dY = \sec Y\,[\sin\alpha\cos\epsilon\,(\xi\sin\alpha - \eta\cos\alpha)\tan\epsilon + \cos\alpha\sin\epsilon\,(\xi\cos\alpha + \eta\sin\alpha)]$$

But $\tan\epsilon = \frac{\sin\epsilon}{\cos\epsilon}$, so we have

$$dY = \sec Y\,[\xi\sin\epsilon\,(\sin^2\alpha + \cos^2\alpha)]$$

Finally, using (6) we get $\underline{\underline{dY = \xi\cos X.}}$ (8)

As can be seen from (7) and (8) the corrections to the X- and Y- angles are of the same order as the tilt components and, thus, the deflections of the vertical.

In a datum, well determined for a single continent, these deflections may average about 3 or 4 seconds in each component, but may reach 20 or 30 seconds. On a world geodetic system, such as the Mercury Datum, deflection components, particularly in mountainous areas and on islands, can easily reach about 30 seconds and 60 or 70 seconds ($0^\circ 018$) are known to exist

Deflection components at the unified S-band sites, with the exception of Guam and the Canary Islands, do not exceed 23 seconds ($0^\circ 006$) Accordingly, errors in X and Y-angles, due to ignoring the astro-geodetic deflections, will not be serious and could pass by unnoticed Deflection components are not available yet for Guam and the Canaries where they could be large, as these locations have not been connected to any major geodetic datum

B DETERMINATION OF ANTENNA TILT BY Y-WHEELHOUSE LEVELS

The Y-wheelhouse levels can be used to good advantage in monitoring the attitude of an antenna which has been carefully checked out by star shots for solution of the error equations If such a method is to be made dependa there should be at least two, and preferably three, sets of X- and Y-levels. For example, the tilt of the antenna can not only be monitored for changes, it can be determined itself, once the relations between the spirit levels and X- and Y-axes are known.

Assume the following constants have been well determined by star calibration·

Z_x = X-encoder bias, (encoder reading, X-axis level),

Z_y = Y-encoder bias, (encoder reading, Y-axis level),

ξ = tilt in meridian (plus north),

η = tilt in prime vertical (plus east),

C = optical to Y-axis lack of orthogonality (plus east).

Assume further that·

L_x and L_y are X- and Y-readings when Y-wheelhouse levels are centered,

X_e = X-level error in relation to optical axis (plus, east end up),

Y_e = Y-level error in relation to optical axis (plus, north end up),

E_x and E_y are the same as X_e and Y_e except that the latter pair is in relation to mechanical axis or X- and Y-axes).

A step by step example, which develops these relationships follows

Assume the antenna is in perfect adjustment and level, i.e., both X- and Y-axes are level and the mechanical axis is in the zenith, and further that the X-encoder bias (Z_x)is -1.7 (in hundredths of a degree).

Now suppose the whole structure is tilted to the east so that $\eta = +0.8$ and the optical axis is tilted to the west of the mechanical axis so that $C = -0.5$. The X-encoder reading is still -1.7. Now to point the optical axis (the axis used in the star shots) to the zenith we must rotate on the X-axis to the west by $-\eta$ or -0.8 and to the east by -C or +0.5, a net of -0.3. The X-encoder will now read -1.7 -0.3 or -2.0.

It should be noted that up to this point the Y-wheelhouse spirit levels have not been used or even considered. Now with $\eta = +0.8$, $C = -0.5$, X-reading = -2.0, and the optical axis in the zenith, rotate the antenna until the X- and Y-spirit levels in the Y-wheelhouse are centered. Assume the X-encoder now reads L_x or -4.6. This means that, with the optical axis in the zenith, the east end of the X-level is 2.6 too low ($X_e = -2.6$).

We have, then, $-2.6 = +1.7 + 0.8 - 0.5 - 4.6$ or

$$X_e = -Z_x + \eta + C + L_x \qquad (1)$$

and by analogy $$Y_e = -Z_y + \xi + L_y \qquad (2)$$

It will be noted that (2) has no counterpart of C in (1). This lack of parallelism of the optical with the mechanical axis, as projected on the meridional plane, must show up as a part of the Z_y, it cannot be separated by star observations as can the C from Z_x.

If we are interested in the relation of the spirit levels to the X- and Y-axes, and thus to the true mechanical axis, then C is omitted from (1) and we have

$$E_x = -Z_x + \eta + L_x$$

and $$E_y = -Z_y + \xi + L_y.$$

Having determined E_x and E_y, we may monitor the tilt components, η and ξ, by the relation

$$\eta = Z_x + E_x - L_x \qquad (3)$$

and $$\xi = Z_y + E_y - L_y. \qquad (4)$$

Since the Z and E terms are constants, changes in η and ξ may be monitored directly by L_x and L_y.

C OBSERVATION EQUATIONS FOR OPTICAL STAR SOLUTIONS

Observation equations for star calibrations were developed during the previous study phase For the seven coefficient model the observation equations were

$$V_{x_i} = Z_x + \frac{\tan e_i \cos \alpha_i}{A_i} d\alpha - \frac{\sin \alpha_i \cos \alpha_i \sec^2 e_i}{A_i} \xi$$

$$- \frac{\sin^2 \alpha_i \sec^2 e_i}{A_i} \eta + \tan Y_i \; \theta + \frac{C}{\cos Y_i} - dX_i$$

and

$$V_{y_i} = Z_y - \frac{\sin \alpha_i}{\sqrt{A_i}} d\alpha - \frac{\tan e_i \cos^2 \alpha_i}{\sqrt{A_i}} \xi -$$

$$- \frac{\tan e_i \cos \alpha_i \sin \alpha_i}{\sqrt{A_i}} \eta - dy_i$$

where Vx_i and Vy_i are the residuals of the observations of the X and Y angles resulting from the data reductions,

and where

Zx	=	X encoder bias
Zy	=	Y encoder bias
$d\alpha$	=	azimuth misalignment
ξ	=	tilt component in the meridian (plus north)
η	=	tilt component in the prime vertical (plus east)
θ	=	X-axis to Y-axis lack of orthogonality
C	=	optical axis to Y axis lack of orthogonality

In the formulation of the seven-coefficient model, the effect on the $d\alpha$ term due to tilt of antenna was not included This was done under the assumption that the maximum tilt would be small, about ± 0 01 It can be shown that the maximum effect on dX and dY due to this assumption is small, i.e , on the order of the tilt components themselves The purpose of making such an assumption was to allow the approximate determination of the values of both tilt components (η and ξ) at the time the observations were taken This was desirable as an effort was being made to monitor the relative changes in the antenna, via the level bubbles, on a near-real-time basis.

The effect of the assumption is to produce only approximate values for the tilt components as well as the other terms that are highly related to these terms (Z_x, Z_y and C)

Further studies of the seven coefficient model, using the various star distributions accumulated during this study phase, led us to include terms to account for structural deflection or sag. These terms were suggested as being the most likely additional terms to included from a review of the models used by Collins Radio Company and the Operations Evaluation Branch, Tracking and Data Systems Directorate, GSFC The expressions for sag used at GSFC had the most straightforward formulation and were the ones adopted for inclusion in our model

Two variables (called A_5 and A_6) are used to allow for the total effect of sag in the X-axis, while a single variable (called B_3) is used to express the effect of sag in the Y-axis. The total expressions for these terms are

(sin X sec Y) A_5, (sin X) A_6, and (cos X sin Y) B_3

In these expressions,

A_5 = X direction sag (moment between X-axis and Y-axis)
A_6 = X direction sag (moment between Y-axis and Dish)
B_3 = Y direction sag

Results obtained while including all three terms in the model were not satisfactory (see section 3 1 3) The main reason being that there was no justification in attempting to solve for the effect of both the A_5 and A_6 terms in the various star distribution available In light of this, our adopte model only includes the A_5 term for expressing the X-axis coefficient of sag and our adopted observation equations are as follows

$$V_{x_i} = Z_x + \frac{\tan e_i \cos \alpha_i}{A_i} d\alpha - \frac{\sin \alpha_i \cos \alpha_i \sec^2 e_i}{A_i} \xi$$

$$- \frac{\sin^2 \alpha_i \sec^2 e_i}{A_i} \eta + \tan Y_i \ \theta + \frac{C}{\cos Y_i} + (\sin X \sec Y) A_5 - dX$$

and

$$V_{y_i} = Z_y - \frac{\sin \alpha_i}{\sqrt{A_i}} d\alpha - \frac{\tan e_i \cos^2 \alpha_i}{\sqrt{A_i}} \xi - \frac{\tan e_i \cos \alpha_i \sin \alpha_i}{\sqrt{A_i}} \eta$$

$$+ (\cos X \sin Y) B_3 - dY_i$$

APPENDIX III
THEORETICAL CAPABILITY OF USB ANTENNA FOR DETECTING CELESTIAL RADIO SOURCES

Prior to conducting experiments, calculations were made to determine the theoretical flux density of a radio source which the unified S-band antenna (30-foot) should be able to detect

The theoretical power (in watts) required for detection can be calculated from the following equation

$$d = 10 \log (W_2/W_1)$$

where d is the difference in two power levels W_2 and W_1 From this formula we can obtain the following expression for the ratio of the two power levels

$$W_2/W_1 = (10)^{0\ 1d}$$

or if W_1 is known, the formula for W_2 is

$$W_2 = W_1\ (10)^{0\ 1d} \qquad (1)$$

Assuming that the minimum discernable signal of the unified S-band is -147 dbm when the system is not equipped with a cryogenic preamplifier and -150 dbm when the system is so equipped, we can use equation (1) to compute the minimum power required for detection by the system With the signal strength expressed in these terms, W_1 is by definition equal to 0 001 watt

Case I — No cryogenic preamplifier (d = - 147)

$W_2 = 0\ 001\ (10)^{-14\ 7}$

$W_2 = 2\ 0\ (10)^{-18}$ watt

Case II — With preamplifier (d = - 150)

$W_2 = 1\ 0\ (10)^{-18}$ watt

Kraus [1] gives the following formula for the total power received by an antenna

$$W = \tfrac{1}{2} A_e S_o \Delta\nu \qquad (2)$$

where W = total received power, in watts,
A_e = effective aperture of antenna, in m^2,
S_o = observed flux density, in watts m^{-2} Hz^{-1}, and
$\Delta\nu$ = bandwidth (between ν and $\nu + \Delta\nu$), in Hz

Equation (1) is based on two assumptions: (a) that the antenna pattern is aligned with the source, and (b) that the flux density is constant over the bandwidth $d\nu$

Solving this equation for the flux density, S_o, we get

$$S_o = \frac{2W}{A_e \Delta\nu} \tag{3}$$

For this antenna system the effective aperture of the antenna, A_e, is approximately equal to 55 square meters and the bandwidth, $\Delta\nu$, equals 4 MHz

We can use equation (3) to determine the flux densities corresponding to the minimum power requirements derived above The results are

Case I $S_o = 1\ 8\ (10)^{-26}$ watts m^{-2} Hz^{-1} = 1 8 flux units, and

Case II $S_o = 0\ 9\ (10)^{-26}$ watts m^{-2} Hz^{-1} = 0 9 flux unit

From these results it appears that any radio source having a flux density equal to or greater than 2 flux units in Case I and 1 flux unit in Case II can theoretically be detected by the unified S-band antenna There are a number of celestial sources with power flux considerably greater than these values For example, those listed in table 1 of the report vary from 70 to 1700 flux units Therefore, it seemed feasible that celestial radio sources could be utilized for rf pointing calibration

---

[1] Radio Astronomy, John D Kraus, McGraw - Hill Book Co , New York, N Y

APPENDIX IV
ANGULAR REFRACTION CORRECTIONS FOR OBSERVATIONS OF RADIO SOURCES

The Smith - Weintraub [1] constants have been used by Barton [2] and Sloanmaker and Nichols [3] in the equation for the atmospheric refraction of radio waves at frequencies below approximately 25,000 MHz The expression for refractivity, N, using these constants is·

$$N = (n_o - 1)\, 10^6 = \frac{77.6}{T}\left(p + 4810\,\frac{e}{T}\right) \qquad (1)$$

where n_o is the index of refraction at ground level, T is the temperature of the air in °K, p is the total atmospheric pressure in millibars, and e is the partial pressure due to water vapor in millibars

The authors of [3] also give the following expression or its equivalent for the refraction correction to an observed angle of elevation greater than 5° or 10°

$$R = N\,(10^{-6})\cot \varepsilon_o \text{ radians} \qquad (2)$$

where ε_o is the observed elevation angle*

Converting the coefficients in equation (1) for use with p and e in inches of mercury instead of millibars (1 in Hg = 33.86389 mb) and separating the right-hand side into two terms, a "dry-air" term and a "moist-air" term, the equation becomes

$$N = \frac{2628\,p}{T} + \frac{12{,}641\,e\,10^6}{T^2} \qquad (3)$$

Since e = the saturation vapor pressure (e') at temperature T multiplied by the relative humidity (H), equation (3) becomes

$$N = \frac{2628\,p}{T} + \frac{12{,}641\,e'\,H\,10^6}{T^2} \qquad (4)$$

*An evaluation of this expression by Data Evaluation Branch, GSFC indicated that this formula is not adequate for tracking purposes when elevation angle are less than 20°

The correction for refraction, equation (2), can be converted to seconds of arc by dividing the right-hand side by arc 1"

$$R'' = 206265\ R$$

$$R'' = 0\ 206265\ N \cot \epsilon_o \qquad (5)$$

Combining equations (4) and (5) results in the expression

$$R'' = \left(\frac{542\ 1\ p}{T} + \frac{2\ 607\ e'\ H\ 10^6}{T^2}\right) \cot \epsilon_o \qquad (6)$$

Equation (6) is the required formula With p and e' in inches of mercur T in degrees Kelvin, H as a decimal fraction from 0 to 1, and ϵ_o the observe elevation angle, R" is the correction to ϵ_o in seconds of arc The saturation pressure e' can be obtained from the Smithsonian Meteorological Tables (195 pp 354-357 The computed correction for refraction is subtracted from the observed elevation angle to obtain the actual elevation angle

A much simpler method of computing the refraction correction is obtained by equating the parenthetical expression of the right-hand side of equation (6) to the product of the "dry-air" term times a correction term

Let $$\left(\frac{542\ 1p}{T} + \frac{2\ 607\ e'\ H\ 10^6}{T^2}\right) = \left(\frac{542\ 1\ p}{T}\right)\ F$$

where $F = 1 + \mu H$ Solving for μ we get

$$\mu = \frac{4809\ e'}{T\ p}$$

This moist air correction factor, μ, increases with temperature (because of the variation of e' which also depends upon temperature) and is inversely proportional to the pressure Numerically it varies from near zer at low temperatures to 1 24 at a temperature of 40° C and a pressure of 27 inches of mercury The values at 30 0 in Hg at normal temperatures are as follows

t °C	-20	-15	-10	-5	0	+5	+10	+15	+20	+25	+30	+35	+4
μ	0 023	0.035	0.051	0 074	0 106	0.148	0 205	0.280	0 377	0 503	0.663	0 864	1 1

Very little error is introduced by using the values of μ given in the preceding table for normal pressures at sea level, particularly at the lower temperatures. Even at 100 percent relative humidity, a change of 2 inches in the pressure only causes the following changes in F at normal temperatures below 5°C, less than 1%, at 20°C, about 2%, at 30°C, about 3%, and at 40°C, about 4%

Using the factor μ the formula for the correction for refraction (in seconds of arc) is

$$R'' = \frac{542.1\ p}{T} (1 + \mu H) \cot \varepsilon_0 \qquad (7)$$

As an example, compute R'' for the following conditions p = 30.0 in Hg, T = 20°C = 293.16°K, relative humidity = 100% (H = 1), and $\varepsilon_0 = 45^\circ$ ($\cot \varepsilon_0 = 1$). From the table above μ = 0 377 and F = 1.377 Then R'' = 76''. A change of 2 inches of mercury in the pressure changes R by only 2 seconds of arc. At an elevation angle of 26° 33' ($\cot \varepsilon_0 = 2.00$) the error would be 4''

Now compute R'' for T = 40°C = 313.16°K, with the other conditions remaining constant. μ = 1.115, H = 1, and F = 2.115. With $\varepsilon_0 = 45^\circ$, R'' = 123''. At 28.0 in. Hg, R'' = 128'', at 32.0 in. Hg, 119''. Here a 2-inch change in pressure causes a change of 5'' in the refraction correction At an elevation angle of 26° 33', the change would be 10''. Since the least count of the encoders is 0°.001 which is about 4'' of arc, the error introduced by using the values of μ in the table above for normal values of sea level pressure and temperature should be negligible in most instances.

---

[1] "The Constants in the Equation for Atmospheric Refractive Index of Radio Frequencies," Ernest K. Smith and Stanley Weintraub, NBS Rept. No. 1938, Sept. 1952.

[2] "Radar System Analysis," David K. Barton (Raytheon Co.), Prentice-Hall, Publ., 1964.

[3] "Positions, Intensities, and Sizes of Bright Celestial Sources at a Wave Length of 10.2 Cm., "R.M. Sloanmaker and J.H. Nichols, Astron. Journal, Vol. 65, No. 3, April 1960.